ÉCOLE POLYTECHNIQUE
FÉDÉRALE DE LAUSANNE

Colorado State University

Senior Project in Civil Engineering 1998/99
Travail de Diplôme en Génie Civil 1998/99

Armoring of the Irrigation Canals in the San Luis Valley, Colorado

Study Report

by Christoph Oehy

Fort Collins, 1999

Abstract

Armoring of the Irrigation Canals in the San Luis Valley, Colorado

The main objective of this study was to reinvestigate the irrigation canals in the San Luis Valley to extend the knowledge of stable channel design and the armoring process at prototype scale. To achieve this objective several field trips were conducted to complete the data sets gathered by *LANE AND CARLSON* (1953) in their 1950-1953 studies.

Six test sections were selected for reinvestigation and measurements completed of the discharge, the slope, the geometry, and the grain size distribution of the armor layer. For the armor layer sampling, several methods were tested, compared, and calibrated to an area-by-weight sample as used by *GESSLER* (1965). Excellent agreement was found for the transect-by-number method and the GoldSize photographic sizing computer program.

The bottom shear stress of the canals was determined and corrected with respect to the bank effect. The analysis of this computation led to the conclusion that in determining the bottom shear stress in canals, a significant error might occur if only the depth of flow or the overall hydraulic radius is used, instead of the hydraulic radius of the bed. The sensitivity analysis furnished new findings about the importance of the different input variables to the resulting bottom shear stress, and showed that the variation of the slope, the discharge, and the roughness of the banks mainly define the standard deviation of the bottom shear stress.

An armoring computation using Gessler's prediction procedure was performed, and the resulting grain size distribution of the predicted armor layer was compared to the armor layer measured during the field trips. All the test sections showed significant differences from computed values; the predicted armor layer systematically appeared to be finer than the measured armor layer. Hence, a conversion method proposed by *PROFFITT* (1980) has been applied to the measured grain size distribution and the resulting corrected armor layer showed good agreement with the computed armor layer in most of the test sections.

The stability coefficient and safety factor of all test sections was calculated and clearly confirmed the assumption that the irrigation canals in the San Luis Valley are very stable. During the field trips, miscellaneous observations reported in flume studies such as the typical imbricated armor pattern, or the sheltered fine material on the lee side of coarser grains were also observed at prototype scale.

Finally, it can be stated that the irrigation canals in the San Luis Valley still offer an excellent opportunity to study static armoring, and permit the verification of flume theories at prototype scale.

Acknowledgements

The author wishes to express his sincerest gratitude and appreciation to his major professor, Dr. J. Gessler, for the excellent guidance, advice, and the continuous encouragement he provided throughout the planning of the field trips, the analysis and interpretation of the results, which to a large extent made the completion of this study possible.

The author's grateful appreciation is extended to Dr. A. Schleiss, who made this study possible by his support of this unique exchange.

Further, the author wishes to thank Dr. R. Wittler for providing the historic literature from the archive of the Bureau of Reclamation, and Dr. G. Annandale from Golder Associates Inc., who provided the computer program for the grain size distribution analysis.

Thanks are also due to Dr. D. Gessler for his keen help and support during this study, as well as the ERC staff for providing the instrumentation for the field investigation.

The writer is also indebted to Mr. St. Baer and Mr. B. Cannon for their assistance during the field trips and for providing helpful information about discharge measurements. Their cooperation was very much appreciated.

Table of contents

1 Introduction

The practice of distributing water through channels excavated in the earth extends back beyond the dawn of recorded history. In China there are canal systems which have been in continuous operation for 2,000 years. Compared to this history, it is only recently, that science has developed to the point where fundamental physical principles involved in such canals have been studied. The idea is to improve their performance, and secure channels which would give a maximum of service with a minimum of expenditure.

For this purpose, during the years from 1950-1953, personnel of the Bureau of Reclamation under the direction of E. W. Lane and E. J. Carlson did studies to perfect methods for designing canals in coarse, non-cohesive materials. A number of stable canals were located in the San Luis Valley of southern Colorado, which formed the basis for this study.

The San Luis Valley is a large, open valley formed between the Sangre de Cristo and the San Juan Mountains in south-central Colorado. Its location is shown on Fig. 1.1. The valley has a length of about 130 kilometers and a width of about 65 kilometers. The bottom is formed by sediments brought down from the surrounding mountains and deposited on the bottom by water. Near the sides of the valley the slopes are rather steep, but they flatten as the distance from the sides increases; in the center the slopes are practically level. The canals on which the observations were made, are located where the Rio Grande River leaves the mountains on the southern end of the valley and flows onto an alluvial cone. Due to the confinement of the hills, the deposits have formed a section of a cone, with slopes of about 0.3 %. Near the apex of the cone the subsoil consists of sand, gravel, and cobbles. The size of the cobbles decreases with the distance from the apex.

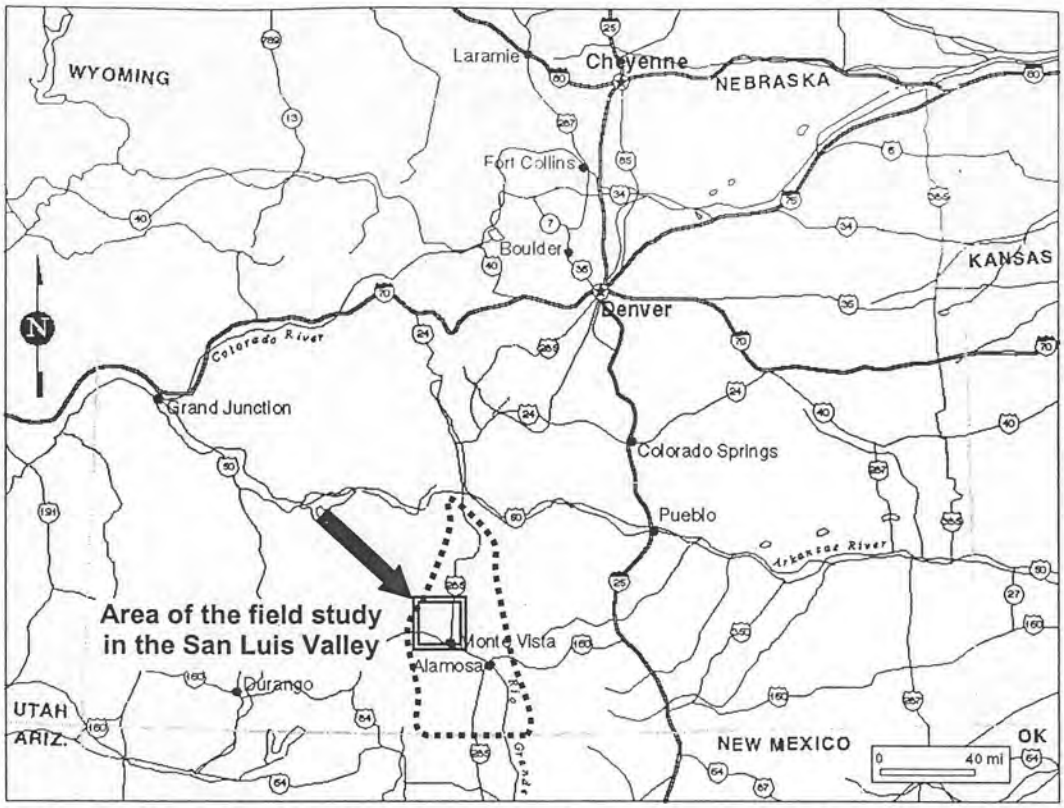

Fig. 1.1. Map of Colorado with the location of the area of the field study in the San Luis Valley

As shown on Fig. 1.2, seventeen reaches of canals were investigated in the area of the field study in the 1950's, covering a wide range of conditions of discharge, slope, and bed material size. These canals presented an unusually favorable condition for studies of stable channels and formed a broad database.

The canals were constructed by slip scrapers drawn by horses. The Rio Grande Canal was constructed in 1879, and the Farmer Union and Prairie Canals were constructed in 1887. Most of the canals and laterals are very stable, very straight and regular in section, and are steep enough to give reasonably high velocities and shear stresses. Unfortunately, the original dimensions are not available, and it is not known to what extent their shape has been modified by the flowing water or by cleaning operations since they were constructed. The nature of the canals is shown on the photographs in Appendix II (Fig. II.1-II.10).

During most of the years of operation of the canals, some coarse material entered through the head gate. But in the 1950's in the Rio Grande Canal, a trap was installed just below the head gate so most of the moving material above sand sizes seemed to be ejected from the canal. Therefore, it can be considered that the canals are mostly conveying clear water without any sediment transport from the intakes of the Rio Grande River.

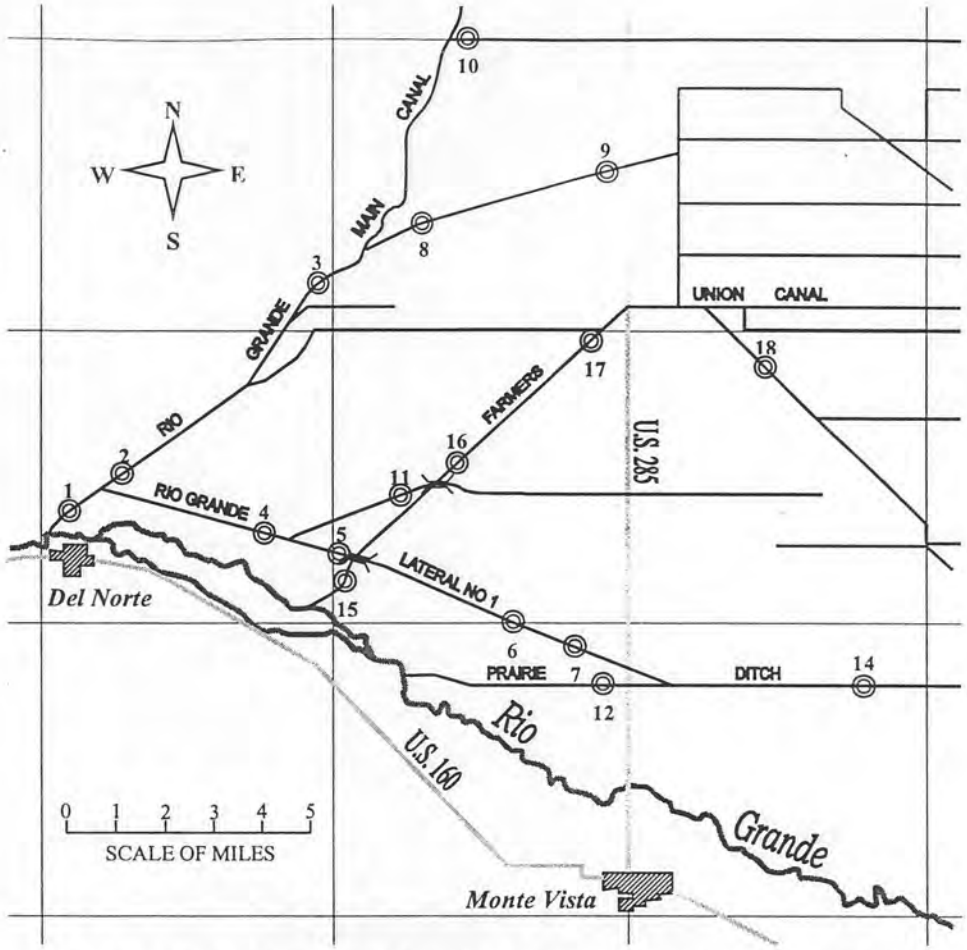

Fig. 1.2. Map of the area of the field study in the San Luis Valley with the location of the test sections investigated by Lane and Carlson 1950-1953

Because of the relatively high velocities and shear stresses, the finer material has been removed from the top layer of the bed and a natural armoring layer has been formed. Therefore, the canals in the San Luis Valley provide, an excellent opportunity to study natural, static armoring at prototype scale.

In his dissertation *GESSLER* (1965) used the hydraulic data and the grain size distribution curves of the irrigation canals in the San Luis Valley, given in the study of *LANE AND CARLSON* (1953), to verify his theory about natural armoring. With respect to the hydraulic characteristics, the canals were ideal because in the irrigation canal the controlled maximum water discharge is known relatively well, and remains constant for a relatively long period of time. These characteristics are very similar to armoring experiments in the laboratory.

However, for such an analysis the data pertaining to the grain size distribution curves was insufficient because the grain fractions were chosen too wide and in the case of the top layer no

numerical data for the coarse material was given. The limits of the size fractions stated by Lane and Carlson formed a geometric series with a factor 2. As a result, the computations of the probabilities of remaining still for the individual fractions were far apart of the measured data, especially in the entire range of the important larger components. Therefore, an accurate analysis of the data has not been possible.

Hence, the motivation for this field study was to complete and verify the data sets collected by *LANE AND CARLSON* (1953), especially the measurements concerning the grain size distributions of the surface material. A comparison of this new data with the data collected almost 50 years earlier will allow conclusions about the long term stability of these canals. The application of Gessler's armoring prediction theory to these data sets should confirm or allow adaptation of the knowledge about the armoring process and stable channel design at prototype scale. In addition, the field study will also present a good opportunity to test and compare recent sampling methods for the armored bed surface.

Therefore, chapter 2, a review of the literature, presents previous experimental, theoretical, and field studies of armoring. Chapter 3 describes the field procedures and data collection in the Poudre River and the San Luis Valley. Chapter 4, is devoted to the analysis and interpretation of the field data, and chapter 5 contains the conclusions. Appendix I concerns the methodologies used in the measurements of grain size distribution curves and their conversion. Appendix II documents photographically the field trips and the measuring procedures used in this study. Appendices III through V include notations, references, and descriptions of the test sections. Appendix VI shows the calculation sheets of the different computations made in this study.

2 Literature review and theoretic bases

2.1 Stable channel design

LANE (1952) defined a stable channel as follows: *"A stable channel is an unlined earth channel for carrying water, the banks and bed of which are not scoured by the moving water, and in which objectionable deposits of sediment do not occur."* He provides the term stable channel to an equilibrium state in which no erosion nor sedimentation occurs. This equilibrium state is called static, instead of a dynamic stability in which erosion equals the sedimentation and therefore, the average values of width, depth, slope, and meander pattern do not vary significantly over extended periods of time.

The analysis of earth channels normally requires knowledge of a great many factors. In general, the problem of stable channel design involves a study of the relationships between the following variables:

- *Geomorphologic properties:* a typical diameter or grain size distribution of the bed material, as well as shape and specific gravity of the grains. – These parameters determine the force needed for dislodgement and transport of grains and the roughness of the bed.

- *Hydraulic properties:* the energy slope, the wetted perimeter, and the cross sectional area. – These parameters determine the water discharge, depth of flow and turbulence.

There are also a number of practical considerations, three of which are the ease of construction, the economy of cleaning, and absence of weeds. To secure the best possible design all of these factors must be considered and, in some cases, balanced against each other to obtain the combination of factors which will give an optimum.

In the stability analysis of channels, it is possible to approach the problem from either the standpoint of shear stress distribution along the banks and bed, or from the standpoint of velocity distribution. Physically the shear stress approach is more directly related to the movement of grains, because the grains get moved by the shear stresses and not the velocity. Further, it is usually easier to get quantitative values in a given case for shear stresses than it is for values of velocity. For this reason the shear stress approach is usually used in the analysis of problems involving the movement of coarse particles.

2.2 Shear stress

The approach of shear stresses was developed from consideration of the forces acting on the soil particles and is based on the fact that the stability of bed and bank material is a function of their ability to resist erosion resulting from the shear stress exerted on them by the moving water. In fact, the total shear stress on the perimeter of a canal, for a unit length in the direction of flow, has to be equal to the component of the weight of the water volume in this unit length of canal, or the force which causes this volume of water to flow down the canal. Assuming that there is no acceleration of this water volume, the force causing motion must be balanced by the force exerted by the banks and bed of the canal on the volume of water. This force or stress is called the shear stress or sometimes also referred to as "tractive force" or "drag force".

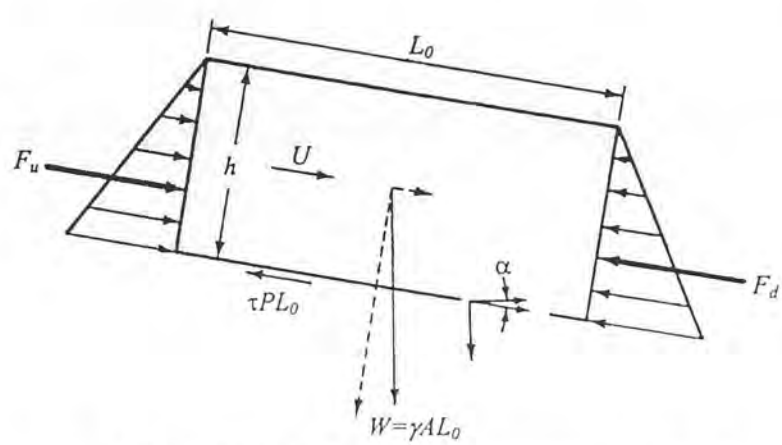

Fig. 2.1. Free-body diagram of a segment of water

The magnitude of this shear stress can be derived by considering the free body of a segment of the full width of a channel as shown in Fig. 2.1. A summation of the forces in the flow direction, assuming steady flow conditions, yields

$$F_u + W \sin\alpha = F_d + \tau P L_0 \qquad [2.1]$$

where F_u and F_d are the upstream and downstream hydrostatic forces, P the wetted perimeter, W the weight of the segment of fluid, α the slope angle, L_0 the length of the free-body segment, and τ the average shear stress that retards the flow. Assuming that F_u=F_d (uniform flow), Eq. 2.1 can be rearranged to solve for the shear stress:

$$\tau = \frac{W \sin\alpha}{P L_0} \qquad [2.2]$$

By substituting $\gamma A L_0$ for the weight W and the slope S for $sin\ \alpha$, Eq. 2.2 reduces to the familiar form for the average shear stress:

$$\tau = \gamma R S \qquad [2.3]$$

where R is the hydraulic radius and equals the cross-sectional area divided by the wetted perimeter. When the channel is very wide relative to the depth, the depth approximates the hydraulic radius, and the expression for average shear stress becomes

$$\tau = \gamma h S \qquad [2.4]$$

where h is the depth of flow in the channel. For armoring consideration often the mean bottom shear stress τ_b is used. It is defined as following

$$\tau_b = \gamma R_b S \qquad [2.5]$$

where R_b is the hydraulic radius of the bed.

Modern advancements in fluid mechanics suggested the desirability of expressing turbulent flow conditions with a quantity u_*. This term u_* is called shear velocity, and is a measure of the intensity of turbulent fluctuations. The relationship between the shear velocity and shear stress is given by

$$u_* = \sqrt{\frac{\tau}{\rho}} \qquad [2.6]$$

where ρ is the density of the fluid.

It is important to realize that in practice, the bottom shear stress never quite reaches the theoretical maximum value of γhS. Attempts were made to determine the distribution of the shear stress on the perimeter of canals from published data on the velocity distribution in trapezoidal channels. By drawing the isovels (lines of equal velocity) it was possible to divide the cross section of the flowing water into a series of subareas by orthogonal lines or lines running perpendicular to the isovels and the perimeter of the canal, and ending in the point of maximum velocity. Since these lines are perpendicular to the lines of equal velocity, there is no velocity gradient across the lines, hence no net exchange of momentum across them and therefore no net shear. The tractive force due to the weight of the water enclosed between the lines originating from the bottom and sides of the canal is therefore exerted on that part of the bottom or sides between the respective lines. By planimetering these partial areas, and thus determining the volumes of water involved, it is possible to compute the tractive force exerted on each of the parts of the canal perimeter and thus establish the shear stress distribution over the bottom and sides.

Recent studies have shown that due to secondary currents, momentum exchange across the section occurs. These currents move in approximately rectangular cells as shown in Fig. 2.2 and help equalize the bottom shear stresses. If indeed the shear stress varies substantially across the width, the armoring characteristics would have to vary as well. Such variation has never been observed in flume or prototype studies.

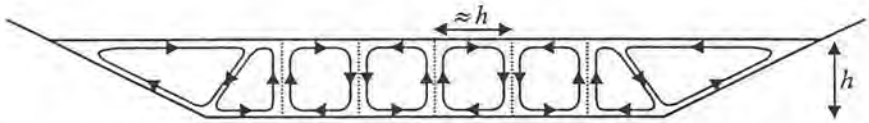

Fig. 2.2. Scheme of secondary currents in trapezoidal cross section

As the flow velocity increases, the shear stress is increased until it reaches a value known as the critical shear stress of the particle, which occurs at the threshold of particle motion. The conditions necessary to cause the motion of this particle lying on a canal bed are very complex, due to the variation of velocity with depth above the bed, the rapid fluctuations of velocity due to the turbulence in the flowing water, and due to the geometry of support for each grain. Like many threshold conditions, an exact value cannot be precisely defined. At first, a grain or two become detached at a certain rate of flow. Then, as the flow rate increases, more grains become detached and are transported until the process is general over the whole bed. Hence, it is easy to understand the difficulty encountered in visually defining the exact state at which the critical tractive force is reached.

Early research in the mechanics of sediment transport, trying to quantify this critical state, was reported by *SHIELDS* (1936). His data was obtained from flume experiments with fully turbulent

flow over artificially flattened sediment beds. He found that for the special case of uniform grains, the relationship becomes

$$\tau_* = \frac{\tau_c}{(\gamma_s - \gamma)d} = f\left(\frac{u_* d}{\nu}\right) \qquad [2.7]$$

where τ_* is the dimensionless shear stress or Shields parameter, τ_c the critical shear stress, γ_s the specific weight of sediment, γ the specific weight of water, d the grain diameter, u_* the shear velocity, and ν the kinematic viscosity of water. The term $u_* d / \nu$ is usually referred to as the grain Reynolds number $\mathbf{Re}_*$.

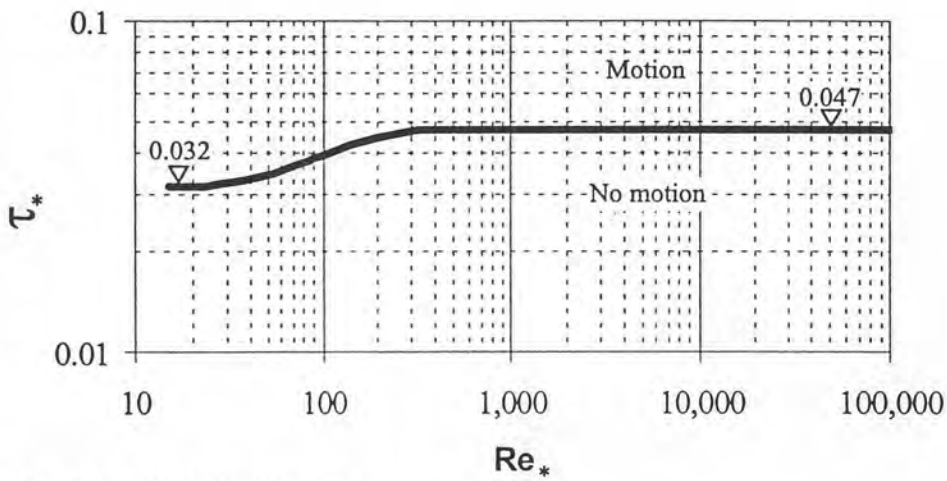

Fig. 2.3. Shields diagram

Shields determined the function f using the data obtained from his experiments. Due to the fact that all the grains of uniform size did not begin to move at the same time, the difficult question of the definition of incipient motion arose. He defined critical shear stress of a grain size as the value of bed shear stress for zero bed load transport obtained by extrapolating to zero a graph of observed bed load transport rate versus shear stress. This indirect yet objective procedure was used to avoid the implications of the random orientation of grains and variations in local flow conditions that may result in grain movement even when $\tau/(\gamma_s-\gamma)d$ is considerably below the critical value. Shields indicated the relationship between Shields parameter and grain Reynolds number by a band of appreciable width, but he did not fit a curve through his data. The curve shown on Fig. 2.3. and termed the Shields diagram was first proposed by *ROUSE* (1939).

However, *GESSLER* (1965) pointed out that the Shields function has the considerable disadvantage that it was not measured directly, but had to be extrapolated in turn from a number of plotted points. As a consequence, this indirect procedure resulted in numerous possible

inaccuracies leading to a considerable scattering of the points determined by Shields. Gessler shows that some of Shields bed load measurements were under conditions where ripples and small dunes prevailed. Nevertheless, Shields used the overall bed shear stress without differentiating between losses due to bed deformation and those due to grain roughness. This resulted in values up to 10 percent too high for the Shields parameter at incipient motion.

Hence, *GESSLER* (1965) determined the critical shear stress by a basically new method. He computed the critical shear stress for a given grain assuming that the probabilities of erosion and of non-erosion are equal. In this case the median shear stress becomes equal to the critical shear stress.

2.3 Armoring process

Armoring may be expected when a flow occurs that is sufficient to move some of the finer particles and yet insufficient to move all the larger particles. Armoring thus becomes an incipient motion problem.

In their study, *LANE AND CARLSON* (1953) expressed concisely and clearly the problem of canal design in widely graded coarse non-cohesive materials where armoring occurs.

"Canals constructed through coarse, non-cohesive material rarely, if ever, pass through a material of a narrow range of particle sizes. In practically every case the material covers a considerable range, usually extending from sand on up to gravel or cobbles. Unless the boundary shear values and velocities are very low, some material will be scoured out of such a canal when it is put into operation. Whether or not the results are satisfactory depends upon whether or not the amount moved out produces unsatisfactory conditions. In the San Luis Valley canal sections on which measurements were made, the finer material had been removed from the top layer of the bed and a paving of coarser material was left. Between the larger particles, however, were found smaller ones; and even sand particles were present immediately under the top particles. It was hoped that substantially all of the material below a certain size would be found to have been removed from the bed so that this size could be used as an index of design, but this was found not to be the case; and no satisfactory analysis of the data based on a specific size left in the bed was found."

The fact that the armor layer is composed mainly of coarse material one particle diameter thick arranged in a shingled or imbricated manner, and that, between the larger particles, finer, sheltered particles are present such that all sizes present in the original bed are present in the

armor layer has been confirmed by subsequent studies from *GESSLER* (1965), *LITTLE AND MAYER* (1976) and *PROFFITT* (1980).

GESSLER (1965) made detailed observations and measurements during selective erosion from a non-uniform sediment bed under essentially constant hydraulic conditions. In the first phase of the experiments transverse gravel bars or ripples formed rapidly. These ripples formed simultaneously along the entire length of the channel. During this process the formation of the top layer was clearly observed. The larger stationary grains formed an identifiable layer that was only temporarily covered by the travelling ripples. This phase was concluded after the most upstream ripple had reached the channel end and the bed could be said to have been partially armored.

During the second phase of the experiment the sediment transport had already strongly died away, in that no more ripples were formed. The transport was now in the form of continuous motion of individual particles over the whole bed. At this stage a preferential orientation for the larger particles can be seen.

PROFFITT (1980) described continuous observations of the larger apparently stable particles. He observed that very few do not move at all while most show one or more quite pronounced movements. These may be a rotation to better align the long axis perpendicular to the flow, a tumbling over from a perched position as finer material is eroded from around the particle, or translation over a distance equivalent to many particle diameters. Typically the particle would arrive at its new location and disturb the finer material nearby, particularly that in its wake. Some would be removed but most would settle down again near the larger stone and aid in stabilizing it. Further stability was often achieved by a smaller stone lodging against its upstream face. This would reduce any flow under the larger stone and inhibit its further movement by acting as a physical restraint. These effects become more and more pronounced as armoring proceeds.

2.4 Prediction of the armor layer

GESSLER (1965) duplicated the conditions described by *LANE AND CARLSON* (1953) in an experimental study. Both studies clearly showed that there is no cutoff point at which all grains smaller are removed and that of prime importance is the stochastic nature of the flow and the exposed bed material.

Grain removal, for example, may occur by a vertical lift, sliding, rolling about a downstream particle, or by a combination of these mechanisms. The resistance offered to such removal is

determined primarily by grain weight. It will vary among particles of any given sieve fraction by virtue of small changes in particle size and density. Variations in shape can also influence interlocking and placement of particles. On the other side the particles comprising a particular sieve size, exposed to a turbulent flow, experience a wide range of applied stresses.

In Gessler's approach, an attempt was made to measure the probability that grains of a specific size will stay. The study was based upon measuring the grain size distribution of the eroded as well as the armor layer material. It was shown that this probability depends mainly upon the Shields parameter and slightly on the grain Reynolds number. In this case, the Shields diagram shown on Fig. 2.3 represents then the 50 percent curve for removal. The probability that a grain will stay depends on how large the mean bottom shear stress is relative to the critical shear stress of this grain. Gessler assumes that the probability function of the ratio τ_c/τ_b equals a Gaussian distribution with a mean value of μ=1, and a standard deviation of σ=0.57. In equation form this probability to remain as part of the top layer is

$$q = \frac{1}{\sigma\sqrt{2\pi}} \int_{-\infty}^{[\tau_c(d)/\tau_b]-1} \exp\left(-\frac{x^2}{2\sigma^2}\right) dx \qquad [2.8]$$

where q is the probability of non-removal, σ the standard deviation, $\tau_c(d)$ is the critical shear stress for grain size d (e.g. according to the Shields diagram Fig. 2.3), τ_b the mean bottom shear stress, and x the variable of integration. The value 0.57 for σ also accounts for what frequently is referred to as hiding. Fig. 2.4. shows schematically the meaning of Eq. 2.8 for a certain grain size d. For purpose of representation the dimensionless τ_{b*} is used instead of τ_b

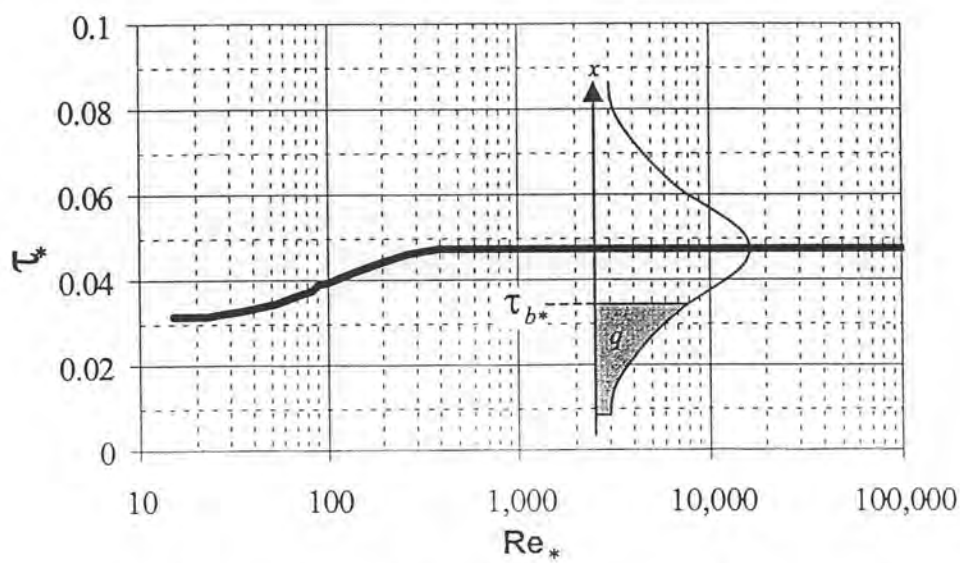

Fig. 2.4. Scheme of Gessler's probabilistic approach for armoring prediction

It is now possible to determine the grain size distribution of the armor layer as soon as the mean shear stress and the initial grain size distribution are given. The initial grain size distribution $P_0(d)$ is

$$P_0(d) = \int_{d_{\min}}^{d} p_0(d)\mathrm{d}d \qquad [2.9]$$

with $p_0(d)$ the frequency function of the initial grain size distribution.

Then for the armor layer the grain size distribution becomes

$$P_A(d) = \frac{\int_{d_{\min}}^{d} q p_0(d)\mathrm{d}d}{\int_{d_{\min}}^{d_{\max}} q p_0(d)\mathrm{d}d} \qquad [2.10]$$

where q varies with the grain size d.

If the probability of the largest grain to stay is high enough, only a certain amount of degradation is necessary to accumulate enough coarse material in the top layer to stabilize the bed. The amount of degradation required will be the same everywhere along the channel as long as the underlying material and the shear stress remain the same. Nevertheless, the shear stress at the beginning of the armoring process (e.g., in a new irrigation canal) could be so high that even the coarsest fraction of the bed material has a reasonably high probability to be moved. Under these conditions an armor layer develops, but it does not become strong enough to stabilize the bed.

GESSLER (1970) suggested that the mean value of the probabilities for the armor layer grains to stay should be a good indicator of bed stability

$$\overline{q} = \frac{\int_{d_{\min}}^{d_{\max}} q^2 p_0(d)\mathrm{d}d}{\int_{d_{\min}}^{d_{\max}} q p_0(d)\mathrm{d}d} \qquad [2.11]$$

in which p_0 is the density function of the initial grain size distribution, and q the probability of the grain size d not to be removed, as defined by Eq. 2.8.

For τ_b=0 the stability coefficient becomes $\overline{q}$=1. For $\tau_b \rightarrow \infty$ the stability coefficient approaches approximately 0.04. Based on field observations in the San Luis Valley and some limited laboratory results *GESSLER* (1970) indicates that a value of approximately $\overline{q}$=0.5 might describe the critical conditions. For $\overline{q} > 0.5$ minor degradation without slope adjustment would occur, while for $\overline{q} < 0.5$ the bed only could become stable after slope reduction. For purposes of design *GESSLER* (1970) recommended a stability coefficient of $\overline{q}$=0.65, which gives a factor of safety, in regard to shear stress, of approximately 1.3.

The main reason for introducing the stability coefficient was because it incorporates the stabilizing effect of all grain sizes and is not limited to one "characteristic" grain size like other investigators suggested. For example, *LANE* (1952) arbitrarily selected d_{75} (size for which 75 percent by weight of the material is finer) to describe the natural material. The d_{75} Lane used was from the initial substrate material (initial material in which the canal was constructed) and was plotted versus the shear stress of the maximum sustained flow. Lane stated his design criterion in words as follows:

"For ease in remembering this relation, it may be stated in English units as: the limiting tractive force in pounds per square foot recommended for design is equal to four-tenths of the particle size in inches of the sieve opening on which 25 percent of the weight of the natural bank material will be retained."

In metric units this criterion can be formulated as

$$\tau_d \cong 0.754 d_{75} \qquad [2.12]$$

where τ_d is the design shear stress in [N/m^2]; and d_{75} is the size for which 75 percent by weight is finer in [mm].

2.5 Friction factor

Objective prediction of the mean bottom shear stress in an armoring study in open channels is a matter of fundamental importance. Therefore, the effective hydraulic radius of the river bed has to be estimated.

The effects of bank friction on the mean bottom shear stress is considerable when width-to-depth ratios are less than about 10:1. In this case using depth of flow, or overall hydraulic radius in the computation can introduce substantial, systematic errors. Therefore, it is extremely important to correct for the bank effects on the bottom shear stress. The correction is based on

the procedure suggested by *EINSTEIN* (1942), assuming that the cross-sectional area can be divided into three subareas, as illustrated in Fig. 2.5.

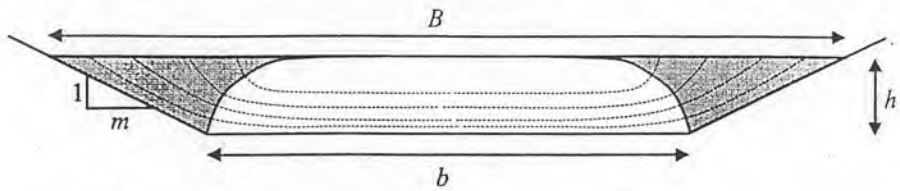

Fig. 2.5. Division in subareas of a trapezoidal cross section

Further it is assumed that each subarea corresponding to a particular section of the wetted perimeter has the same friction slope and the same mean flow velocity. The latter assumption is somewhat questionable, because in nature the velocity in the section over the bed is higher than in the bank subareas. However, it has been proved that the assumption is reasonable.

Resistance to flow is analyzed in terms of the Darcy-Weisbach friction factor. Most existing relationships for grain resistance to flow in gravel-bed channels are based on the friction factor for hydraulically rough boundary like the relationship proposed by *KEULEGAN* (1938) for the case of uniform, fixed roughness:

$$f = \left[2.21 + 2.03 \log\left(\frac{R}{k_s} \right) \right]^{-2} \qquad [2.13]$$

where f is the average friction factor, R the hydraulic radius, and k_s the controlling roughness. The controlling roughness is associated to the coarser fractions of the bed grain size distribution. This relationship is used to determine the friction factor for the banks, f_s. It will be necessary to estimate the absolute roughness of the banks by a characteristic coarse grain size, in this case d_{90}.

For the evaluation of the bottom friction factor f_b the following method developed by *GESSLER* (1990) for armored river beds has been used. He found in a review of previous work of *PROFFITT* (1980), *LITTLE AND MAYER* (1976) and *GESSLER* (1965) that the use of the maximum grain size as the controlling roughness is in many cases not adequate. He suggests that the controlling roughness of an armor layer, developed from an initial mixture, to be a function of the mean bottom shear stress to which the mixture was exposed, and that formed the armor layer.

Therefore, in some cases the controlling roughness can be less than the maximum grain size, and in others even become coarser than the maximum grain size. For grain Reynolds numbers above 150-200 this results in the following dimensionless relationship:

$$\tau_* = \frac{\tau_b}{(\gamma_s - \gamma)k_s} = \frac{\gamma R_b S}{(\gamma_s - \gamma)k_s} = \text{constant} \qquad [2.14]$$

where τ_* is the dimensionless shear stress or Shield parameter, τ_b the mean bottom shear stress, γ_s the specific weight of the sediment, γ the specific weight of the fluid, k_s the controlling roughness height, R_b the hydraulic radius of the bed, and S the slope.

The constant was determined from laboratory data reported by *GESSLER* (1965), *PROFFITT* (1980), and *LITTLE AND MAYER* (1976) and found to be 0.0155. If one combines this value with Eq. 2.13 one obtains

$$f_b = \left[2.21 + 2.03\log\left(\frac{0.0155(\gamma_s - \gamma)}{S\gamma}\right)\right]^{-2} \qquad [2.15]$$

It indicates that due to the process that forms the armor layer, the controlling roughness is independent of the maximum grain size, at least as long as one deals with reasonable grain size distributions. Because a Shields parameter controls the friction factor, the specific gravity of the sediment is another controlling factor. If one assumes a specific gravity of the sediment of 2.65, Eq. 2.15 becomes (after slight modification of the numeric value in the argument of the logarithm for the purpose of best fit)

$$f_b = \left[2.21 + 2.03\log\left(\frac{0.0251}{S}\right)\right]^{-2} \qquad [2.16]$$

If one now applies Darcy-Weisbach's flow equation to each cross-sectional subarea as shown on Fig 2.5, as well as the entire cross section, it leads to the following set of equations:

$$\left.\begin{aligned} U^2 &= \frac{8g}{f_s} R_s S \\ U^2 &= \frac{8g}{f_b} R_b S \\ U^2 &= \frac{8g}{f} RS \end{aligned}\right\} \text{Flow equations} \qquad [2.17]$$

$$\left.\begin{aligned} f_s &= \left[2.21 + 2.03\log\left(\frac{R_s}{k_s}\right)\right]^{-2} \\ f_b &= \left[2.21 + 2.03\log\left(\frac{0.0251}{S}\right)\right]^{-2} \end{aligned}\right\} \text{Friction factor relationships} \qquad [2.18]$$

$$\left.\begin{aligned} R_s &= \frac{A_s}{P_s} \\ R_b &= \frac{A_b}{P_b} \\ R &= \frac{A}{P} \end{aligned}\right\} \text{Hydraulic radius relationships} \qquad [2.19]$$

$$\left.\begin{aligned} P_b &= b \\ P_s &= h\sqrt{1+m^2} \\ P &= P_b + 2P_s \end{aligned}\right\} \text{Wetted perimeter relationships} \qquad [2.20]$$

$$\left.\begin{aligned} A &= h(b+mh) \\ A &= A_b + 2A_s \end{aligned}\right\} \text{Area relationships} \qquad [2.21]$$

$$\left.\begin{aligned} U &= \frac{Q}{A} \\ U &= U_b = U_s \end{aligned}\right\} \text{Velocity relationships} \qquad [2.22]$$

where U is the average flow velocity, f_s the friction factor of the banks, f_b the friction factor of the bed, f the average friction factor, R_s the hydraulic radius for the banks, R_b the hydraulic radius of the bed, R the overall hydraulic radius, g the acceleration due to gravity, S the slope of energy grade line, k_s the controlling roughness for the bank, P_s the wetted perimeter of the banks, P_b the wetted perimeter of the bed, P the overall wetted perimeter, A_s the area of the bank subarea, A_b the area of the bed subarea, A the total cross-sectional area, b the bottom width of the channel, h the depth of flow, m the bank slope (mH:1V), and Q the discharge.

Eqs. [2.17]-[2.22] can be resolved simultaneously to predict the hydraulic radius of the bed R_b for a given discharge, energy grade line slope, controlling bank roughness, bottom width and bank slope. With the hydraulic radius of the bed, the mean bottom shear stress can be determined using Eq. 2.5.

3 Field studies and data collection

3.1 Data collected by Lane and Carlson 1950-1953

During the years from 1950-1953, studies on 18 test sections in the San Luis Valley were made by the personnel of the Bureau of Reclamation under the direction of E. W. Lane and E. J. Carlson. Hydraulic measurements including velocity distributions, energy slope and discharge were made. A summary of the available measured hydraulic data for 15 of the reported 18 test sections is presented in Tab. 3.1.

These measurements were carried out very carefully and can therefore be considered sufficiently accurate and form the reference for all further developments.

ID	d_{50}	1950 measurements						1952 measurements						Q_{max}
		Q	U	S	h	B	n	Q	U	S	h	B	n	
[-]	[mm]	[m³/s]	[m/s]	[%]	[m]	[m]	[s/m^1/3]	[m³/s]	[m/s]	[%]	[m]	[m]	[s/m^1/3]	[m³/s]
(1)	(2)	(3)	(4)	(5)	(6)	(7)	(8)	(9)	(10)	(11)	(12)	(13)	(14)	(15)
1	82	26.73	1.46	0.271	1.25	20.12	0.033	42.48	1.79	0.280	1.48	22.25	0.031	42.48
2	77	10.36	1.19	0.375	0.74	15.85	0.036	18.92	1.78	0.376	0.86	16.76	0.027	20.64
4	76	12.91	1.42	0.362	0.82	14.33	0.032	21.75	1.99	0.359	0.95	14.63	0.025	21.75
5	54	8.18	1.33	0.371	0.69	11.28	0.030	12.69	1.77	0.368	0.76	12.19	0.026	12.69
6	42	2.86	1.09	0.299	0.49	6.37	0.027	4.50	1.40	0.295	0.57	6.61	0.022	4.50
7	41	1.16	0.84	0.290	0.39	4.51	0.029	2.71	1.33	0.290	0.53	4.85	0.022	2.71
8	39	0.31	0.41	0.319	0.17	5.49	0.036	1.30	0.91	0.316	0.29	5.85	0.024	1.30
10	64	0.22	0.46	0.973	0.16	3.26	0.059	0.47	0.88	0.965	0.18	3.38	0.031	0.47
11	48	3.53	0.83	0.213	0.52	9.72	0.030	5.75	1.18	0.235	0.57	9.85	0.025	5.75
12	34	2.80	1.08	0.240	0.49	6.55	0.024	3.62	1.22	0.243	0.54	6.68	0.023	3.82
14	20	1.83	0.78	0.126	0.48	6.28	0.024	3.11	1.00	0.136	0.61	6.52	0.022	3.60
15	50	5.69	1.11	0.194	0.67	10.70	0.025	13.51	1.48	0.199	0.93	12.01	0.026	14.20
16	49	5.49	1.06	0.202	0.55	10.30	0.024	No data taken						14.61
17	38	5.58	1.12	0.267	0.49	11.28	0.026	15.04	1.68	0.274	0.79	12.50	0.024	15.04
18	21	1.77	0.67	0.083	0.52	6.10	0.021	6.65	1.16	0.080	0.90	7.62	0.018	7.87

Tab. 3.1. Data collected by Lane and Carlson 1950-1953

d_{50} is the mean grain diameter of the surface material, Q the discharge, U the average flow velocity, S the energy slope, h the mean depth of flow, B the top width, n Manning's coefficient, and Q_{max} the maximum sustained discharge.

3.2 Selection of the test sections for reinvestigation

For the selection of the test sections to be reinvestigated, the available data from Lane and Carlson was analyzed in regards to the dimensionless shear stresses. Unfortunately, no data concerning the cross sectional area A or the hydraulic radius R of the canals was available, but Lane and Carlson measured these quantities with the intent to determine the average Manning coefficient n for each section (see Tab. 3.1). Therefore, to get an estimation of the missing data a back-calculation was performed, based on the results given in Lane and Carlson's report. To effectuate these computations, the assumption of a trapezoidal cross-sectional geometry as shown in Fig. 3.1 had to be made.

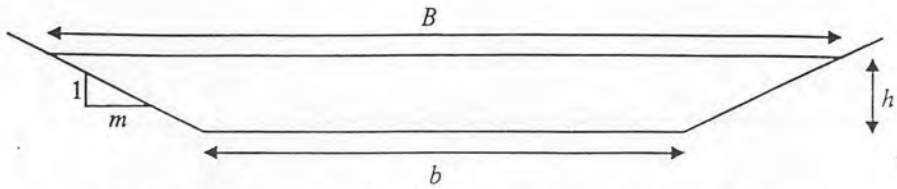

Fig. 3.1. Scheme of trapezoidal cross section

In this case the cross-sectional area A_c can be calculated by

$$A_c = (b + mh)h \qquad [3.1]$$

where $b=B-2mh$ is the bottom width, h the average flow depth, and m the bank slope. The overall hydraulic radius R can then be determined by

$$R = \frac{(b + mh)h}{b + 2h\sqrt{1 + m^2}} \qquad [3.2]$$

Using Manning-Strickler's formula

$$Q = A_c \frac{1}{n} R^{2/3} S^{1/2} \qquad [3.3]$$

the theoretical geometry of the canals (m, A, and R) was then determined with the depth h, the top width B, Manning's coefficient n and the discharge Q of the 1950 and 1952 measurements. The "calculated" area A_c was then compared to the "measured" area A_m defined as

$$A_m = Q / U \qquad [3.4]$$

where U is the measured average flow velocity, and Q the measured discharge.

The results of these computations and the comparison of the ratios A_c/A_m, the ratios R/h, and the m ratios of the 1950 and 1952 measurements showed little variation for most of the canals as can be seen in Tab. 3.2. The R/h ratio (14) and the m ratio (15) have been calculated by dividing columns (7)/(13) and (2)/(8). The results have been classified in regards to their variations (5 and 20%).

ID	1950 measurements						1952 measurements							
	m	R	A_c	A_m	A_c/A_m	R/h	m	R	A_c	A_m	A_c/A_m	R/h	R/h ratio	m ratio
[-]	[-]	[m]	[m^2]	[m^2]	[-]	[-]	[-]	[m]	[m^2]	[m^2]	[-]	[-]	[-]	[-]
(1)	(2)	(3)	(4)	(5)	(6)	(7)	(8)	(9)	(10)	(11)	(12)	(13)	(14)	(15)
1	4.4	0.89	18.22	18.27	**1.00**	0.72	3.9	1.08	24.34	23.70	**1.03**	0.72	**0.99**	***1.12***
2	4.3	0.59	9.40	8.70	***1.08***	0.79	3.5	0.69	11.77	10.64	***1.11***	0.81	**0.98**	***1.20***
4	3.2	0.65	9.54	9.11	**1.05**	0.80	2.8	0.76	11.32	10.93	**1.04**	0.80	**1.00**	***1.14***
5	3.5	0.53	6.07	6.16	**0.99**	0.77	1.6	0.66	8.38	7.15	***1.17***	0.87	***0.89***	2.24
6	2.2	0.39	2.59	2.63	**0.99**	0.80	2.7	0.43	2.91	3.22	***0.90***	0.74	***1.08***	***0.83***
7	2.2	0.31	1.44	1.37	**1.05**	0.78	1.8	0.40	2.05	2.04	**1.00**	0.76	**1.03**	***1.19***
8	7.0	0.13	0.73	0.76	**0.96**	0.78	3.1	0.24	1.45	1.42	**1.02**	0.83	***0.93***	2.29
10	2.2	0.15	0.45	0.46	**0.98**	0.94	3.4	0.15	0.51	0.53	**0.95**	0.81	***1.16***	0.65
11	4.3	0.39	3.87	4.27	***0.91***	0.76	2.6	0.48	4.79	4.86	**0.99**	0.83	***0.92***	1.65
12	2.7	0.38	2.58	2.61	**0.99**	0.78	2.2	0.43	2.96	2.97	**1.00**	0.80	**0.98**	***1.20***
14	2.4	0.38	2.48	2.35	***1.06***	0.79	2.3	0.46	3.14	3.11	**1.01**	0.76	**1.04**	***1.06***
15	3.8	0.50	5.45	5.12	***1.07***	0.75	1.2	0.80	10.10	9.16	***1.10***	0.86	***0.87***	3.11
16	4.2	0.42	4.43	5.19	***0.85***	0.77	No data taken						-	-
17	2.7	0.42	4.86	4.97	**0.98**	0.87	1.9	0.68	8.71	8.95	**0.97**	0.85	**1.02**	1.42
18	3.8	0.34	2.14	2.63	***0.82***	0.66	2.2	0.63	5.07	5.75	***0.88***	0.71	***0.93***	1.75

Note: Accuracy of data: **within 5%**; ***within 20%***;

Tab. 3.2. Geometric analysis of data collected by Lane and Carlson 1950-1953

The hydraulic radius calculated for the higher 1952 discharges was used to determine the dimensionless shear stresses for the given d_{50} and the grain Reynolds number. These results have been plotted together with the Shields diagram in Fig. 3.2 to get an idea of the criticality concerning the shear stresses for the different test sections.

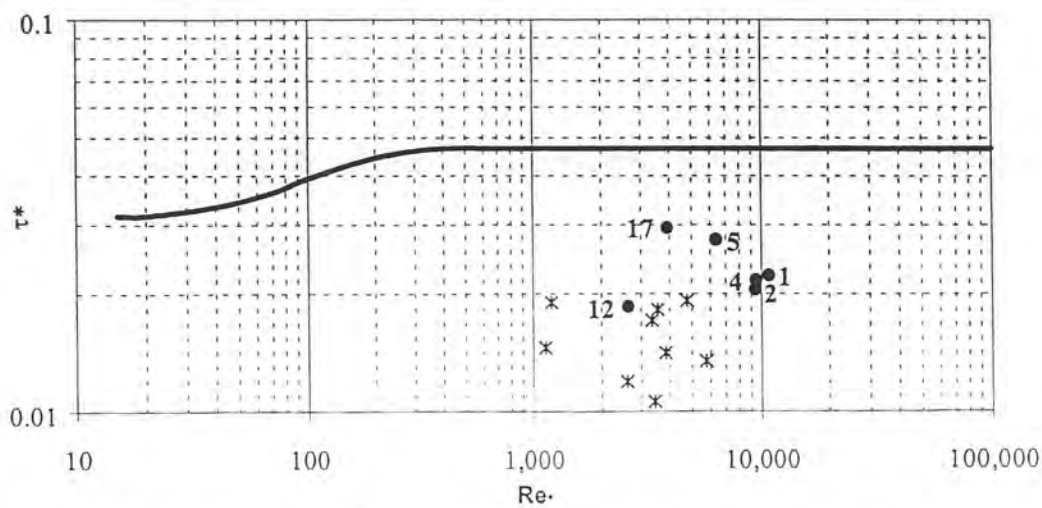

Fig. 3.2. Shields diagram with computed dimensionless shear stresses

A reconnaissance field trip was then made to the San Luis Valley to get a visual idea of the locations and the actual state of the different test sections. It was found that they still are especially good for measurement, in that the sections are straight, the cross sections uniform, as can be recognized on the photographs in Appendix II (Fig. II.4-II.10).

The primary requirements that determined the choice of the canal reaches were the value of the dimensionless shear stress, as well as the consistency of the geometric computations. Six test sections were then selected on canals and laterals of varying slopes, cross sections, and discharges. They cover the Rio Grande Main and Lateral #1 Canal, the Farmers Union Main Canal as well as the Prairie Ditch Main Canal. Referring to the test sections determined by Lane and Carlson (see Fig. 1.2) they were located at test section 1, 2, 4, 5, 12 and 17. Test section 12 has been chosen because this section was used by *GESSLER* (1965) to apply his theory about armoring computations. An exact description of location of the different test sections can be found in Appendix V.

The data, as well as some characteristic hydraulic values of the retained test sections together with the other test sections are summarized on Tab. 3.3.

ID	d_{50}	Q_{max}	Q	U	h	S	R	h/d_{50}	τ_0	τ_*	u_*	Re_*
[-]	[mm]	[m³/s]	[m³/s]	[m/s]	[m]	[%]	[m]	[-]	[N/m²]	[-]	[m/s]	[-]
(1)	(2)	(3)	(4)	(5)	(6)	(7)	(8)	(9)	(10)	(11)	(12)	(13)
1	82	42.48	42.48	1.79	1.48	0.280	1.08	18.1	29.55	0.0223	0.17	10,766
2	77	20.64	18.92	1.78	0.86	0.376	0.69	11.1	25.53	0.0205	0.16	9,387
4	76	21.75	21.75	1.99	0.95	0.359	0.76	12.5	26.65	0.0217	0.16	9,465
5	54	12.69	12.69	1.77	0.76	0.368	0.66	14.2	23.93	0.0275	0.15	6,359
6	42	4.50	4.50	1.40	0.57	0.295	0.43	13.7	12.35	0.0182	0.11	3,555
7	41	2.71	2.71	1.33	0.53	0.290	0.40	12.8	11.38	0.0171	0.11	3,351
8	39	1.30	1.30	0.91	0.29	0.316	0.24	7.5	7.56	0.0119	0.09	2,597
10	64	0.47	0.47	0.88	0.18	0.965	0.15	2.9	13.95	0.0135	0.12	5,770
11	48	5.75	5.75	1.18	0.57	0.235	0.48	11.9	10.98	0.0141	0.10	3,840
12	34	3.81	3.62	1.22	0.54	0.243	0.43	15.9	10.23	0.0186	0.10	2,628
14	20	3.60	3.11	1.00	0.61	0.126	0.46	30.4	5.72	0.0176	0.08	1,158
15	50	14.16	13.51	1.48	0.93	0.199	0.80	18.6	15.56	0.0192	0.12	4,765
16	49	14.61	5.49	1.06	0.55	0.202	0.42	11.3	8.41	0.0106	0.09	3,432
17	38	15.04	15.04	1.68	0.79	0.274	0.68	20.8	18.16	0.0295	0.13	3,920
18	21	7.87	6.65	1.16	0.90	0.080	0.63	42.5	4.97	0.0146	0.07	1,134

Note: $\rho = 2.65\times10^3$ kg/m³; $\nu = 1.31\times10^{-6}$ m²/s (T = 10°C); Selected test sections.

Tab. 3.3. Summary of some characteristic quantities of the test sections

3.3 Test measurements in the Cache la Poudre River

Prior to sampling at the San Luis Valley, a test sampling was conducted on the Poudre River, near Fort Collins, Colorado. The idea was to get familiarized with the sampling concepts and to compare the results of different sampling methods.

A dry bank of the Poudre River (about 100 m upstream of crossing with Shields Avenue) north-west of Fort Collins was selected to effectuate the test measurements. An area-by-weight and a transect-by-number sample was obtained from two spots (upstream and downstream) on the test site. The test site and the field procedures are documented photographically in Appendix II (Fig. II.11-II.13).

For the area-by-weight sample the sampling area was 1 m^2 and has been spray-painted to distinguish the surface layer from the substrate material. The painted stones, typically 800-1000, rocks were removed. The size analysis of the top layer for each test area was determined by sieving to yield area-by-weight grain size distributions. A template containing the openings of common large sieve sizes was used to aid in classifying the particles in terms of size.

For the transect-by-number sample all rocks falling under a straight line (wire) along the sampling line constituted the sample. To ensure that the sample was representative a sample size of minimum 150 stones was taken. The transect-by-number samples, were placed adjacent to the areal samples, were approximately 5 m long and directed in river flow direction. A handmade caliper was used to measure the intermediate *b*-axis of each particle once it was removed from the bed. When large particles, which could not be removed from the bed, were encountered, the minor exposed axes was admitted to be the *b*-axis of the particle, and was measured in place.

While it is true that particles in the small size range (<10 mm) can be picked up by hand, their proportion in a transect-by-number sample may not accurately reflect their presence in the channel bed. In an armored channel bed their occurrence should be negligible, therefore the fraction of all the particles smaller than 10 mm was admitted to be 0 %. To get a more representative grain size distribution the data for both samples was then added together, so a mean grain size distribution for both samples was obtained.

The grain size distribution curves obtained by the transect-by-number method were calibrated to an area-by-weight sample by the method proposed by *KELLERHALS AND BRAY* (1971) and *FEHR* (1986), as described in Appendix I. The data has been analyzed by a least square analysis of the exponent to determine the best fitting functional relationship between the transect-by-

number and the area-by-weight sample. For the transect-by-number sample a conversion exponent of x=1.7 was found.

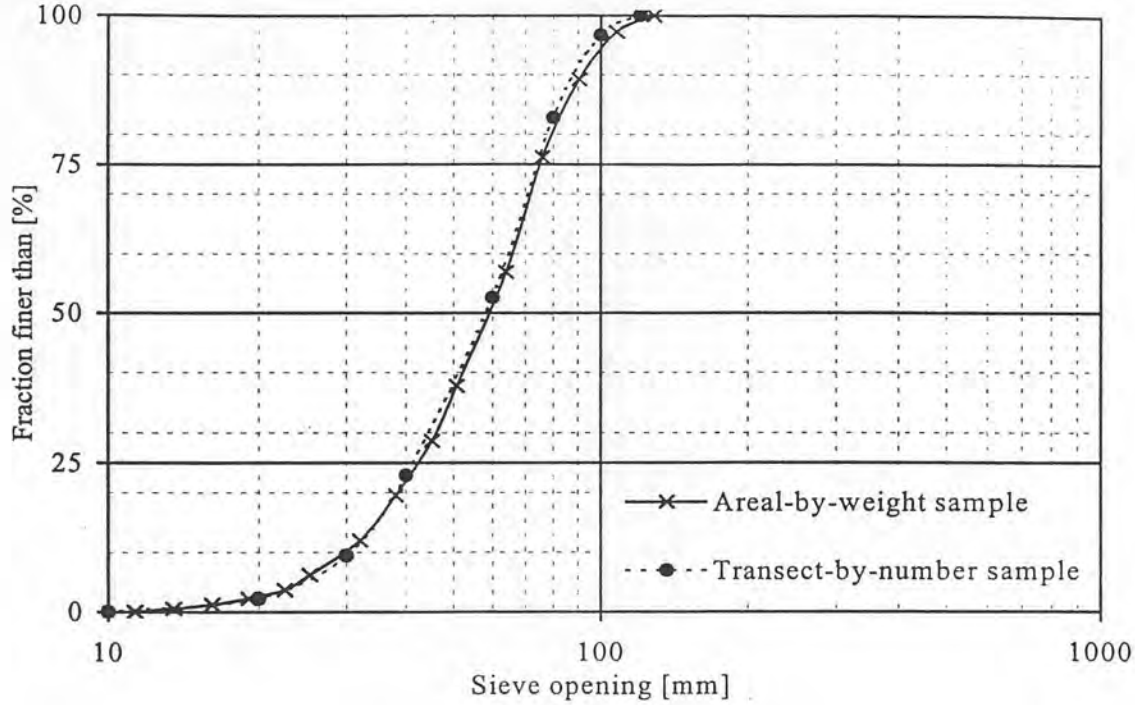

Fig. 3.3. Mean grain size distribution curves of Poudre River test measurements

The comparison of the results on Fig. 3.3 shows that the transect-by-number method gives quite a similar grain size distribution as the area-by-weight sample. Yet, the amount of time for processing a transect-by-number sample is about 5 times smaller than it is for an area-by-weight sample, and, therefore, more samples can be taken for an equal amount of time. If several samples have been collected, the mean can be used which should guarantee an even more reliable and representative sample. In a very coarse channel bed one can even imagine that the sample taken by the transect-by-number method will be more representative than a 1 m^2 area-by-weight sample. First, because with a maximum grain size of 250 mm an area of 1 m^2 seems to be too small, and secondly, the transect sample in this case will have a length of more than 10 m which would allow averaging of small channel bed irregularities. For these reasons it can be admitted that with the transect-by-number method one achieves at least the same accuracy as with an 1 m^2 area-by-weight sample. Although, because the top layer of the irrigation canals in the San Luis Valley is of different nature and fluvial morphology, it is recommended that some more comparisons be completed to confirm the results of the Poudre measurements.

The test measurements in the Poudre River also allowed optimization of the sampling procedure. First, it was found to be more efficient to use a template with the common sieve sizes than a caliper, at least for the sizes smaller than 152 mm. And secondly, the size classes of the transect-by-number method should likely be changed so that they are equivalent to the common sieve sizes to make comparison more feasible.

3.4 Hydraulic measurements in the San Luis Valley

A knowledge of the maximum sustained flows at the test sections is necessary to compute the shear stresses which produced the existing armor layer. For an approximate solution, a best estimate of this maximum discharge for each test section since the canals were constructed, is needed.

Discharge records are available on these canals over the last 90 years only at the intakes from the Rio Grande River. These data are collected by the Water Commissioners in connection with the supervision of the use of the water of this stream for irrigation. From these records of the Water Division's office in Alamosa and the Superintendent's of the irrigation companies the largest daily, weekly, and monthly average flow at the intakes of the canals since the early 1900's was determined. The values with the corresponding year of occurrence is shown on Tab. 3.4. In general there have been slightly higher discharges since the 1950 and 1952 measurements.

ID [-] (1)	Canal [-] (2)	Daily [m^3/s] (year) (3)	Weekly [m^3/s] (year) (4)	Monthly [m^3/s] (year) (5)
1	Rio Grande Main	50.18 m^3/s (1965)	49.62 m^3/s (1965)	46.77 m^3/s (1965)
2	Rio Grande Main		No records available	
4	Rio Grande Lateral #1		No records available	
5	Rio Grande Lateral #1		No records available	
12	Prairie Ditch	10.99 m^3/s (1979)	9.89 m^3/s (1979)	8.10 m^3/s (1979)
17	Farmers Union	24.41 m^3/s (1975)	22.83 m^3/s (1980)	19.23 m^3/s (1979)

Tab. 3.4. Sustained maximum discharges at the intakes of the canals from the Rio Grande River

For the determination of the sustained maximum discharge at the cross sections, the maximum weekly average discharge has been retained. This discharge was considered to occur often enough to form the existing canal bed and to be sufficiently representative.

In the 1950-1953 study, the measurement of the discharge in the test sections was investigated very carefully and the measurements at the intakes corrected by extraction of the flows to the several farm, and lateral turnouts. In some cases the discharge has even been measured with a current meter within the reach of canal or lateral being studied. So, the data reported in the 1950-1953 study, shown on Tab. 3.1, can be considered to be reliable and be used as a reference for further maximum discharge determinations.

For the higher discharges since the 1950's it is assumed that corrections for losses or gains from seepage and turnouts between the measuring stations at the canal intakes and the observation sections, are in the same proportions as in the 1950's and 1952's. As there do not exist any major diversions upstream of test sections 1, 12 and 17 these assumptions are justified. Unfortunately, the data available for test section 17 covers only one value, so it has to be assumed that losses of 18 % are reasonable. For test section 12, the 1952 measurements at the intake seemed to be unreal, or major losses have occurred between the intake and the test section; therefore a value of 44 % was assumed. But for test sections 1, 4, and 5 the proportions of intake and cross section measurement are quite consistent. For test section 2 the percentage corresponding to the higher discharge in the 1952 measurement was retained. With these assumptions it was possible to arrive at a reasonably close estimate of the maximum sustained flow at the experimental sections for the period of 1950-1997. Tab. 3.5 resumes these calculations for the six test sections.

ID	1950 measurements			1952 measurements			Sustained max discharge	Comparison with Report**
	Intakes*	Report**		Intakes*	Report**			
[-]	[m³/s]	[m³/s]	[%]	[m³/s]	[m³/s]	[%]	[m³/s]	[%]
(1)	(2)	(3)	(4)	(5)	(6)	(7)	(8)	(9)
1	29.73	25.73	86.5	48.42	42.48	87.7	43.17 (87 %)	+ 1.6 %
2	No data	10.36	34.8	No data	20.64	42.6	20.84 (42 %)	+ 0.1 %
4	No data	12.91	43.4	No data	21.75	44.9	21.83 (44 %)	+ 0.0 %
5	No data	8.18	27.5	No data	12.69	26.2	13.40 (27 %)	+ 5.6 %
12	3.37	2.80	83.1	8.61	3.82	44.4	4.35 (44 %)	+ 13.9 %
17	No data	5.58	-	18.26	15.04	82.4	18.72 (82 %)	+ 24.5 %

Note: *Measurements at intakes of Rio Grande River; **Measurements of Lane and Carlson.

Tab. 3.5. Determination of the sustained maximum discharge in the test sections

It can be noted that for test sections 1, 2, and 4 the differences between measured values of the discharge in the 1950's and the determined discharge based on the records are negligible. For test sections 5, 12, and 17 this is not the case. Even if the method of determination of these values is not very accurate, it should be taken in consideration that the sustained maximum discharge in these reaches could have been augmented. In these cases the computations of the armoring process will permit further conclusions about the probable maximum discharge.

Because of the current groundwater recharge program in the fall of 1998, the canals were conveying water until the middle of December. So, an opportunity was offered to make certain flow measurements in test sections 1, 2, 12, and 17 to complete the studies in the selected reaches. (Test sections 4 and 5 were already dry!) In the most regular portions of these reaches the assumption of uniform flow conditions was made and therefore, the slope of energy could be measured by topographic survey. A level measuring instrument was used to determine the exact elevation of the water surface. The slope on the water surface in the test sections was determined by leveling in 7.5 m steps over a distance of 60 m in the test reach. The rod was held on the water surface on the side of the canal. The slope was determined by a least square adjustment of the measured values. The instantaneous discharge was determined either by an existing rating station or by a current meter measurement (USGS 0.6-method). The results of these measurements are shown on Fig. 3.4. and summarized in Tab. 3.6, where r^2 is the regression coefficient.

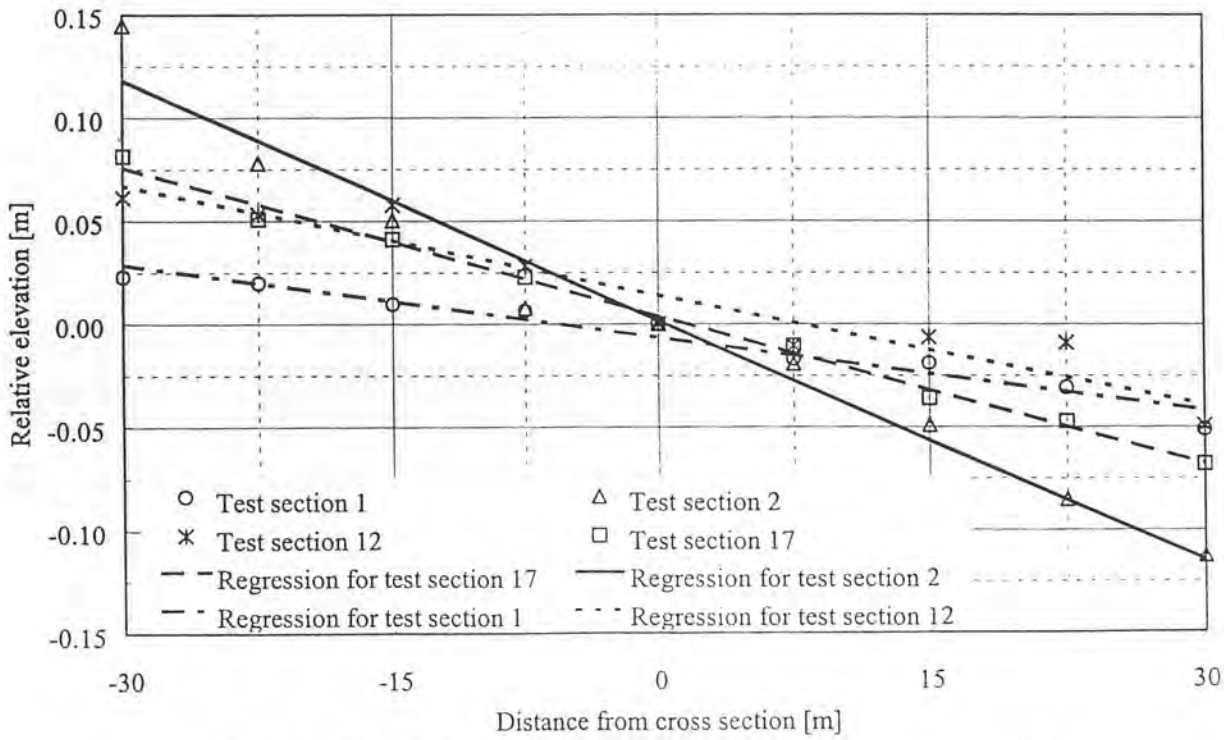

Fig. 3.4. Slope of energy measurements with linear regression

It is important to note that for test sections 1, 12, and 17 the measured discharge was only approximately 1/10 of the discharge in 1952. Therefore, the flow depth was about 0.20-0.25 m for test sections 1, 2, and 17, and only 0.13 m for test section 12. These shallow depths explain the significant difference in the slope measurements of test section 1 and 12, because small irregularities in the canal bed can effect the water surface significantly. In test section 2 the discharge was about 1/5 of the measured discharge in 1952 and the results are more consistent. An important remark concerning the slope measurements is that a distance of 60 m for such little slopes is obviously too short. But unfortunately, the level instrument did not permit making accurate readings for distances more than 15 m.

	Measurements 1998			Measurements 1952		
ID	Q	S	r^2	Q	S	$\Delta\%$
[-]	[m^3/s]	[%]	[-]	[m^3/s]	[%]	[%]
(1)	(2)	(3)	(4)	(5)	(6)	(7)
1	3.79	0.118	0.954	42.48	0.280	-57.9
2	3.37	0.388	0.970	18.92	0.376	3.2
12	0.39	0.177	0.908	3.62	0.243	-27.2
17	1.40	0.240	0.993	15.04	0.274	-12.4

Tab. 3.6. Summary and comparison of slope of energy measurements

For the further computations it is admitted that the slope has not changed in the past 50 years, which is correct if a parallel degradation of the canal bed is assumed. Therefore the slope measurements effectuated in the study of 1950-1952 are considered to be sufficiently reliable and accurate for the purpose of this study.

3.5 Survey measurements in the San Luis Valley

Complete cross sections were taken in reach 2 and 17 when the canals were dry. The data are plotted in Fig. 3.5. It can be noted that the cross sections are quite regular and the assumption of a trapezoidal section is justified.

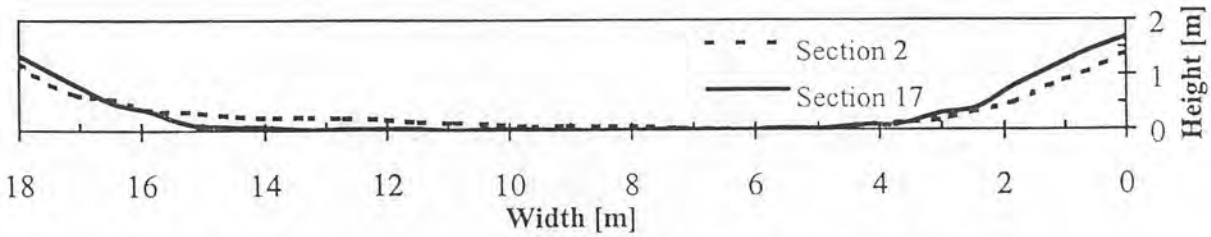

Fig. 3.5. Complete cross sections of the test sections 2 and 17

From every test reach the bottom bed width b and the bank slope m was determined on five cross sections over a distance of 250 m. From the measured values the mean was taken and a standard deviation based on the variation of the measured values was estimated. The bank roughness, d_{90} was determined by visual estimation. The retained values for further computations are summarized on Tab. 3.7.

ID [-] (1)	b [m] (2)	σ_b [m] (3)	m [-] (4)	σ_m [-] (5)	d_{90bank} [mm] (6)
1	12.7	0.3	2.4	0.15	200
2	13.6	0.5	2.0	0.20	300
4	9.2	0.4	2.3	0.10	200
5	8.0	0.3	2.3	0.10	250
12	5.9	0.8	1.5	0.15	30
17	11.6	0.2	2.0	0.10	60

Tab. 3.7. Summary of geometric measurements of the test sections

3.6 Fluvial morphologic measurements in the San Luis Valley

In test section 2, 2 area-by-weight samples and 4 transect-by-number samples were taken to again compare the results of the different sampling methods. In test section 17, 1 area-by-weight sample and 2 transect-by-number samples were collected to have a data set with finer material. A rigid frame, constructed of 1" x 2" redwood, was placed on the river bed and the inside area was spray-painted. The mean of the 2 corresponding transect-by-number samples was then taken. The least square analysis confirmed the choice of the exponent to be x=1.7. The 3 data sets (3 area-by-weight and 3 transect-by-number) are represented on Fig. 3.6.

As can be noted on Fig. 3.6 the adapted transect-by-number method represents the area-by-weight samples very well. For the 2 area-by-weight samples of test section 2 there is a significant differences in the mid-grain sizes. However, the transect-by-number samples differ much less and show remarkably that the transect-by-number method might be even more reliable and representative, because of the "longer" sample size.

Several transect-by-number samples in test sections 1, 4, 5, and 12 were then taken and averaged. The resulting grain size distribution curves are represented in Fig. 3.7. The retained surface layer grain size distribution curves are also summarized in Tab. 3.8, whereas for test section 2 the average of the upstream and downstream test sites was taken.

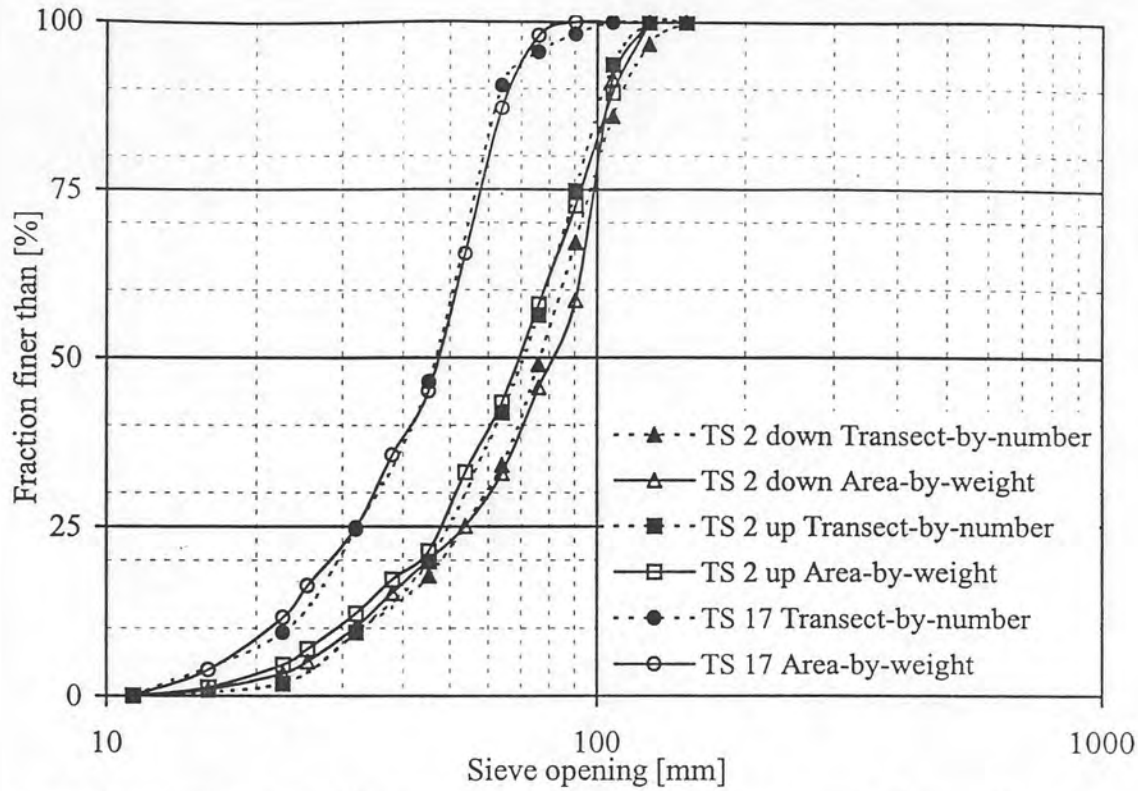

Fig. 3.6. Comparison of transect-by-number and area-by-weight samples for test sections 2 and 17

d_i [mm] (1)	Σp_i^A TS 1 [%] (2)	TS 2 [%] (3)	TS 4 [%] (4)	TS 5 [%] (5)	TS 12 [%] (6)	TS 17 [%] (7)
215.3	100.0	100.0	100.0	100.0	100.0	100.0
181.0	92.6	100.0	100.0	100.0	100.0	100.0
152.2	84.3	100.0	100.0	100.0	100.0	100.0
128.0	78.1	98.7	93.7	97.0	100.0	100.0
107.6	65.9	90.6	79.5	93.6	100.0	100.0
90.5	51.0	71.7	58.3	82.7	97.8	98.2
76.1	31.5	53.4	46.5	70.1	96.1	95.5
64.0	24.5	38.8	35.8	54.7	90.0	90.4
45.3	10.7	19.0	16.3	29.0	63.9	46.4
32.0	4.1	9.4	7.0	13.7	40.0	24.6
22.6	1.6	1.8	2.3	4.5	19.1	9.4
11.3	-	-	-	-	-	-

Tab. 3.8. Retained area-by-weight grain size distribution curves

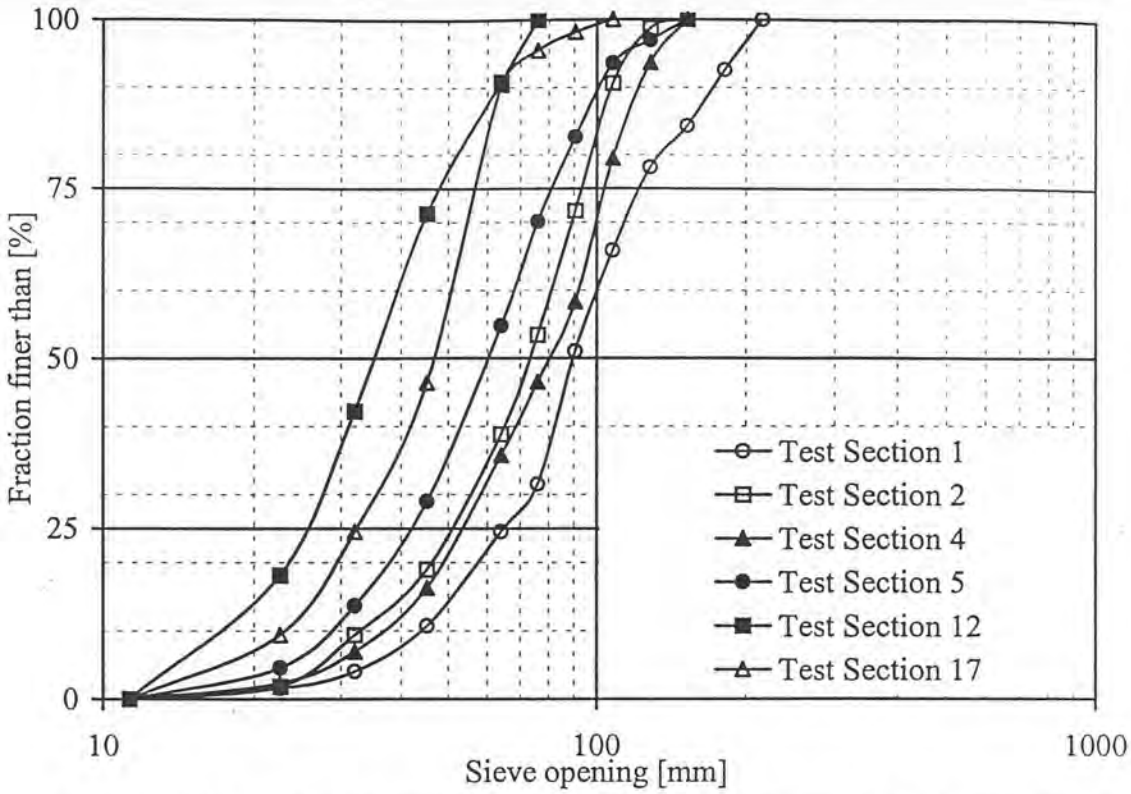

Fig. 3.7. Retained area-by-weight grain size distributions of all the test sections

Because of the frozen ground and the limited amount of time available it was not possible to get any new data concerning the grain size distribution of the initial substrate material. But as the canals are assumed to be stable, the initial substrate material should not have changed during the last 50 years.

In the 1950's, samples of the initial substrate material, approximately 150 kilos each, were collected. The sample size was determined by the amount of material that could practically be extracted and transported from the sampling site. This sample size seems to be too small for the coarser test sections, and therefore, the grain size distribution curves have to be considered prudently, and a considerable variation might be possible.

The maximum sieve size in the report of *LANE AND CARLSON* (1953) was 76.1 mm which for certain test sections was much too small, and the limits of the size fractions published in the report formed geometric series with a factor 2. For the use of these initial substrate material distributions for an armoring prediction, the missing size fractions was completed by fractions formed of geometric series with a factor of $\sqrt[4]{2}$ up to the maximum grain size found with the area samples. This completion of the grain size distributions introduces an uncertainty, which is difficult to quantify.

However, the armoring computation will give further information about the sensitivity of the computations to errors in the initial substrate material. The initial substrate material grain size distribution curves are represented in Fig. 3.8 and summarized in Appendix VI.

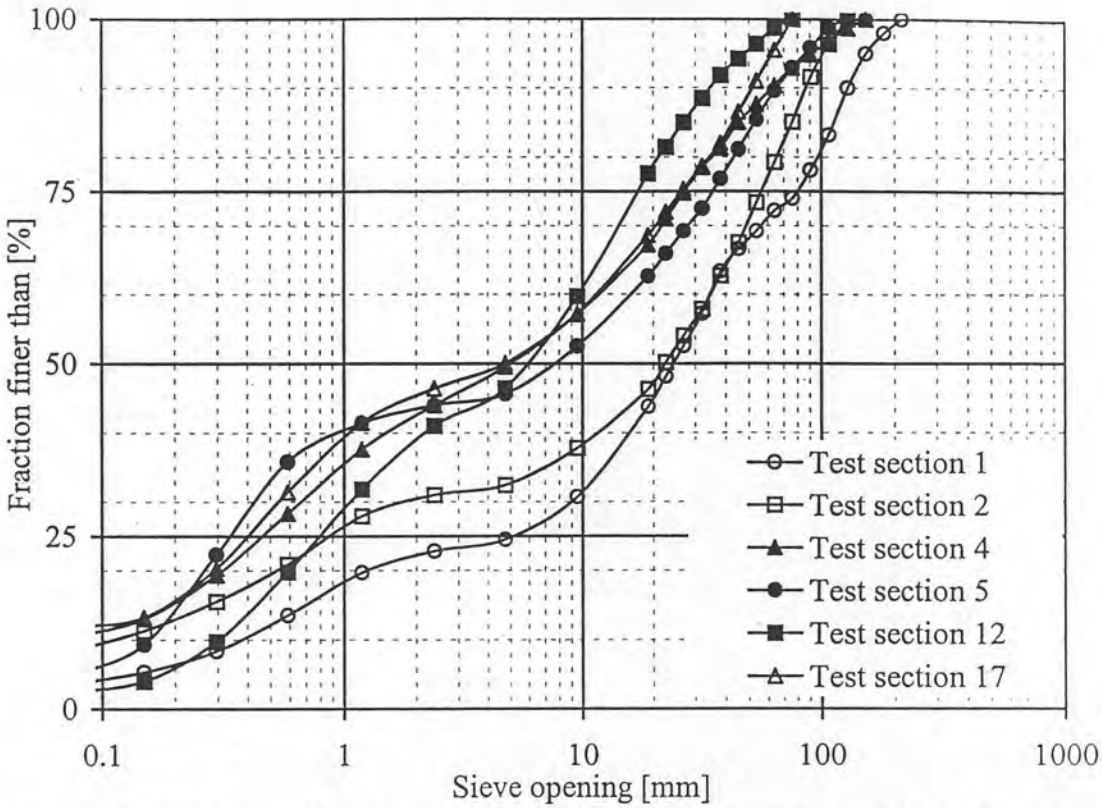

Fig. 3.8. Initial substrate material grain size distribution curves of all test sections

3.7 Miscellaneous field observations in the San Luis Valley

Most of the typical armoring effects described by *GESSLER* (1965) and *PROFFITT* (1980) were also observed in this study of the canals in the San Luis Valley. In Fig. 3.9 it can be recognized that the large rock has grouped around it both very small particles in its wake and moderate sized particles on its upstream side. Comparisons of such photographs show that armoring is not just the transport of the more easily eroded particles but a rearrangement of all particles making up the bed.

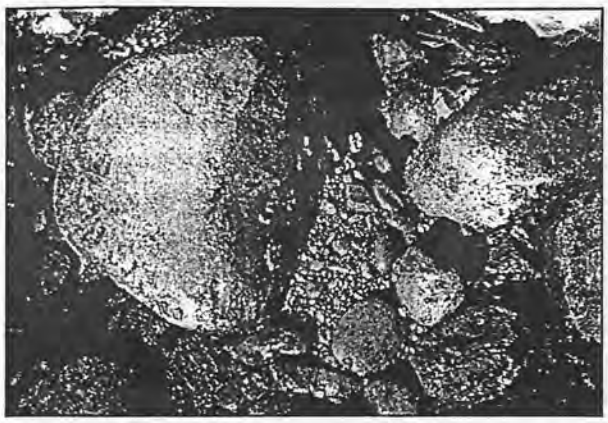

Fig. 3.9. Sheltering of fine material on the lee side of a large rock

One of the most important observations made on the canals inspected was the natural "imbrication" or "shingling" of the bed, due to the cobbles arranging themselves in an overlapping manner, under the action of the flowing water. It is believed that this action causes the bed material to resist movement by the water to a greater extent than would otherwise be the case, and therefore probably exerts considerable influence on the stability of canal sections.

This action was particularly noticeable in the larger canals where the cobbles were large. For example, Figs. 3.10 and 3.11 were taken in test section 5 from the same angle of view, Fig. 3.10 looking downstream and Fig. 3.11 looking upstream. It is important to note how much smaller the cobbles appear to be in Fig. 3.11 than in Fig. 3.10, although they are the same cobbles, only photographed from the opposite directions. This is because Fig. 3.11 looks at the edges of the flat rocks, while figure 3.10 looks on the back sides. The cobbles tend to arrange themselves

Fig. 3.10. Shingling looking downstream

Fig. 3.11. Shingling looking upstream

such that the longest axis is normal to the direction of flow, the intermediate axis is in the direction of flow, and tends to be tipped upward somewhat in the direction of flow, and the smallest axis is nearly vertical, but tipped somewhat upstream.

Fig. 3.12 was taken of the same rocks, but photographed from the side. The direction of flow was from right to left. Note that a large number of the flatter cobbles are arranged with their flatter faces sloping upward in a downstream direction or, in other words, that they were arranged like shingles on a roof and tend to overlap the cobble next to it in a downstream direction, forming a sort of "shingling" or "imbrication". The tendency of the flat faces of the cobbles to be tipped upward in the direction of flow causes the force of the water flowing over them to exert a pressure downward on the cobbles, thus helping to prevent them from rolling down the canal.

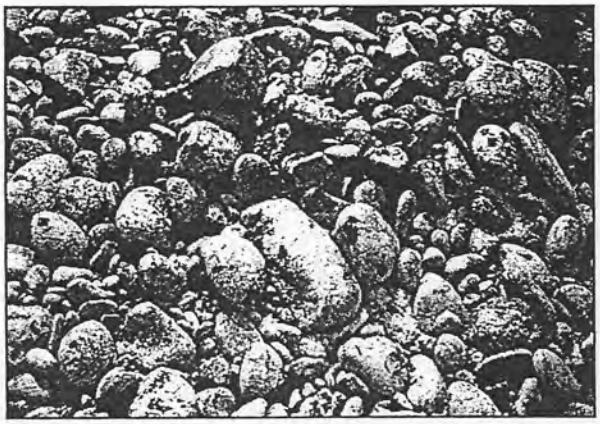

Fig. 3.12. Shingling from side view

This "imbrication" of the bed material was not so noticeable where the cobbles were smaller (test sections 12 and 17). In general, the smaller canals, which were further from the point where the Rio Grande left the mountains, had smaller bed material and it appeared to be more spherical in shape than further upstream, thus having less tendency to imbricate.

It was also noticed that, except for some of the top cobbles which rested only on other cobbles, most of the large cobbles which formed the bed rested on sand which fits closely around the lower portion of the cobble. When these cobbles were raised from the bed, an impression or cast of the shape of the cobble remained in the sand (see Appendix II, Figs. II.12 and II.13).

4 Computations and analyses

4.1 Shear stress computations

The input data for the shear stress computations included the discharge Q, the slope of energy grade line S, the channel bottom width b, the channel bank slope m, and the characteristic diameter for the bank roughness d_{90} as presented in chapter 3. By resolving Eqs. 2.17-2.22 simultaneously, the hydraulic radius, R_b, was calculated and the mean bottom shear stress determined following Eq. 2.5. The results are summarized in Tab. 4.1.

ID	Q	S	b	m	d_{90}	h	A	U	f_b	f_s	f	R_b	τ_b
[-]	[m³/s]	[%]	[m]	[-]	[mm]	[m]	[m²]	[m/s]	[-]	[-]	[-]	[m]	[N/m²]
(1)	(2)	(3)	(4)	(5)	(6)	(7)	(8)	(9)	(10)	(11)	(12)	(13)	(14)
1	43.17	0.280	12.70	2.4	200	1.37	21.85	1.98	0.058	0.069	0.062	1.03	28.42
2	20.84	0.376	13.60	2.0	300	0.81	12.25	1.70	0.066	0.096	0.073	0.65	23.99
4	21.83	0.359	9.20	2.3	200	1.03	11.93	1.83	0.065	0.079	0.070	0.77	27.18
5	13.40	0.368	8.00	2.3	250	0.84	8.28	1.62	0.066	0.093	0.075	0.59	21.47
12	4.35	0.243	5.90	1.5	30	0.52	3.45	1.26	0.055	0.049	0.053	0.46	10.88
17	18.72	0.274	11.60	2.0	60	0.84	11.23	1.67	0.058	0.053	0.056	0.75	20.05

Note: Input data

Tab. 4.1. Shear stress computations for all the test sections

It can be noted that the difference between the depth of flow, and the hydraulic radius of the bed is very different for each test section. It is mostly dependant on the ratio b/h and the bank friction factor. For example, for test section 12 and 17, where the banks are relatively smooth and the ratios b/h are higher than 10, the relative difference between depth of flow and hydraulic radius of the bed is about 10%. If this value is compared to a relative difference of about 25 – 30% for test sections 1, 4, and 5, where the banks are rough and the ratio b/h less than 10, it can be stated that the magnitude of the error of using the depth of flow or the overall hydraulic radius, instead of the hydraulic radius of the bed can be significant.

It is also important to note that in flume studies the error in using the depth of flow or the overall hydraulic radius is much less than it is in channel studies at prototype scale, because the side walls are frequently glass and relatively smooth. Therefore the side effect is less developed.

4.2 Sensitivity analysis of shear stress

To get an idea of the importance of the errors in the measurement or estimation of all the input variables to the computations of the mean bottom shear stress, a sensitivity analysis was performed.

Using the Gaussian error propagation law of random and independent errors, the standard deviation in the calculated bottom shear stress, due to the error in measuring discharge, slope, bottom width, side slope and bank controlling roughness, was calculated to be

$$\sigma_{\tau_b}{}^2 = \left(\frac{\partial \tau_b}{\partial Q}\right)^2 \sigma_Q^2 + \left(\frac{\partial \tau_b}{\partial S}\right)^2 \sigma_S^2 + \left(\frac{\partial \tau_b}{\partial b}\right)^2 \sigma_b^2 + \left(\frac{\partial \tau_b}{\partial m}\right)^2 \sigma_m^2 + \left(\frac{\partial \tau_b}{\partial d_{90}}\right)^2 \sigma_{d_{90}}^2 \qquad [4.1]$$

where σ_i is the error in measuring the parameter i, $\partial \tau_b / \partial i$ is the partial derivative of τ_b with respect to parameter i.

In irrigation canals where the discharge is measured by rating stations which are calibrated several times a year, it can be reasonably assumed that an error of about ± 5% can be expected in the measured discharge. The error in the slope is due to the error in the level readings and the positioning of the surveying rod; it can be assumed to be ± 3%. Therefore, the standard deviation of the measured values for the discharge and the slope was assumed to be 5% and 3%, respectively. For the bottom width and the bank slope, a standard deviation was determined

by analyzing the measured values (see Tab. 3.7) and for d_{90} a standard deviation was simply estimated by considering reasonable gathering of the value of d_{90}.

To calculate the partial derivatives all the input variables were varied by +1% for each test section separately. The results of the analysis for the different test sections together with each squared term of Eq. 4.1 are presented in Tab. 4.2.

ID	$(d\tau/di)^2\sigma_i^2$ for Q	S	b	m	d_{90}	σ_τ^2	σ_τ	τ_b	σ_τ/τ_b
[-]	[N²/m⁴]	[N²/m⁴]	[N²/m⁴]	[N²/m⁴]	[N²/m⁴]	[N²/m⁴]	[N/m²]	[N/m²]	[%]
(1)	(2)	(3)	(4)	(5)	(6)	(7)	(8)	(9)	(10)
1	0.60	0.63	0.03	0.16	0.54	1.96	1.40	28.42	4.9
2	0.49	0.41	0.12	0.13	0.21	1.35	1.16	23.99	4.9
4	0.51	0.59	0.10	0.07	0.56	1.83	1.35	27.18	5.0
5	0.34	0.37	0.04	0.05	0.45	1.25	1.12	21.47	5.2
12	0.11	0.08	0.43	0.01	0.05	0.69	0.83	10.88	7.6
17	0.35	0.28	0.02	0.01	0.24	0.91	0.95	20.05	4.7

Tab. 4.2. Sensitivity analysis of the shear stress computations

The results of the sensitivity analysis show that, the standard deviation of the mean bottom shear stress depends highly on the discharge Q, the slope S, and on the characteristic roughness diameter of the bank d_{90}. The geometric properties b, and m have little influence on the standard deviation of the bottom shear stress, except for test section 12, which is very variable.

The relative error in the bottom shear stress was calculated in column (10) and found to be about 5% for test sections 1, 2, 4, 5, and 17. For test section 12 the relative error was slightly higher and about 7.5%.

The sensitivity analysis clearly shows which data should be improved for a more accurate determination of the bottom shear stress. The discharge and slope measurements can hardly be ameliorated without investing a lot of time and money. The parameter which can easily be improved is the characteristic diameter of the banks. But even if the d_{90} term in column (6) would be in the same order of magnitude as m, and b, the relative error would still be approximately 4%. Hence, for the armoring computations the accuracy of the mean bottom shear stress can be assumed sufficiently exact.

4.3 Armoring prediction

As mentioned previously, *GESSLER*'s method was used to predict the armor layer grain size distribution. Given the mean bottom shear stress, τ_b, and the initial grain size distribution of the sediment mixture, the following steps were effectuated to predict the armor layer (see Appendix VI for the computation sheets):

1. By using the modified Shields diagram after *GESSLER* (1965), Fig. 2.3, the critical shear stress for the mean grain diameter, d_{gi}, corresponding to each fraction was determined.

2. After calculating the ratio τ_c/τ_b, the probability of a grain to stay as part of the armor layer, q, as defined by Eq. 2.8, was found.

3. The grain size distribution curve of the armor layer was determined, using Eq. 2.10.

As the predicted armor layer was compared to the measured armor layer in the canals, a significant difference could be observed. The divergence always occurred against the coarser fractions, which led to the finding that the difference had to be of systematic origins.

Several researchers questioned the sampling method used by *GESSLER* (1965), and *LITTLE AND MAYER* (1976). Therefore, a conversion procedure developed by *PROFFITT* (1980) and based on the work by *KELLERHALS AND BRAY* (1971) was used to correct the measured armor layer in favor of the finer grains. A description of the complete conversion procedure and a comparison of its effects on the flume data reported by *GESSLER* (1965) is given in Appendix I.

The comparison between the measured armor layer as defined by *GESSLER* (1965), the corrected measured armor layer as proposed by *PROFFITT* (1980), the initial substrate material grain size distribution and the predicted grain size distributions of the armor layer are shown in Figs. 4.1 through 4.6.

The represented band of the predicted armor grain size distribution curve corresponds to a bottom shear stress of $\tau_b \pm 1.96\sigma$. This band shows the 95 % probability of the gathering of the armor layer grain size distribution curve due only to the variations of the mean bottom shear stress, i.e. assuming the distribution of the substrate material is correct.

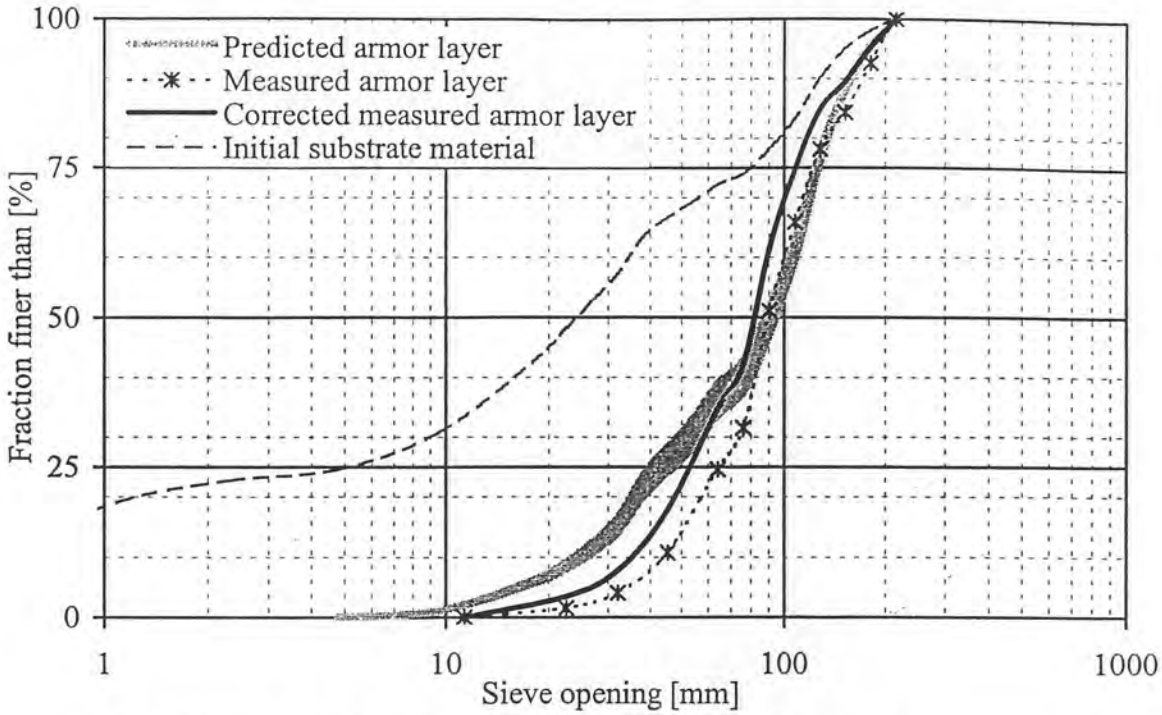

Fig. 4.1. Armor layer grain size distributions of test section 1

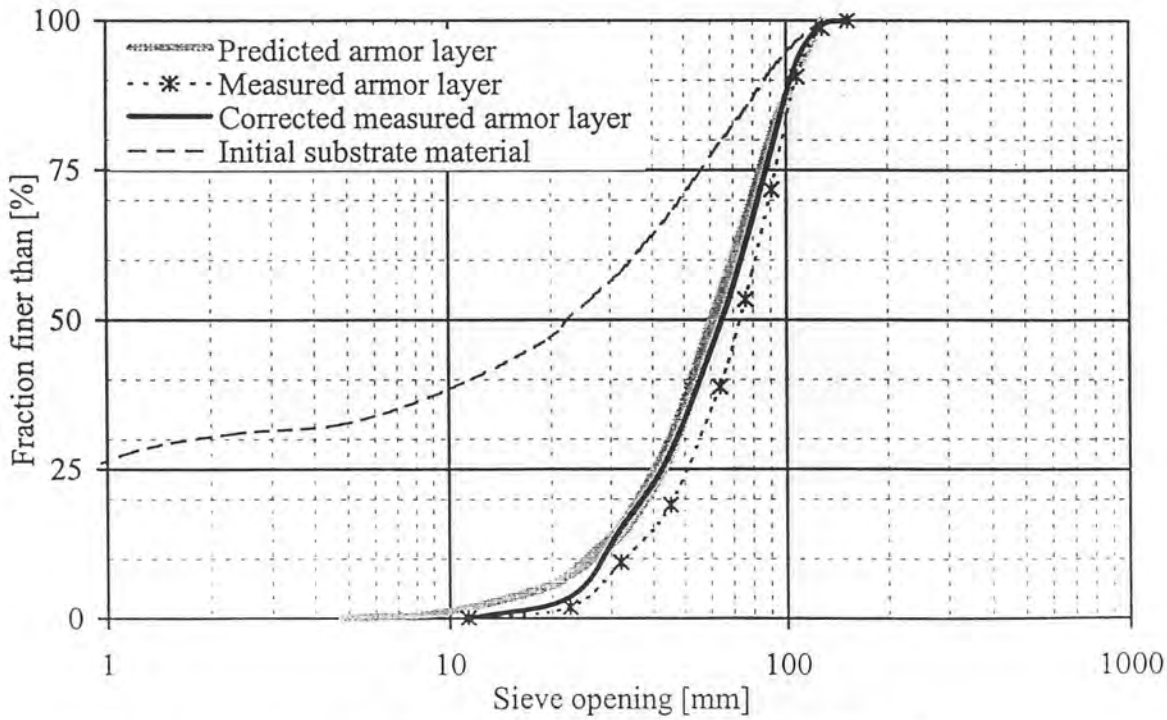

Fig. 4.2. Armor layer grain size distributions of test section 2

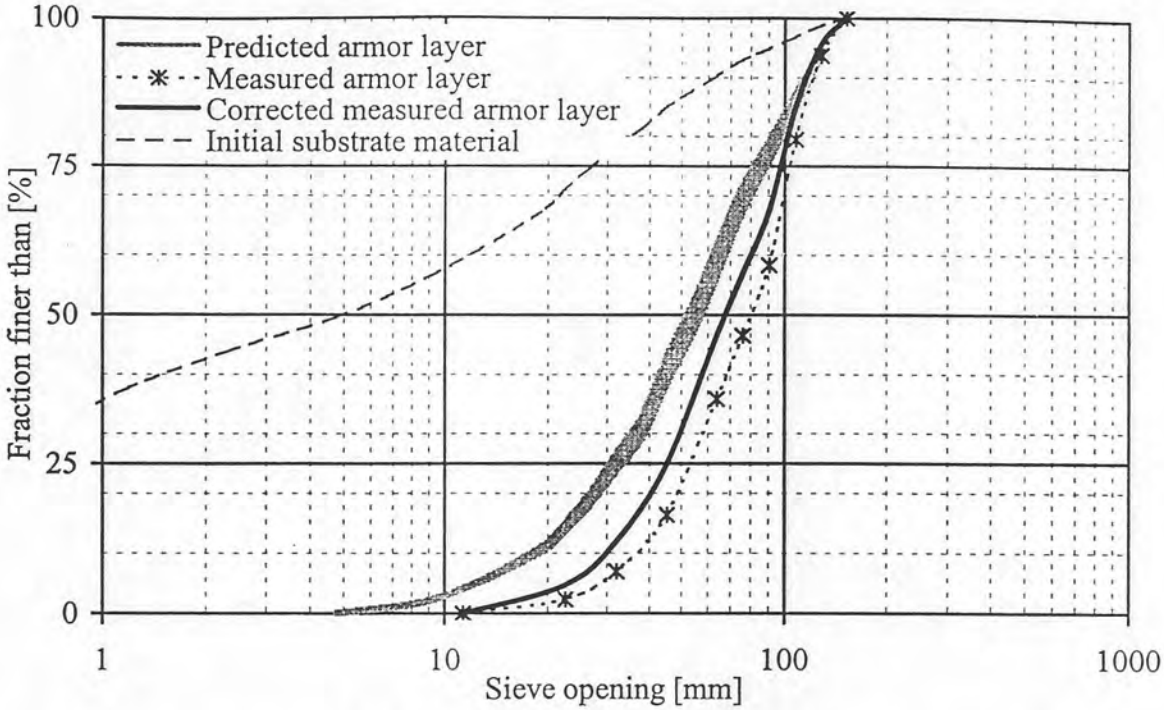

Fig. 4.3. Armor layer grain size distributions of test section 4

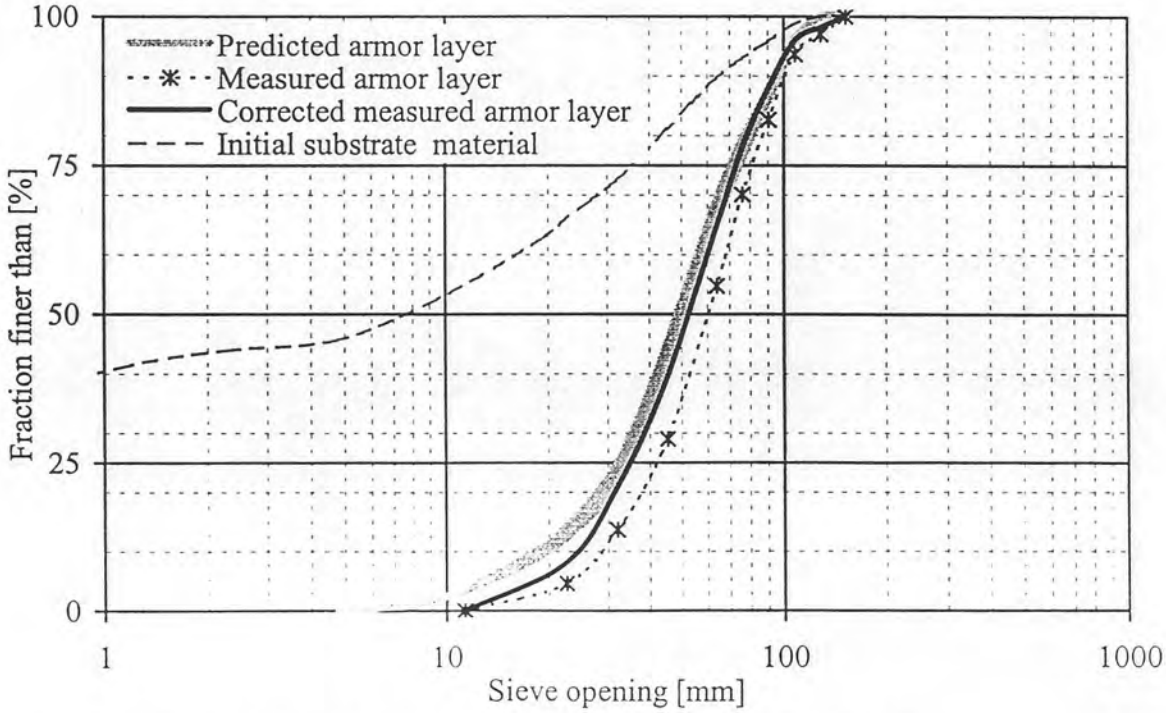

Fig. 4.4. Armor layer grain size distributions of test section 5

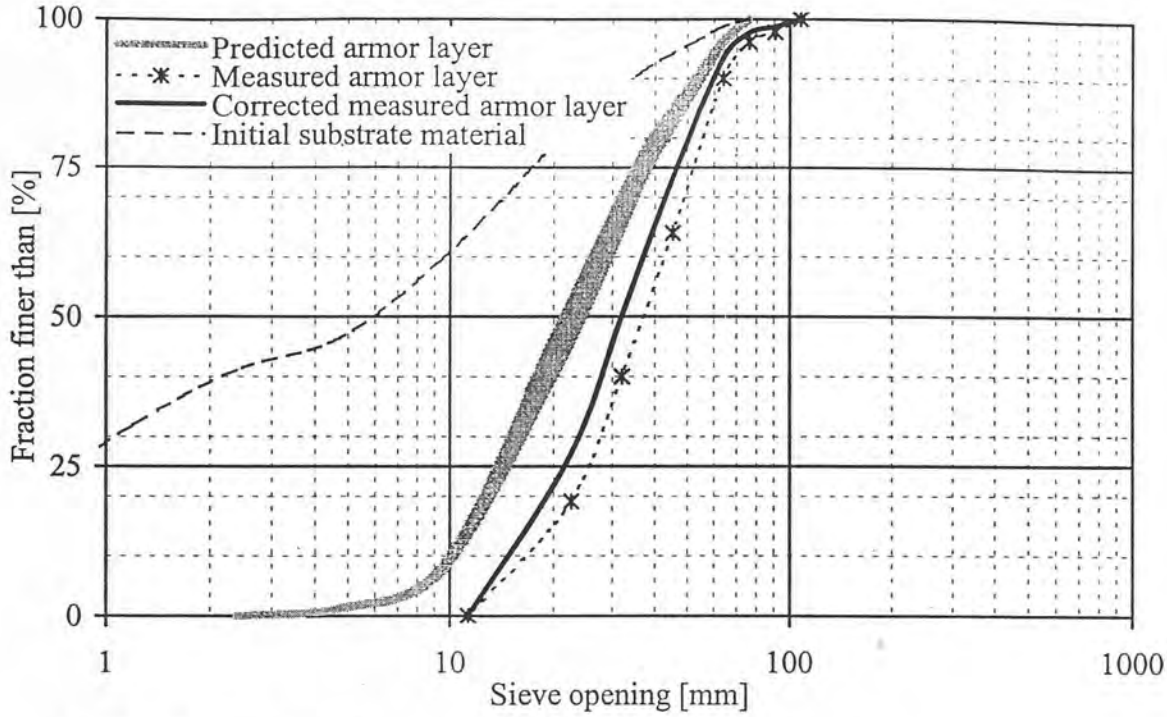

Fig. 4.5. Armor layer grain size distributions of test section 12

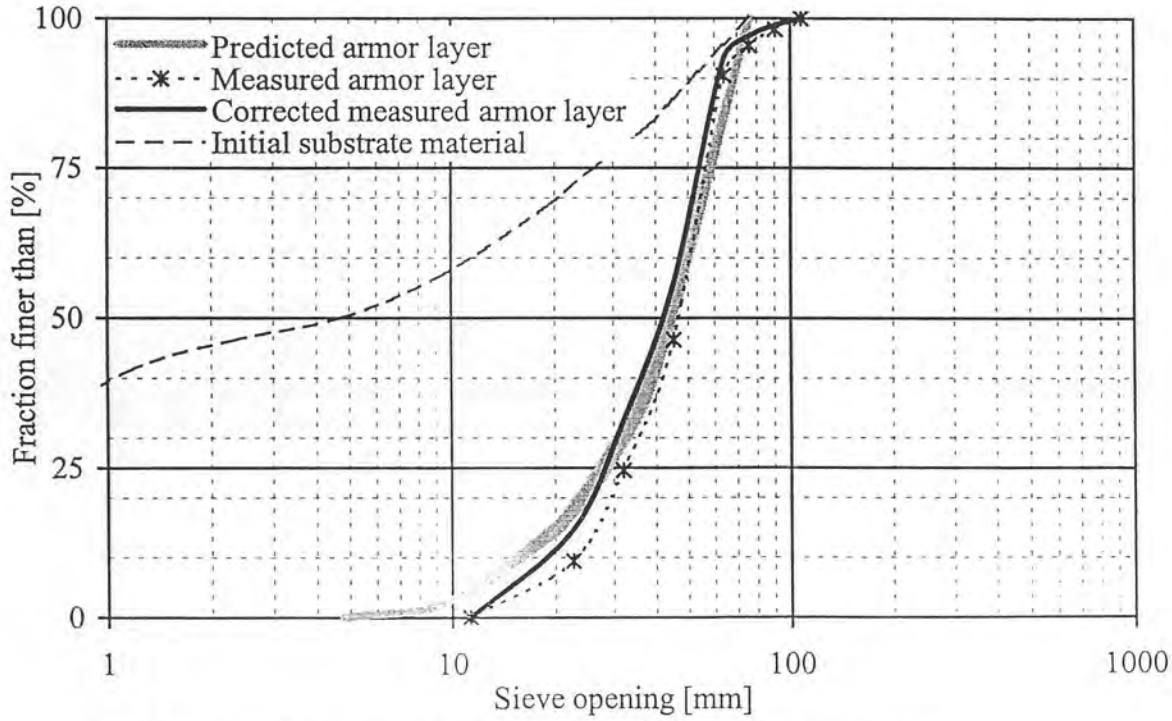

Fig. 4.6. Armor layer grain size distributions of test section 17

It can be noted that for test sections 2, 5, and 17 the predicted armor layer corresponds very well to the corrected measured armor layer. In these cases the difference of the grain size distribution curve in the smaller grain size fractions can be explained by the fact that the sampling methods were not very accurate for grain sizes smaller than 20 mm.

The predicted armor layer of test sections 1 and 4 fit well in the coarser fractions, but in the smaller fractions the measured armor layer tends to be biased to the coarser fractions. In these cases, the initial sample or the armor layer sample might not be representative or might be biased. This statement can be even more confirmed by two facts: First, test sections 1 and 4 are the coarsest test sections and therefore, only one transect-by-number sample could be taken. And secondly, the largest sieve size in the report of *LANE AND CARLSON* (1953) was 76.1 mm which had to be completed by fractions formed of geometric series with a factor of $\sqrt[4]{2}$ up to the maximum grain size found in the armor layer samples. As already mentioned in chapter 3.6, this completion introduces an uncertainty which is difficult to quantify.

In test section 12 the prediction fails significantly as compared to the measured armor layer. There might be several reasons for this divergence. First, the canal geometry has important irregularities, which favors local disparities in the bottom shear stresses. Secondly, the maximum discharge could be largely underestimated, which might be possible in regard to the contradictions observed in the historic discharge records (see Tab. 3.5). But the most probable explanation is that in this test section the transect-by-number method is not adequate because the fractions finer than 20 mm represent about 40% of the predicted armor layer. For the applied transect-by-number method this would correspond to about 250 stones in the size range < 11.3 mm. It is difficult to judge if this is reasonable.

However, it has been noticed that the armoring computation is very sensitive to the initial grain size distribution and that an error of 5% in the middle sieve sizes can change the resulting armor layer prediction considerably.

4.4 Stability coefficient

By analyzing the predicted armor layer grain size distributions, some information can be gained concerning what safety factor should be used in a design criterion. The required safety factor largely depends on the reliability of the measured initial grain size distribution curve and the uncertainties in predicting the maximum bottom shear stress. The latter problem is not too difficult in an irrigation canal, where the maximum discharge is relatively well determined. In natural channels, it is considerably more difficult to develop a design shear stress.

The stability coefficient of the predicted armor layer for each test section was calculated using Eq. 2.10. The critical shear stress, τ_{cp}, corresponding to a stability coefficient, $\overline{q}$ =0.5, was then determined by back-solving the armoring computation. Based on the measured bottom shear stress, τ_b, and the predicted critical shear stress, τ_{cp}, the safety factor, F, which is defined as the ratio between τ_{cp} and τ_b, for these test sections was calculated.

The results of the calculation are presented in Tab. 4.3, where τ_b is the bottom shear stress, $\overline{q}$ the stability coefficient, τ_{cp} the predicted critical shear stress, corresponding to $\overline{q}$ =0.5, and F the calculated safety factor. The computation sheets can be found in Appendix VI.

ID [-] (1)	τ_b [N/m^2] (2)	$\overline{q}$ [-] (3)	τ_{cp} [N/m^2] (4)	F [-] (5)
1	28.42	0.80	84.09	3.0
2	23.99	0.82	55.46	2.3
4	27.18	0.70	53.09	2.0
5	21.47	0.78	47.89	2.2
12	10.88	0.79	25.68	2.4
17	20.05	0.75	35.67	1.8
Average	$\overline{q}$ =	0.77	F =	2.3

Tab. 4.3. Stability coefficient and safety factor for all test sections

For the purpose of design, a safety factor must be assigned. As already mentioned before, the choice of the required safety factor is closely related to the reliability of the measured initial grain size distribution curve, to the uncertainties in predicting the maximum bed shear stress to be expected and to how much temporary instability can be tolerated under flood conditions.

It can be noted that in the canals investigated in the San Luis Valley, the stability coefficient was between 0.70 and 0.82 with an average of 0.77. The safety factor varied between 1.8 and 3.0 with an average value of 2.3.

Based on the analysis of the data collected from the irrigation canals in the San Luis Valley, it can clearly be stated that with a safety factor of more than 2.0 the canals can be considered very stable. Since these canals were built more than a hundred years ago, when the knowledge of stable channel design was only based on experience, it is not amazing that the safety factor is so high.

If these canals would be constructed with current know-how, maybe they would have smaller cross sections leading to higher shear stresses. The design of a new irrigation canal given the

maximum required discharge, the required slope of the canal and the grain size distribution of the initial bed material, would be effectuated by the following procedures:

1. The critical shear stress, τ_{cp}, corresponding to a stability coefficient of $\overline{q}$ =0.5, using *GESSLER*'s method (1965) is determined by Eqs. 2.8, 2.10, and 2.11.

2. The design shear stress, τ_d, is calculated by dividing the critical shear stress with the safety factor.

3. The friction factor associated with the bed, f_b, is found assuming a slope and using Eq. 2.16.

4. Knowing the design discharge and the slope, the hydraulic radius of the bed can be calculated using Eq. 2.5.

5. The average flow velocity in the channel is calculated using Eq. 2.17.

6. Knowing the design discharge and the average flow velocity, from step 5, the cross sectional area of the channel can be calculated.

Finally, the shape of the canal cross section will depend on many parameters, such as the required side slope which is a function of the angle of repose of the side material, the minimum required bottom width for the machinery, and mostly on economic considerations.

5 Conclusions

The analysis of the bottom shear stress computations clearly showed that the magnitude of the error in using the depth of flow, instead of the hydraulic radius of the bed, is significant if the banks are rough and the channel width is not at least 10 times the flow depth. Therefore, it is of primary importance to correct for this bank effect by dividing the cross-sectional area into subareas.

The sensitivity analysis permitted an estimation of the standard deviation of the computed shear stress in relation to the accuracy of the input variables. It has been found that the variation of the shear stress mainly depends on the variation of the discharge, the slope, and the roughness of the bank. Hence, the best improvement of the computations could be done by collecting more reliable data on these variables.

With the knowledge of the shear stress, its standard deviation, and the initial substrate material distribution an armoring prediction was performed using *GESSLER*'s armoring prediction method. The resulting grain size distribution of the armor layer was compared to the armor layer measured in the canals during the field trips to the San Luis Valley.

A discrepancy between the predicted and the measured armor layer was observed in all the test sections. The fact that the measured armor layer was always significantly coarser than the predicted armor layer led to the assumption that the difference had to be of systematic origin.

The sampling method used in this study was identical to the sampling procedures described by *GESSLER* (1965) and *LITTLE AND MAYER* (1976). It corresponds to a true area-by-weight sample, which is considered to be equivalent to a volumetric analysis. This definition is still

controversial with other investigators, who claim that a surface layer one grain thick cannot be recovered on a volumetric basis since it does not occupy a volume that can be predetermined (*KELLERHALS AND BRAY* (1971)). Therefore, the correction proposed by *PROFFITT* (1980) was applied to the measured armor layer distribution. The resulting corrected measured armor layer showed good agreement in most of the test sections.

Another reason for the discrepancies in the predicted armor layer could be the uncertainty concerning the initial substrate material distributions. With only one sample for the whole test section and a sample size of 150 kg, an error in the initial substrate material distribution can have a significant influence to the armor layer prediction.

A more intuitive argument, which could explain the fact that all measured armor layers are coarser than the predicted distributions, is the age of these canals. They have been conveying water for more than a hundred years and therefore, they could be "completely armored". The flume experiments on which the prediction method is based lasted about a hundred hours. After this time, the sediment transport almost died off and armoring was considered to be accomplished. It might be possible that this difference in time scale explains the observed differences between the measured and the predicted armor layers. One could call this phenomenon, an "aging effect".

However, the differences observed between the armor layer predicted from the initial material and the armor layer measured in situ are most probably related to the sample accuracy, and the sampling method. The main conclusion drawn from the analysis of the results in the San Luis Valley is that the variation of these factors might well outweigh the differences caused by hydraulic effects. Therefore, considering the engineering application, the efforts in stable channel design should mainly be on the accuracy of the initial grain size distributions, because errors in the estimation of the bottom shear stress have relatively little influence on the prediction of the armor layer and the stability coefficient.

The armoring study in the San Luis Valley clearly showed that for prediction of the stability of the canal bed (a main engineering problem in stable channel design), *GESSLER*'s method combined with *PROFFITT*'s sampling correction give a reliable and consistent estimation of the armor layer grain size distribution curve.

A second objective of this study was to get data for the stability coefficient and the safety factor of stable channels. For purposes of design *GESSLER* (1970) recommended a stability coefficient of $\overline{q}$ =0.65. This criterion corresponds to a safety factor in bottom shear stress of approximately 1.4 to 1.5. In terms of discharge the safety factor is approximately 1.6 to 1.9. The stability coefficients found in the present study of the irrigation canals in the San Luis Valley varied

between $\overline{q}$ =0.70 to 0.82 with an average of $\overline{q}$ =0.77. The safety factor in terms of bottom shear stress was determined to be between 1.8 and 3.0 with an average of 2.3.

These safety factors of more than 2.0, clearly confirm the assumption that the irrigation canals in the San Luis Valley are stable. For design such a safety factor would be rather conservative and the values proposed by *GESSLER* (1970) appear to be more reasonable.

During the field trips most of the armoring phenomenon observed in the flume experiments by many researcher were also found at prototype scale in the irrigation canals of the San Luis Valley (see chapter 3.7). It was astonishing how well the typical armoring pattern was developed. One can very well imagine that the critical shear stresses of such mixtures will be slightly higher, because of the imbricated manner the surface material is arranged.

The results of this study have identified areas which require more investigation to further refine the knowledge of the armoring process at prototype scale:

As was previously mentioned, the predicted armor layer and the stability coefficient largely depend on the initial grain size distribution. It would be interesting to further investigate the influence of variations in the initial grain size distribution to the results of the predicted armor layer and the stability coefficient. This investigation could lead to a better definition of the needed safety factor, and a more economic channel design.

For further field investigations of the irrigation canals in the San Luis Valley one should first try to ameliorate the data concerning the initial substrate material, for example by taking 2 samples of 200 kg in each test section. And secondly, the characteristic roughness diameter of the canal bank should be determined, for example by using the photographic sizing program tested in the present study (see Appendix I.). With these data it should be possible to considerably ameliorate the input data of the computations and permit further conclusions about armoring prediction.

Appendix I. Determination of surface grain size distributions

Surface sampling methods

To determine grain size distribution curves (cumulative frequency curves $p_i = f(d_i)$) there are several sampling methods of assigning size and frequency values:

(1) ***Transect sampling.***- All rocks larger than 10 mm, falling under a straight wire along the sampling line constitute the sample. In this case only one dimension of the sample is predetermined and the volume of the sample collected is entirely dependent on one grain dimension. To ensure that the sample is representative *FEHR* (1986) proposes a sample size of minimum 150 stones. The class boundaries should follow a geometric progression with the ratio of $\sqrt{2}$ or even $\sqrt[4]{2}$. The stones are measured on the intermediate or *b* principal axis by ruler or calipers, or classified using square openings in a template. The latter technique provides a measure of size that is equivalent to conventional sieving. The size distribution is then determined on a frequency-by-number basis. The frequency of each size interval is expressed as the percentage-by-number of the total number of particles in the original sample that fall into the interval.

(2) ***Areal sampling.***- All stones exposed within a predetermined area are sampled (e.g. *LANE AND CARLSON* (1953); *GESSLER* (1965)). In this case only two of the three dimensions of the sample volume are independent of particle dimensions. The rocks can be marked by spray paint and picked up. The frequency of each size interval is expressed as the percentage-by-weight of the original sample falling into the interval.

(3) ***Photographic sampling.***- This method utilizes a camera which records the particle size distribution of the river bed surface. A grid or scale is required to quantify the particle sizes. The photographic sampling can either be a grid or an areal sampling depending on how the photo is analyzed.

Grain Size distribution curve conversion

KELLERHALS AND BRAY (1971) noted that different methods of selecting material for size analysis lead to non-equivalent results. The formal conversion of Kellerhals and Bray is based upon the dimensions of the sample that are predetermined by the sampling technique. The general conversion relationship is

$$f_{ci} = \frac{f_{oi} d_{gi}^{x}}{\sum_{i=1}^{n} f_{oi} d_{gi}^{x}} \qquad [I.1]$$

where f_{oi} is the observed proportion of the sample in the ith size class with mean size d_{gi}, x is the integer dimension required for the conversion (determined by the method of sampling), n the number of size classes, and the sum effects a renormalization of the distribution to give the converted proportions f_{ci}.

To determine the exponent x a model proposed by *FEHR* (1986) is used. The conversion between a frequency-by-number and frequency-by-weight grain size distribution curve differ by a weighting factor proportional to d^3. Therefore, for the same type of sample, a grain size distribution curve evaluated by number, to one evaluated by weight has to be converted by the following relationship:

$$p_i = \frac{q_i d_{gi}^{3}}{\sum_{i=1}^{n} q_i d_{gi}^{3}} \qquad [I.2]$$

where p_i is the percentage-by-weight, q_i the percentage-by-number, n the number of fractions, and d_{gi} is the geometric mean diameter of the ith class.

To map the frequency of a given size class in a transect sample onto the frequency of the same size class in an areal sample. Fehr assumes that the percentage-by-number in a given class for volumetric, areal and transect samples of the same material is inversely proportional to the diameter cubed, the diameter squared and the diameter respectively, as shown in Eq. I.3:

$$q_i^{\,V} \propto \frac{1}{d_{gi}^3}$$
$$q_i^{\,A} \propto \frac{1}{d_{gi}^2} \qquad [I.3]$$
$$q_i^{\,T} \propto \frac{1}{d_{gi}}$$

where the indices represent the sampling method (V = volumetric sampling; A = areal sampling; and T = transect sampling).

Thus the ratio of the percentage-by-number in a size class for areal samples to the percentage-by-number of the same size class for transect samples is:

$$q_i^{\,A} = q_i^{\,T} \frac{1}{d_{gi}} \qquad [I.4]$$

and the ratio of the percentage-by-number in a size class for volumetric samples to the percentage-by-number of the same size class for transect samples would be:

$$q_i^{\,V} = q_i^{\,T} \frac{1}{d_{gi}^2} \qquad [I.5]$$

The two types of mapping described above give the rules for converting one grain size distribution curve to another. For example an areal-by-number curve can be converted to a areal-by-weight curve by simply using Eq. I.2:

$$p_i^{\,A} = \frac{q_i^{\,A} d_{gi}^3}{\sum_{i=1}^{n} q_i^{\,A} d_{gi}^3} \qquad [I.6]$$

and a transect-by-number curve can be converted to an areal-by-weight curve by using Eqs. I.2 and I.4:

$$p_i^{\,A} = \frac{q_i^{\,T} d_{gi}^2}{\sum_{i=1}^{n} q_i^{\,T} d_{gi}^2} \qquad [I.7]$$

Thus in the case of a transect-by-number sample the conversion factor is proportional to d_{gi}^2 and for an areal-by-number sample the conversion factor to an area-by-weight sample is proportional to d_{gi}^3.

These conversion exponents are purely theoretic and would only apply to cubical grains on a river bed surface without any coarsening. For the gravel found in rivers and canals the situation is somewhat more complicated because a variety of shapes and different packing densities occur. In reality, the river bed has also been exposed to a certain grade of static or dynamic armoring by selective transport, which could influence the conversion factor as well.

Armor layer sampling

Several researchers questioned the sampling method used by *GESSLER* (1965), and *LITTLE AND MAYER* (1976). *KELLERHALS AND BRAY* (1971) was the first, who demonstrated that areal samples tend to be biased in favor of the coarser grains. As *PROFFITT* (1980) argued, the final prediction of the armor layer is very sensitive to the sampling procedure and the comparison of the initial volume-by-weight sample type with the final area-by-weight sample type can lead to conflicting results. He developed a conversion procedure based on work by *KELLERHALS AND BRAY* (1971) to convert the areal sample to the equivalent volume sample:

$$p_i^V = \frac{p_i^A d_{gi}^{-0.5}}{\sum_{i=1}^{n} p_i^A d_{gi}^{-0.5}} \qquad [I.8]$$

where p_i^V and p_i^A are the percentage of the fraction with mean diameter d_{gi} on a volume-by-weight, respectively area-by-weight basis. The exponent of –0.5 has been determined by an analysis of experiments performed by *PROFFITT* (1980) and *SUTHERLAND* (1987).

This conversion procedure was used in the present study and has also been applied to the flume data of run number 5, reported by *GESSLER* (1965) to compare the results. Fig. I.1 shows the comparison of the armor layer predicted with the armoring computation to the armor layer sampled on an areal-by-weight basis, and the armor layer corrected by *PROFFITT*'s conversion procedure.

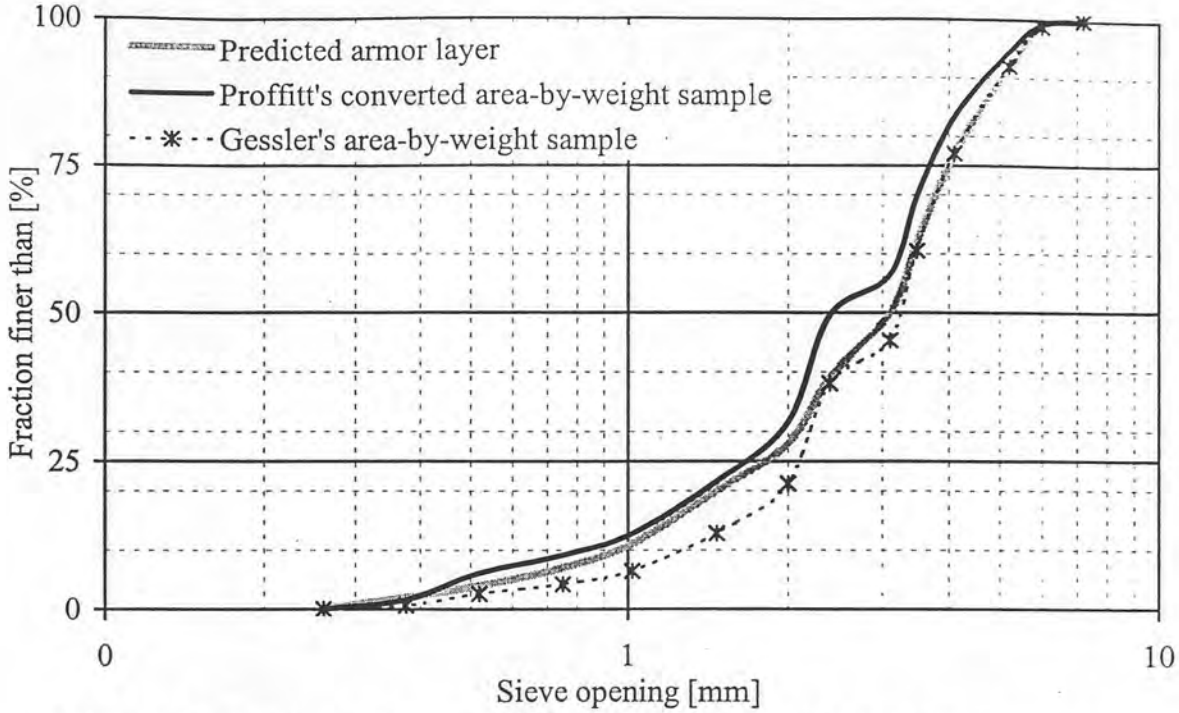

Fig. I.1. Comparison of Gessler's area-by-weight and Proffitt's corrected volume-by-weight samples

It can be noted that no significant difference occurs for smaller grain sizes. Gessler's area-by-weight sample fits better in the range between 3 and 7 mm and Proffitt's corrected volume-by-weight sample shows good agreement from 0.3 to 2 mm. Therefore, no conclusion about which method better represents the armor layer distribution can be made from this comparison of Gessler's experiment.

Photographic sizing with GoldSize 2.0

GoldSize originally was designed by Golder Associates Inc. to measure, calibrate and predict blast fragmentation. It is ideal for quarries, open pit mines, in fact for any bench blasting. GoldSize is a Windows™ based computer program to estimate the sizes of blast fragmentation size distributions. The present study was an opportunity to test this program for its reliability in prediction of river surface grain size distributions.

The process of sizing is divided into three steps:

1. The user photographs the particles using either a digital camera, a single lens reflex camera, or a video camera. The photographs can be taken in a vertical position or in perspective.

2. Then the photographs will be processed into Windows™ bitmap images. In this step, a digital camera creates digital images directly for downloading to the computer. With a single lens reflex camera the photographs are printed and scanned with a flat bed scanner. A video camera can be connected to a frame grabber to capture digital images from the tape.

3. The object digitizing, the most technically challenging component of the GoldSize sizing program, is totally manual. It is performed by tracing around each rock using the computer's mouse.

4. The scaling links the top and bottom of the image to the back and front of the collection of objects in the picture, assuming that all objects lie on one flat surface. The sizing program needs 2 reference objects in the case of a perspective photograph and only 1 reference object for a vertical picture.

5. Calculating the size distribution is then simply a matter of selecting the desired menu item. The sizes are calculated based on object width (shortest visible axis), because this most closely corresponds to sieving behavior of rocks.

In this study a single lens camera was used and all the test samples were photographed vertically. The difficulty was to get the whole areal sample (1 m^2) onto one photograph, therefore, several photographs had to be taken for every sample. The use of a digital camera would considerably simplify this process. It was also found that the contours and contrast of the image are slightly ameliorated by using a spray painted area, which later will be processed into a black and white photograph.

In the present study golf balls (∅ 4.27 cm) were used as reference sizing objects. They were found to be well adapted for gravel beds, but do not assure a very exact scaling. By using a wooden frame around the sample, the accuracy of the scaling process significantly improves. The sample area of 1 m^2 was found to be adequate for manageable handling and sufficiently large for a good accuracy for grains equal to or greater than 10 mm.

The initial photograph before sizing with the 2 golf balls is shown in Fig. II.2. The image represents exactly 1 m^2 and is prepared for processing.

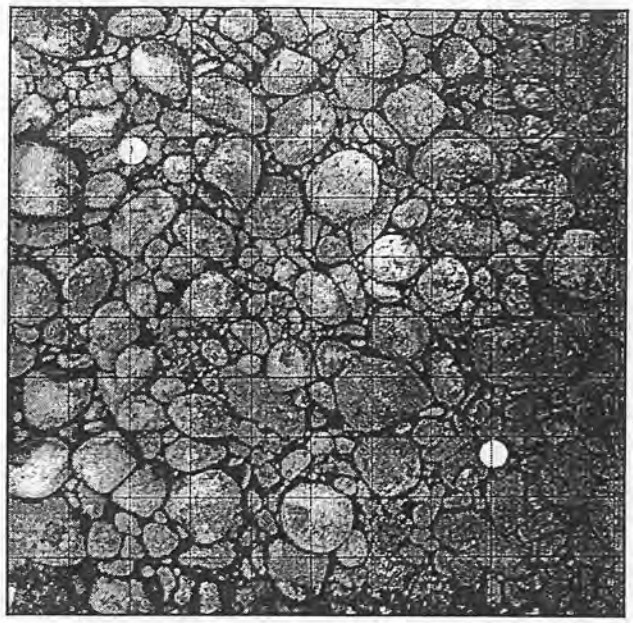

Fig. I.2. Initial area sample before sizing

Figs. I.3 and I.4 show the area sample with all the rocks traced around. The sizing program analyzes every rock in regards to the two principal axis and assumes that the shortest visible axis corresponds to the intermediate principal axis *b*. The rocks then are classified by number in the size classes, assuming the intermediate principal axis *b* corresponds to the sieve opening *D*.

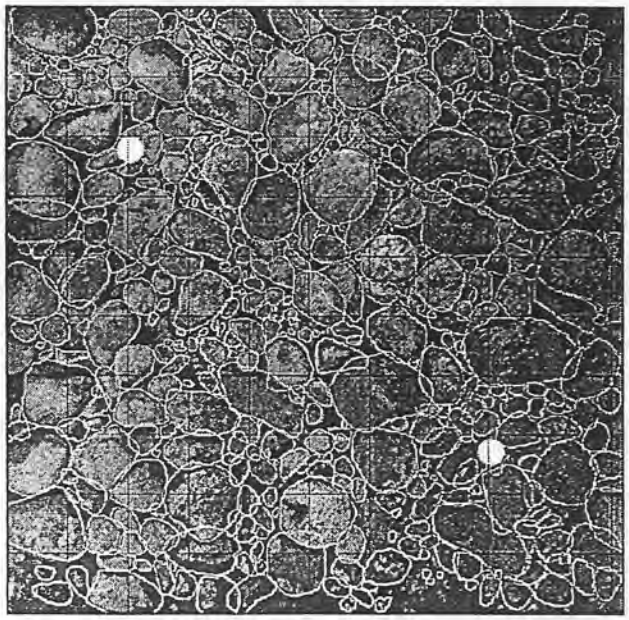

Fig. I.3. Processed image with all rocks traced

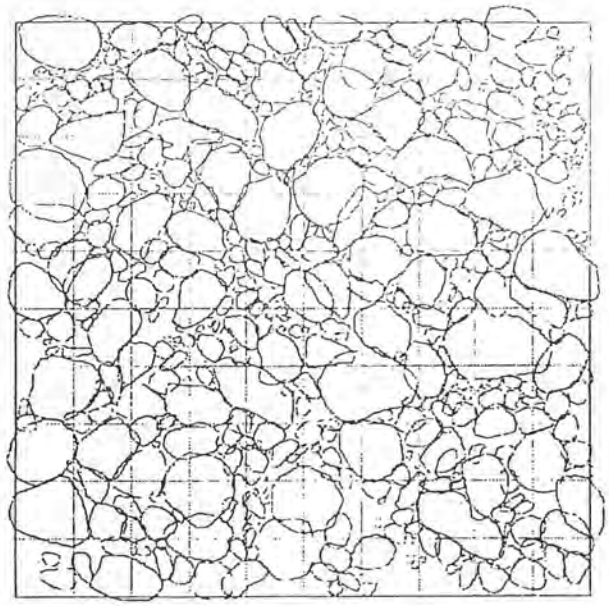

Fig. I.4. Traced rocks as processed by the program

It was found that an analysis can be accomplished at a rate of one image every 45 minutes. But if one takes into account the time for the image acquisition (scanning, converting, ...) the total amount of time can be doubled.

To convert the area-by-number grain size distribution found automatically by the program into an area-by-weight distribution, using the procedure presented previously, a least square analysis of the available data for the exponent x was effectuated. The best fitting exponent x for the photographic sizing was found to be $x = 2.6$ (theoretically $x = 3.0$). The computation sheets are presented in Appendix VI.

In the case of the photographic sizing a second conversion or correction is necessary, because the shortest visible axis (intermediate principal axis) does not correspond directly to the sieve openings. To correct for this overestimation with the photographic sizing method, the measured diameters had to be multiplied by a factor $C = 0.9$. This factor can be explained by the fact that in standard sieving the grains can also pass diagonally. The relationship between the shortest visible axis b and the sieve opening D depends upon the ratio of the shortest principal axis c to the intermediate principal axis b and can be defined as following

$$\frac{D}{b} = \frac{1}{\sqrt{2}}\left[1 + \left(\frac{c}{b}\right)^2\right]^{1/2} \qquad [I.9]$$

where D is the sieve opening, b the intermediate principal axis or shortest visible axis, and c the shortest principal axis. If one assumes a common c/b ratio of 0.7, the factor D/b becomes 0.86, which is close to the $C = 0.9$. The comparison of the converted photographic sample and the measured area-by-weight sample for the test sections in the San Luis Valley is shown on Fig. I.5.

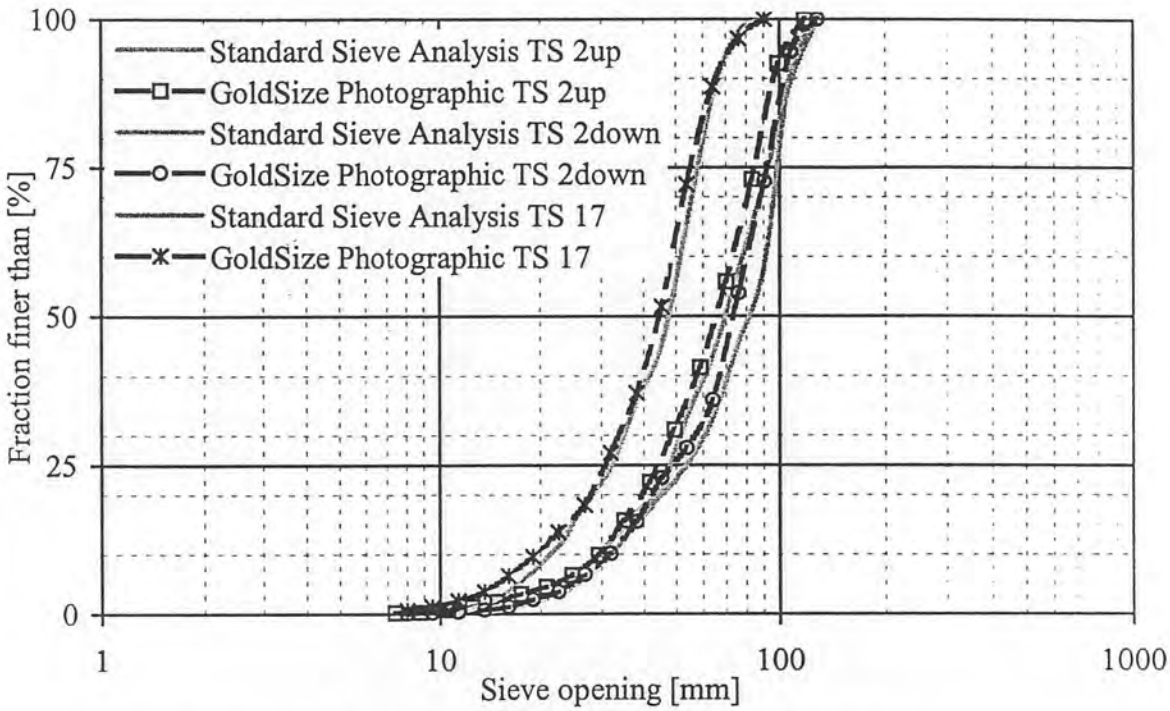

Fig. I.5. Comparison of the GoldSize photographic sizing and the measured area-by-weight samples in the San Luis Valley

The comparison shows almost perfect agreement for all the test sections in the San Luis Valley. The two test sites on the Poudre River were also compared and the results were the same. Hence, the GoldSize photographic sizing program is very well adapted for measurement of river bed surface grain size distributions. The settings in the program to get an area-by-weight sample as used by *GESSLER* (1965) are as following:

Menu Tools-Options:

Sizing (Metric units):	"Mass Power":	2.6
	"Sieve Shift":	0.9
	"Fines. Cor. Size":	0.002 m

To get an area-by-weigh samples as proposed by *PROFFITT* (1980) the settings are:

Sizing (Metric units):	"Mass Power":	2.6-0.5=2.1
	"Sieve Shift":	0.9
	"Fines. Cor. Size":	0.002 m

To get the standard sieve openings in the project reports the settings are:

Sizing (Metric units):	"Number of bins":	42
	"Top Size" (Maximum grain size):	1.024 m
	"Bottom Size" (Minimum grain size):	0.001 m

It was found that the best choice of the mouse sensitivity is "Fine Sensitivity 0.003" in the menu Tools-Options-Appearance.

To compare the results of photographs taken vertically and photographs taken in perspective, an upstream and a downstream photograph of test section 2 (TS 2up) were taken. Figs. I.6 and I.7 show the images with all the rocks sized.

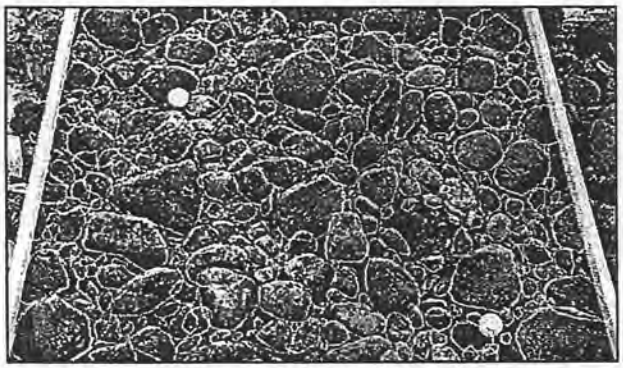

Fig. I.6. Test section 2 (upstream) looking downstream

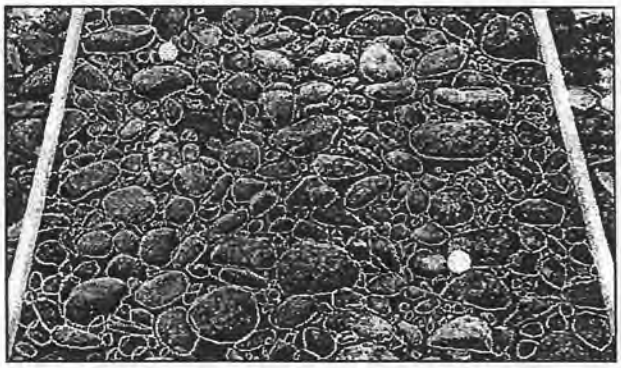

Fig. I.7. Test section 2 (upstream) looking upstream

Apparently there is no significant difference in appearance between the two viewing directions. In the case of a perspective photograph the sizing program needs two reference scaling objects, one in front and one in the back of the picture, as can be recognized on Figs. I.6 and I.7.

The resulting grain size distributions of the three directions (upstream, downstream, and vertical) are represented on Fig. I.8.

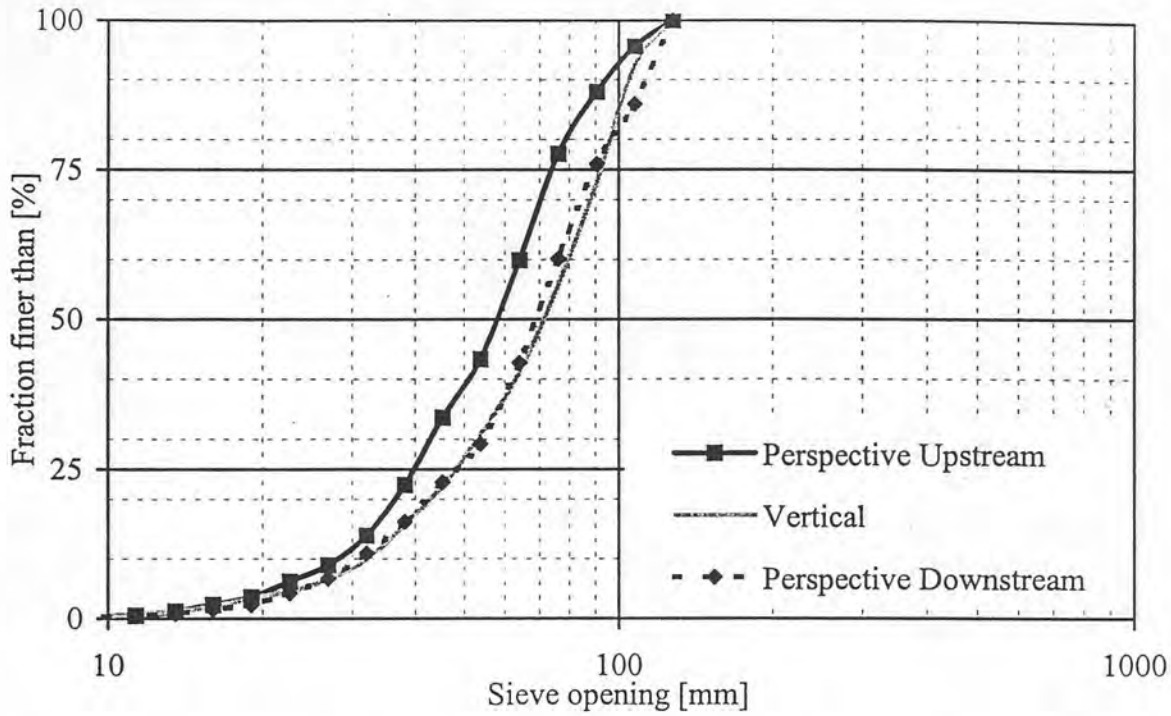

Fig. I.8. Comparison of the GoldSize photographic sizing in perspective

It can be noted that there is little difference between the "true" vertical distribution and the grain size distribution in downstream direction. Nevertheless, the difference between the image taken in upstream direction and the other images is significant. The discrepancy can be explained by the fact that in downstream and vertical view one always sees the longest and intermediate principal axis of a rock, therefore, the grain size distribution is correct as the program assumes the shorter visible axis to be equivalent to the intermediate axis. In the case of the upstream image one more likely recognizes the longest and the shortest principal axis of a rock, hence, the program assumes the shorter axis to correspond with the intermediate axis. As a result the sample photographed in an upstream direction seems to be slightly finer than in the other views.

This phenomenon can be explained by the nature of armored canal beds that show these typical imbricated patterns. The analysis by the photographic sizing program permits for the first time to quantify this difference in appearance of armored river beds.

The GoldSize 2.0 photographic sizing program is a powerful tool for surface grain size distribution analysis of river beds. The new version of GoldSize is supposed to add fully automated image acquisition and analysis, which could significantly improve the whole photograph sizing process.

By converting the area-by-number sample as presented herein, the photographic sample can be corrected for imbrication effects. From the measurements in the Poudre River and the irrigation canals in the San Luis Valley it can be concluded that the exponent x and factor C conceivably might be consistent for the surface.

The effects of partial hiding of the rocks by sand, shadow or another rock, need further investigation and could largely depend on the nature of the river. Photographic sizing also appears to be more adequate for gravel and larger material (< 20-30 mm). It is also recommended to check and eventually calibrate the grain size distribution for each study area situated in a different sedimentary environment. After this check the sizing program permits consistent results to be obtained within one river, or one geological province. In hydraulic calculations that are insensitive to grain size, or when a summary estimate of grain size is to be based upon data pooled from many sites, these methods may allow substantial saving in field effort.

Appendix II. Photographs

During the present armoring study and the study of E. W. Lane and E. J. Carlson, many photographs were taken to document the field procedures and miscellaneous observations. A selection of the most descriptive pictures is published in this appendix.

Field investigation trip to the San Luis Valley 1950

The following photographs were taken by E. W. Lane and E. J. Carlson during the field trip to the San Luis Valley, October 31 – November 5, 1950.

Fig. II.1. Looking downstream at test section 1

Fig. II.2. Looking upstream at test section 1

It can be noted that the appearance of the rocks on Fig. II.1 and II.2 is different because of the imbricated pattern. This phenomenon is quite characteristic for armored canal beds and it was also recognized on the field trips of the present study (see chapter 3.7).

Fig. II.3 shows another view of the canal in test section 4 as it was in the 1950's.

Fig. II.3. Looking upstream at test section 4

Field investigation trip to the San Luis Valley 1998

The following photographs were taken by the author during the field trip, November 11 – 13, 1998. The purpose of this field investigation trip was to locate the different test sections and to get an idea of their actual conditions.

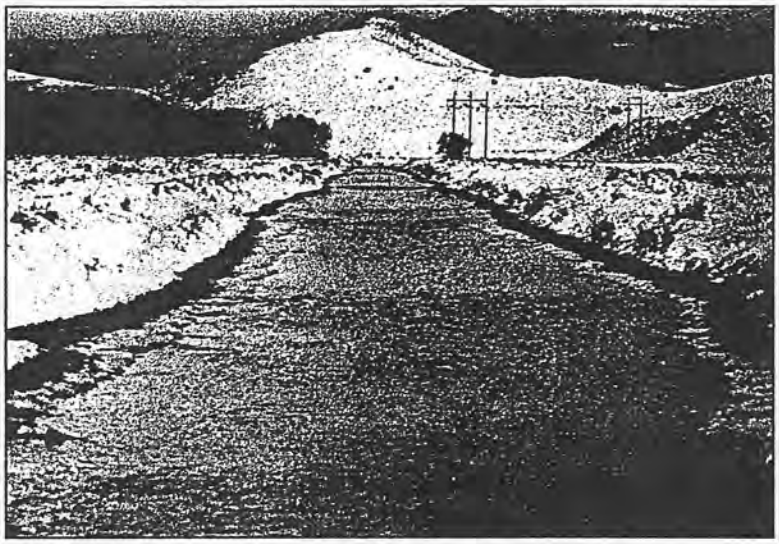

Fig. II.4. Looking upstream at test section 1

As can be seen on Fig. II.4 and II.5, the canals were still conveying water. The reason was the winter recharge program which supplies the aquifer.

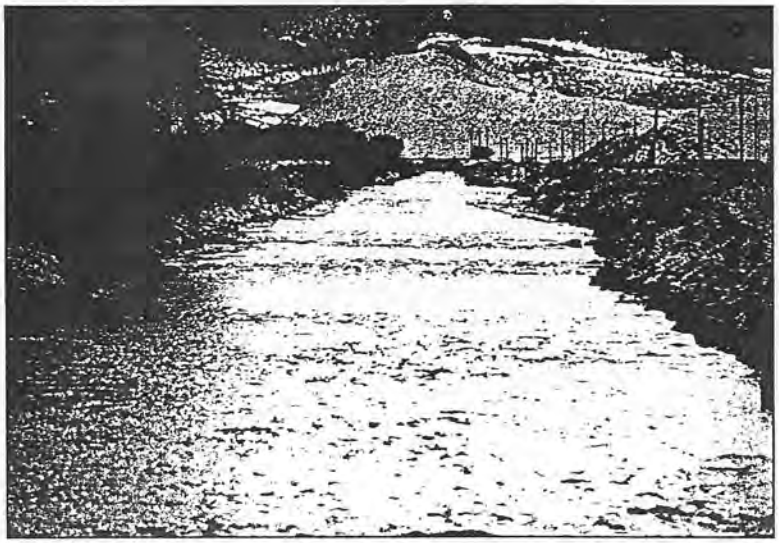

Fig. II.5. Looking upstream at test section 2

Test sections 4 and 5 were dry and partially covered with ice. On the left hand side of Fig. II.6 a center pivot can be seen. This equipment turns around a center point which is connected to the aquifer. The aquifer is supplied by the infiltration of the water in the canal. The whole valley is irrigated by this procedure, which is much more effective than simple irrigation by small ditches.

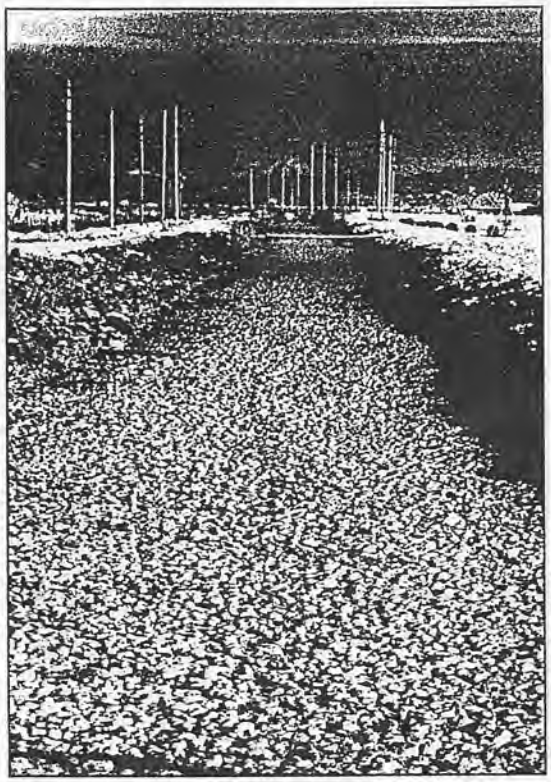

Fig. II.6. Looking downstream at test section 4

Fig. II.7. Looking downstream at test section 5

Fig. II.8 was taken between test section 4 and 5. As a consequence of the frozen ice layer, it illustrates very well that the characteristic grain size for the roughness of a canal bed is formed of a diameter close to the maximum grain size.

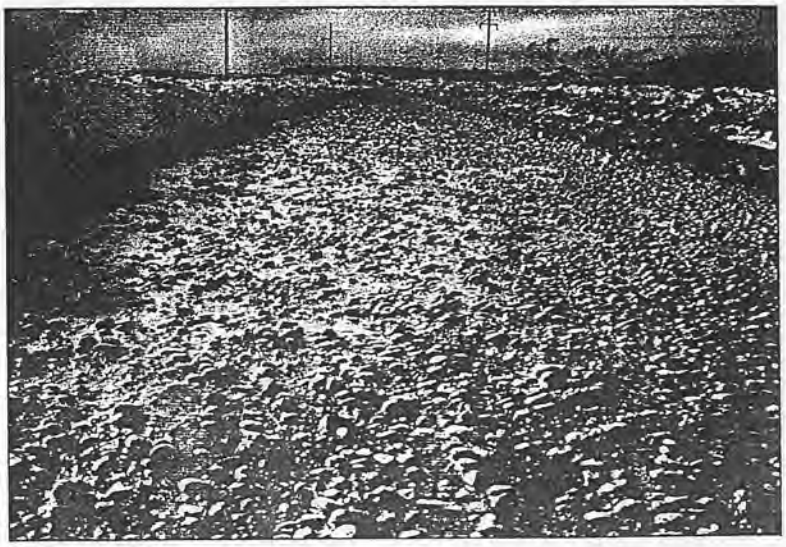

Fig. II.8. Frozen canal bed between test section 4 and 5

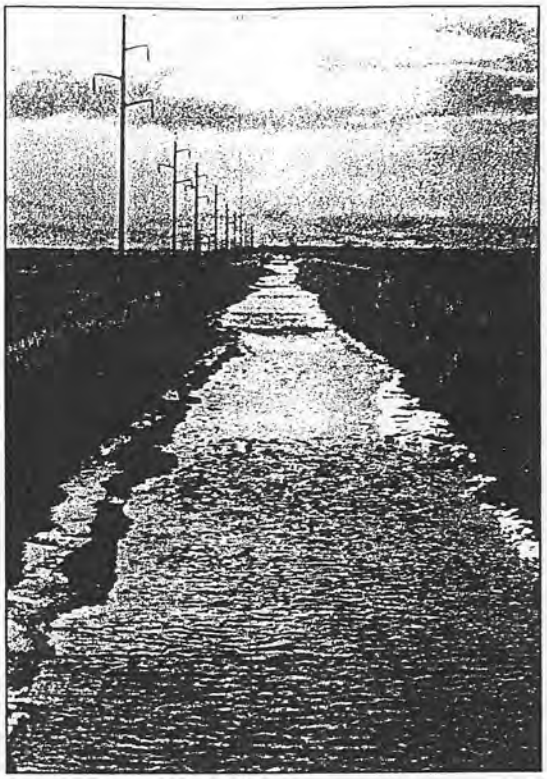

Test section 12 is shown on Fig. II.9 and represents the canal section documented in several papers. Its side slopes are very steep and unstable as can be noted on the photograph. The gravel piles on the left side of the canal indicate considerable cleaning operations.

As can also be recognized on the photograph, the geometry of this test section shows significant irregularities and therefore, in this case the assumption of an uniform cross section is questionable.

Fig. II.9. Looking upstream at test section 12

In test section 17 relatively high accumulations of snow were observed as shown on Fig. II.10. An explanation might be the alignment of the canal to the dominant wind direction which favors the snow accumulation.

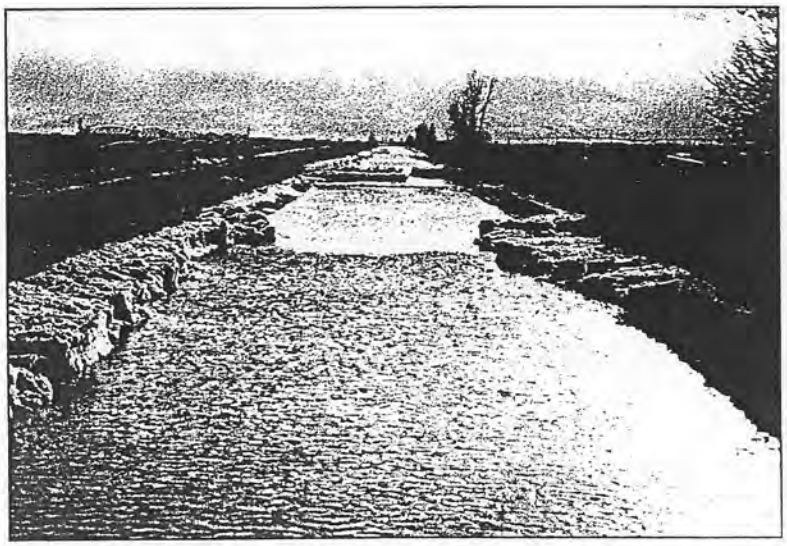

Fig. II.10. Looking upstream at test section 17

Poudre River test measurements

During the test measurements on the Poudre River near Fort Collins, CO, photographs were taken to document the different sample collection methods. The measurements were made on November 25, 1998.

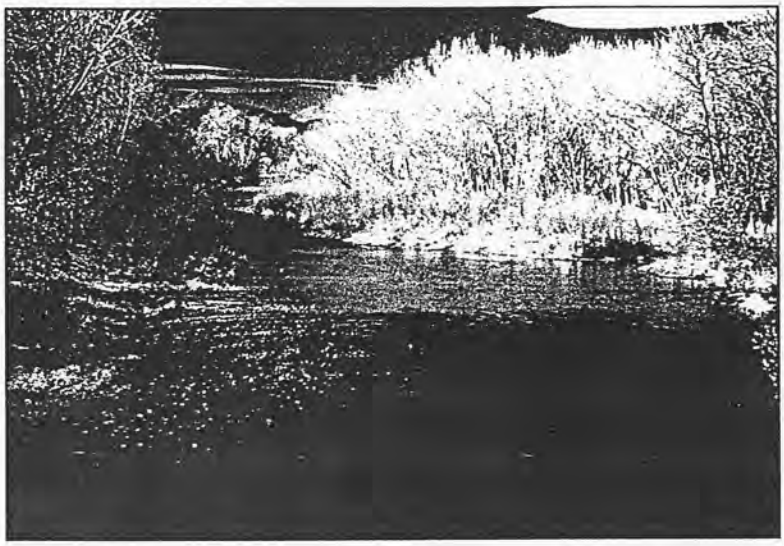

Fig. II.11 shows the location of the test site on the inner side bank of the Poudre River, on the left hand side of the picture.

Fig. II.11. Test site location on the Poudre River

On the test site two areal and two transect samples were collected. Fig. II.12 shows one transect sample adjacent to the areal sample.

In the transect sample every rock falling under the wire was measured and classified. Approximately 150 rocks formed a sample.

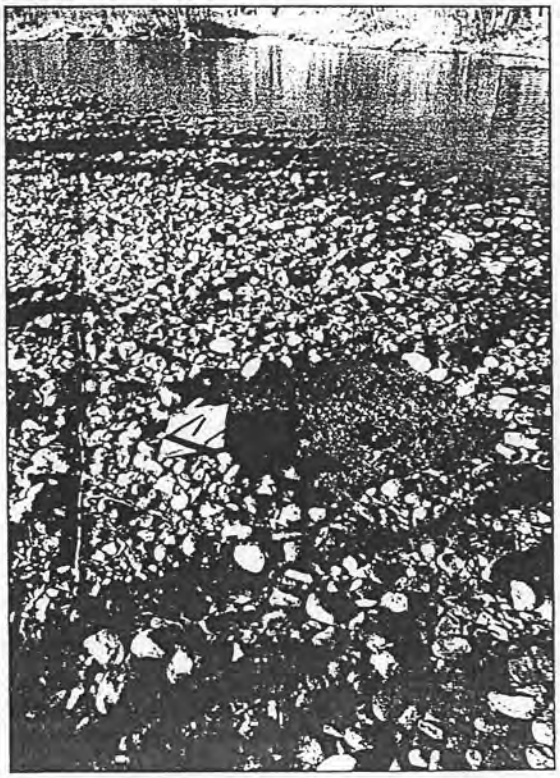

Fig. II.12. Transect sample adjacent to the areal sample

In the areal sample all the spray painted rocks on the surface within 1 m^2 were collected. The surface exposed after removal of the armor coat consisted of a layer of fine material, as can be seen on Fig. II.13. The golf ball was used as reference scale for the photographic sizing.

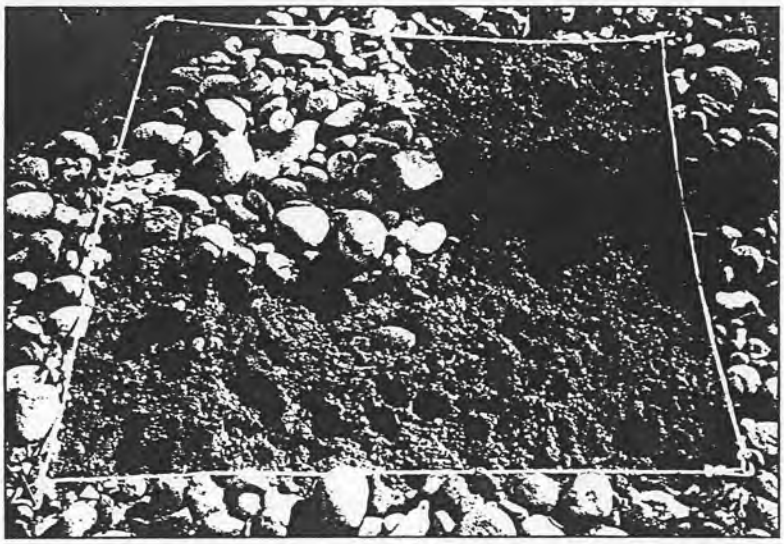

Fig. II.13. Areal sample partially collected with golf ball for photographic sizing

Data collection in the San Luis Valley

During the data collection trip on December 1 – 5, 1998, to the San Luis Valley, several photographs of the field procedures were taken.

Fig. II.14 shows an areal sample prepared for collection, after a heat burner was used to melt the ice and snow. The wooden frame defined 1 m^2.

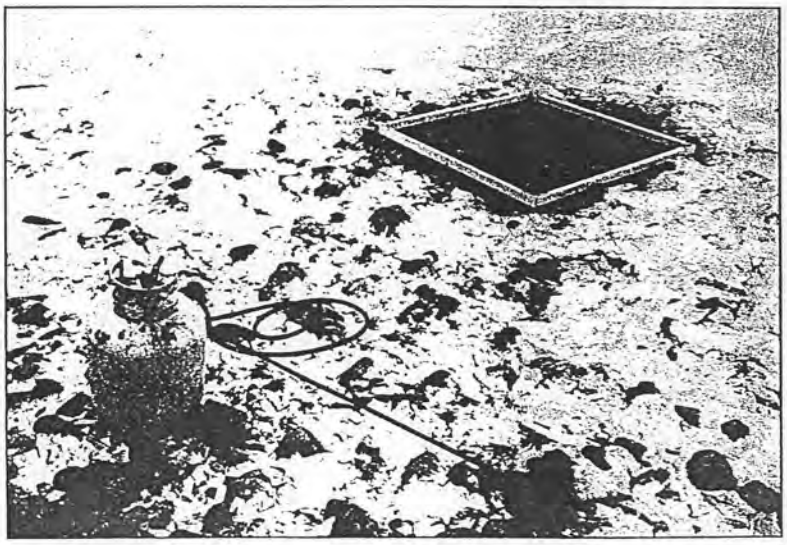

Fig. II.14. Areal sample prepared for collection

Appendix III. References

Einstein, H. A. (1942). "Formulas for the transportation of bed load," Trans., ASCE, Reston, Va., 107, pp. 561-573.

Fehr, R. (1986). " A Method for Sampling Very Coarse Sediments in order to reduce Scale Effects in Movable Bed Models," IHAR, Symposium on Scale Effects in Modeling Sediment Transport Phenomena, pp. 383-397.

Gessler, J. (1965). "Der Geschiebetriebbeginn bei Mischungen untersucht an natürlichen Abpflästerungserscheinungen in Kanälen," Mitteilung No. 69, Versuchsanstalt für Wasserbau und Erdbau, ETH, Zurich, Switzerland.

Gessler, J. (1970). "Self-stabilizing Tendencies of Alluvial Channels," J. of the Waterways and Harbors Division, ASCE, Vol. 96, No. WW2, pp. 235-249.

Gessler, J. (1990). "Friction Factor of Armored River Beds," J. of Hydr. Engrg., ASCE, Vol. 116, No. 4, pp. 531-543.

Kellerhals, R., and Bray, D. I. (1971). "Sampling Procedures for Coarse Fluvial Sediments," J. Hydr. Div., ASCE, Vol. 97, No. 8, pp. 1165-1180.

Keulegan, G. H. (1938). "Laws of Turbulent Flow in Open Channels," J. Nat. Bureau of Standards, Res. Paper 1151.

Lane, E. W. (1952). "Progress Report on Results of Studies on Design of Stable Channels," Hydr. Lab. Report No. 352, Bureau of Reclamation, Denver, Colorado.

Lane, E.W., and Carlson E. J. (1953). "Some Factors affecting the Stability of Canals constructed in Coarse Granular Materials," Hydr. Lab. Report No. 318, Bureau of Reclamation, Denver, Colorado.

Little, W. C., and Mayer, P. G. (1976). "Stability of Channel Beds by Armoring," J. Hydr. Div., ASCE, Vol. 102, No. 11, pp. 1647-1662.

Proffitt, G. T. (1980). "Selective Transport and Armouring of Nonuniform Alluvial Sediments," thesis presented to the University of Canterbury, Christchurch, New Zealand, in partial fulfillment of the requirements for the degree of Doctor of Philosophy.

Rouse, H. (1939). "An Analysis of Sediment Transportation in the Light of Fluid Turbulence," Soil Conservation Service, Rep. No. 25, U.S. Dept. of Agriculture, Washington D.C.

Shields, A. (1936). "Anwendung der Ähnlichkeitsmechanik und der Turbulenzforschung auf die Geschiebebewegung," Mitteilungen der Preussischen Versuchsanstalt für Wasserbau und Schiffbau, Heft 16, Berlin, Germany.

Sutherland, A. J. (1987). "Static Armour Layers by Selective Erosion," In: Thorne, C. R., Bathurst, J. C. and Hey, R. D. (Eds), Sediment Transport in Gravel-Bed Rivers. Wiley, Chichester, U.K., pp.243-268.

Appendix IV. Notation

The following symbols are used in this report:

A = cross-sectional area;
A_b = subarea of bed;
A_c = calculated cross-sectional area;
A_m = "measured" cross-sectional area;
A_s = subarea of bank;
b = intermediate axis of grain, and bottom width of canal;
B = top width of canal;
c = shortest axis of grain;
d = size of grains forming the bed;
d_{75} = bed-material size such that 75 % by weight of sediment sample is finer (d_{50}, and d_{90} are defined in a similar manner);
f = average friction factor;
f_b = friction factor of bed;
f_s = friction factor of bank;
F = safety factor;
F_d = downstream hydrostatic force;
F_u = upstream hydrostatic force;
g = acceleration due to gravity;
h = depth of flow;
k_s = controlling roughness;
L_0 = length of free-body segment;
m = bank slope (mH;1V);
n = Manning's coefficient;
p_i = percent of bed material in size range i;
P = overall wetted perimeter
P_b = wetted perimeter of bed;
p_A = density function of predicted armor layer;
p_{Am} = density function of measured armor layer;
p_{Ac} = density function of corrected measured armor layer;
P_A = grain size distribution of armor layer;
P_s = wetted perimeter of bank;
p_0 = density function of initial grain size distribution;
P_0 = initial grain size distribution;
q = probability of non-removal;
$\overline{q}$ = stability coefficient;
Q = discharge;
Q_{max} = maximum sustained discharge;
r^2 = coefficient of determination in regression analysis;
R = overall hydraulic radius;
R_b = hydraulic radius of bed;

R_s = hydraulic radius of bank;
$\mathbf{Re}_*$ = grain Reynolds number;
S = energy slope;
u_* = shear velocity;
U = average flow velocity;
W = weight of fluid mass;
x = variable of integration;
α = slope of channel bed in degrees;
γ = specific weight of water;
γ_s = specific weight of sediment;
μ = mean value;
ν = kinematic viscosity of water;
ρ = density of water;
σ = standard deviation;
τ = average shear stress;
τ_b = mean bottom shear stress;
τ_{b*} = dimensionless mean bottom shear stress;
τ_c = critical shear stress at incipient motion;
τ_{cp} = predicted critical shear stress of armor coat;
τ_d = design shear stress; and
τ_* = dimensionless shear stress or Shields parameter.

Superscripts used in this report:

A = area-by-weight sample;
P = photographic sample;
T = transect-by-number sample; and
V = volume-by-weight sample.

Appendix V. Description of test sections and contact addresses

Description of test sections as of Nov. 1998

Test section	*Begin*	*End*	*Remarks*
1	Approximately 1 km downstream from diversion at Rio Grande	60 m upstream from county bridge due north of Del Norte. 2.2 km downstream from diversion	No trees. No obstacles. Some stumps. Some cobbles as large as 250 mm. Maximum water flow height clearly visible.
2	800 m downstream from turnout for Rio Grande Lateral #1 (Travelers)	Steel truss bridge approximately 1.6 km downstream from Lateral #1	Some trees. Material smaller than in No. 1 test section. No flume rating station.
4	Approximately 400 m downstream from west side of Section 26	1 km downstream at turnouts with some rocks	No trees. No flume rating station.
5	North-south county bridge on west side of Section 30	600 m downstream at small turnout on left side of lateral. Just upstream from Farmers Union crossing	No trees. No flume rating station.
12	At bridge 1.6 km west of Gun Barrel Road	700 m downstream from beginning approximately 100 m upstream from check structure 800 m west of Gun Barrel Highway	Some effect of backwater at downstream end. Free of trees.
17	Approximately 800 m above east-west bridge of Section 1	To turnout in Section 16	No trees. Straight. Flat bottom.

Contact addresses

Dr. Johannes Gessler
Professor of Civil Engineering and
Interim Dean of Engineering
Colorado State University
Fort Collins, CO, 80523
Tel: 970-491-3366
Fax: 970-491-5569
E-mail: jgessler@engr.colostate.edu

Dr. Rodney J. Wittler
Hydraulic Engineer
Water Resources Research Laboratory
Bureau of Reclamation, D-8560
P.O. Box 25007
Denver, CO, 80225
Tel: 303-445-2156
Fax: 303-445-6324
E-mail: rwittler@do.usbr.gov

Dr. George A. Annandale
Director Water Resources Engineering
Golder Associates Inc.
44 Union Boulevard, Suite 300
Lakewood, CO, 80228
Tel: 303-980-0540
Fax: 303-985-2080
E-mail: george_annandale@golder.com

Steve Baer
Div. III, Dist. 20
Water Commissioner
P.O. Box 106
Monte Vista, CO, 81144
Tel: 719-852-4351
Fax: 719-852-4319

Appendix VI. Computation sheets

Initial grain size distributions 1950 - 1953

d_i [mm] (1)	Σp_i^V TS 1 [%] (2)	TS 2 [%] (3)	TS 4 [%] (4)	TS 5 [%] (5)	TS 12 [%] (6)	TS 17 [%] (7)
215.3	100.0	100.0	100.0	100.0	100.0	100.0
181.0	98.0	100.0	100.0	100.0	100.0	100.0
152.2	95.0	100.0	100.0	100.0	100.0	100.0
128.0	90.0	100.0	98.7	100.0	100.0	100.0
107.6	83.2	96.4	96.8	98.7	100.0	100.0
90.5	78.1	91.6	94.8	95.8	100.0	100.0
76.2	74.0	85.1	92.9	92.9	100.0	100.0
64.0	72.2	79.3	90.3	89.6	98.7	95.5
53.8	69.2	73.4	87.6	85.4	96.4	91.0
45.3	66.6	67.6	85.0	81.1	94.2	86.5
38.1	63.3	62.7	81.3	75.8	91.8	82.0
32.0	57.2	57.9	78.5	72.5	88.5	78.7
26.9	52.6	54.0	74.8	69.2	85.0	75.3
22.6	48.2	50.2	71.0	65.9	81.4	72.0
19.1	43.8	46.3	67.2	62.6	77.6	68.6
9.53	30.7	37.8	57.1	52.5	59.7	57.2
4.76	24.5	32.4	49.5	45.6	46.4	50.0
2.38	22.8	31.0	44.0	44.0	41.0	46.4
1.19	19.7	27.9	37.6	41.4	31.8	41.5
0.590	13.5	20.9	28.3	35.8	19.8	31.4
0.297	8.3	15.5	19.3	22.3	9.7	20.3
0.149	5.3	11.3	13.0	9.3	4.0	13.2
0.074	3.6	8.3	10.3	4.8	2.4	11.9

Least square analysis between transect-by-number and area-by-weight sample for TS 2 (upstream)

Transect-by-number

d_i [mm]	n [-]	q_i^T [%]	Σq_i^T [%]	d_{gi} [mm]	$q_i^T \cdot d_{gi}^x$ [-]	Σp_i^A [%]	$q_i^T \cdot d_{gi}^{1.7}$ [-]	Σp_i^A [%]
152.2	-	-	100.0	139.6	-	100.0	-	100.0
128.0	8	1.5	100.0	117.4	3,642.47	100.0	5,085.79	100.0
107.6	32	6.2	98.5	98.7	10,980.89	93.9	15,146.83	93.7
90.5	42	8.1	92.3	83.0	10,866.77	75.6	14,808.62	74.8
76.1	44	8.5	84.2	69.8	8,584.08	57.5	11,556.85	56.3
64.0	105	20.2	75.7	53.8	13,400.65	43.2	17,715.43	41.9
45.3	103	19.8	55.5	35.0	6,522.85	20.9	8,367.30	19.8
32.0	117	22.5	35.6	26.9	4,824.54	10.0	6,075.71	9.4
22.6	68	13.1	13.1	16.0	1,202.29	2.0	1,459.98	1.8
11.3	-	-	-	3.4	-	-	-	-
$\Sigma =$	519	100.0			60,024.54		80,216.52	

Standard Sieve Analysis

ϕ [-]	d_i [mm]	w_i [kg]	p_i^A [%]	Σp_i^A [%]
-7.00	128.0	-	-	100.0
-6.75	107.6	9.458	10.6	89.4
-6.50	90.5	15.135	16.9	72.6
-6.25	76.1	13.158	14.7	57.9
-6.00	64.0	12.988	14.5	43.4
-5.75	53.8	9.272	10.3	33.0
-5.50	45.3	10.505	11.7	21.3
-5.25	38.1	3.779	4.2	17.1
-5.00	32.0	4.459	5.0	12.1
-4.75	25.4	4.651	5.2	6.9
-4.50	22.6	2.120	2.4	4.6
-4.00	16.0	3.014	3.4	1.2
-3.50	11.3	1.086	1.2	-
	< 11.3	-	-	-
	$\Sigma =$	89.625		

Least Square Analysis

	d^T_i [mm]	d^A_i [mm]
d_{90}	103.7	108.2
d_{80}	94.3	97.7
d_{70}	85.7	87.8
d_{60}	77.9	78.0
d_{50}	69.5	69.3
d_{40}	60.9	60.5
d_{30}	52.1	51.5
d_{20}	44.0	42.9
d_{10}	31.9	29.1
	$\Sigma(d^A_i - d^T_i)^2 =$	46.7

$x = 1.63$

Least square analysis between transect-by-number and area-by-weight sample for TS 2 (downstream)

Transect-by-number

d_i [mm]	n [-]	q_i^T [%]	Σq_i^T [%]	d_{gi} [mm]	$q_i^T \cdot d_{gi}^x$ [-]	Σp_i^A [%]	$q_i^T \cdot d_{gi}^{1.7}$ [-]	Σp_i^A [%]
152.2	2	0.6	100.0	139.6	3,584.95	100.0	2,803.16	100.0
128.0	9	2.8	99.4	117.4	11,914.60	96.6	9,397.04	96.8
107.6	21	6.6	96.5	98.7	20,521.37	85.5	16,325.68	85.9
90.5	27	8.5	89.9	83.0	19,484.84	66.3	15,635.42	67.1
76.1	30	9.5	81.3	69.8	15,989.29	48.1	12,941.61	49.0
64.0	51	16.1	71.8	53.8	17,235.41	33.1	14,132.30	34.1
45.3	54	17.1	55.7	35.0	8,600.64	17.0	7,204.81	17.7
32.0	77	24.4	38.6	26.9	7,737.44	8.9	6,567.23	9.4
22.6	45	14.2	14.2	16.0	1,821.82	1.7	1,586.83	1.8
11.3	-	-	-	3.4	-	-	-	-
$\Sigma =$	316	100.0			106,890.36		86,594.09	

Standard Sieve Analysis

ϕ [-]	d_i [mm]	w_i [kg]	p_i^A [%]	Σp_i^A [%]
-7.00	128.0	-	-	100.0
-6.75	107.6	7.507	8.4	91.6
-6.50	90.5	29.434	33.1	58.5
-6.25	76.1	11.484	12.9	45.6
-6.00	64.0	11.314	12.7	32.9
-5.75	53.8	7.010	7.9	25.0
-5.50	45.3	4.472	5.0	20.0
-5.25	38.1	4.290	4.8	15.2
-5.00	32.0	4.473	5.0	10.1
-4.75	25.4	4.517	5.1	5.1
-4.50	22.6	1.539	1.7	3.3
-4.00	16.0	2.178	2.4	0.9
-3.50	11.3	0.789	0.9	-
	< 11.3	-	-	-
	$\Sigma =$	89.007		

Least Square Analysis

	d^T_i [mm]	d^A_i [mm]
d_{90}	115.4	106.8
d_{80}	102.4	101.3
d_{70}	93.6	96.1
d_{60}	85.2	91.2
d_{50}	77.5	80.7
d_{40}	69.3	70.5
d_{30}	59.9	60.1
d_{20}	48.3	45.3
d_{10}	33.5	31.8
	$\Sigma(d^A_i - d^T_i)^2 =$	142.7

$x = 1.75$

Least square analysis between transect-by-number and area-by-weight sample for TS 17

Transect-by-number

d_i [mm]	n [-]	q_i^T [%]	Σq_i^T [%]	d_{gi} [mm]	$q_i^T \cdot d_{gi}^x$ [-]	Σp_i^A [%]	$q_i^T \cdot d_{gi}^{1.7}$ [-]	Σp_i^A [%]
152.2	-	-	100.0	139.6	-	100.0	-	100.0
128.0	-	-	100.0	117.4	-	100.0	-	100.0
107.6	1	0.3	100.0	98.7	1,166.71	100.0	731.14	100.0
90.5	2	0.6	99.7	83.0	1,707.77	98.0	1,089.24	98.2
76.1	5	1.5	99.1	69.8	3,124.90	95.1	2,028.55	95.5
64.0	68	20.2	97.6	53.8	26,585.36	89.8	17,721.46	90.4
45.3	70	20.8	77.4	35.0	12,612.91	44.5	8,783.64	46.4
32.0	76	22.6	56.5	26.9	8,522.37	23.0	6,096.12	24.6
22.6	114	33.9	33.9	16.0	5,013.19	8.5	3,780.68	9.4
11.3	-	-	-	3.4	-	-	-	-
$\Sigma =$	336	100.0			58,733.21		40,230.82	

Standard Sieve Analysis

ϕ [-]	d_i [mm]	w_i [kg]	p_i^A [%]	Σp_i^A [%]
-7.00	128.0	-	-	100.0
-6.75	107.6	-	-	100.0
-6.50	90.5	-	-	100.0
-6.25	76.1	0.874	2.0	98.0
-6.00	64.0	4.687	10.9	87.1
-5.75	53.8	9.330	21.7	65.3
-5.50	45.3	8.710	20.3	45.1
-5.25	38.1	4.063	9.5	35.6
-5.00	32.0	4.671	10.9	24.7
-4.75	25.4	3.652	8.5	16.2
-4.50	22.6	2.007	4.7	11.6
-4.00	16.0	3.312	7.7	3.8
-3.50	11.3	1.653	3.8	-
	< 11.3	-	-	-
	$\Sigma =$	42.959		

Least Square Analysis

	d^T_i [mm]	d^A_i [mm]
d_{90}	64.4	67.1
d_{80}	59.4	60.5
d_{70}	55.0	55.9
d_{60}	51.0	51.4
d_{50}	47.2	47.2
d_{40}	42.1	41.2
d_{30}	35.8	34.8
d_{20}	29.7	28.1
d_{10}	23.4	21.1
	$\Sigma(d^A_i - d^T_i)^2 =$	18.6

$x = 1.80$

Armor layer computations for TS 1

d_i [mm] (1)	d_{gi} [mm] (2)	p_{Oi} [%] (3)	Σp_{Oi} [%] (4)	τ_c [N/m^2] (5)	τ_c/τ [-] (6)	q [-] (7)	qp_{Oi} [-] (8)	q^2p_{Oi} [-] (9)	Σp_{Ai} [%] (10)	Σp_{Ami} [%] (11)	Σp_{Aci} [%] (12)
215.3	197.4	2.0	100.0	150.18	5.28	1.000	2.00	2.00	100.0	100.0	100.0
181.0	166.0	3.0	98.0	126.27	4.44	1.000	3.00	3.00	95.4	92.6	95.3
152.2	139.6	5.0	95.0	106.19	3.74	1.000	5.00	5.00	88.4	84.3	89.5
128.0	117.4	6.8	90.0	89.28	3.14	1.000	6.80	6.80	76.9	78.1	84.9
107.6	98.7	5.1	83.2	75.07	2.64	0.998	5.09	5.08	61.1	65.9	74.7
90.5	83.0	4.1	78.1	63.14	2.22	0.984	4.03	3.97	49.4	51.0	61.4
76.1	69.8	1.8	74.0	53.09	1.87	0.936	1.69	1.58	40.0	31.5	42.2
64.0	58.7	3.0	72.2	44.64	1.57	0.842	2.53	2.13	36.1	24.5	34.7
53.8	49.4	2.6	69.2	37.56	1.32	0.714	1.86	1.32	30.3		
45.3	41.5	3.3	66.6	31.60	1.11	0.578	1.91	1.10	26.0	10.7	17.9
38.1	34.9	6.1	63.3	26.57	0.93	0.454	2.77	1.26	21.6		
32.0	29.3	4.7	57.2	22.32	0.79	0.353	1.64	0.58	15.2	4.1	7.8
26.9	24.7	4.4	52.6	18.76	0.66	0.275	1.21	0.33	11.4		
22.6	20.8	4.4	48.2	15.79	0.56	0.218	0.95	0.21	8.6	1.6	3.5
19.1	17.5	13.1	43.8	13.28	0.47	0.175	2.29	0.40	6.4		
9.53	6.73	6.2	30.7	5.10	0.18	0.075	0.46	0.03	1.1	-	-
4.76	3.37	1.7	24.5	2.22	0.08	0.053	-	-	-	-	-
2.38	1.68	3.1	22.8	0.90	0.03	0.045	-	-	-	-	-
1.19	0.84	6.2	19.7	0.43	0.02	0.042	-	-	-	-	-
0.590	0.42	5.2	13.5	-	-	0.040	-	-	-	-	-
0.297	0.21	3.0	8.3	-	-	0.040	-	-	-	-	-
0.149	0.11	1.7	5.3	-	-	0.040	-	-	-	-	-
0.074			3.6						-	-	-

Note: $\Sigma qp_{Oi} = 43.23$; $\Sigma q^2 p_{Oi} = 34.79$; $\tau = 28.42$ N/m^2; and $\overline{q} = 0.80$.

Armor layer computations for TS 2

d_i [mm] (1)	d_{gi} [mm] (2)	p_{Oi} [%] (3)	Σp_{Oi} [%] (4)	τ_c [N/m^2] (5)	τ_c/τ [-] (6)	q [-] (7)	qp_{Oi} [-] (8)	q^2p_{Oi} [-] (9)	Σp_{Ai} [%] (10)	Σp_{Ami} [%] (11)	Σp_{Aci} [%] (12)
215.3	197.4	-	100.0	150.18	6.26	1.000	-	-	100.0	100.0	100.0
181.0	166.0	-	100.0	126.27	5.26	1.000	-	-	100.0	100.0	100.0
152.2	139.6	-	100.0	106.19	4.43	1.000	-	-	100.0	100.0	100.0
128.0	117.4	3.6	100.0	89.28	3.72	1.000	3.60	3.60	100.0	98.7	99.1
107.6	98.7	4.8	96.4	75.07	3.13	1.000	4.80	4.80	91.8	90.6	93.3
90.5	83.0	6.5	91.6	63.14	2.63	0.998	6.49	6.47	80.8	71.7	78.4
76.1	69.8	5.8	85.1	53.09	2.21	0.983	5.75	5.66	65.9	53.4	62.6
64.0	58.7	5.8	79.3	44.64	1.86	0.935	5.47	5.11	52.8	38.8	48.9
53.8	49.4	5.9	73.4	37.56	1.57	0.839	4.91	4.12	40.3		
45.3	41.5	4.8	67.6	31.60	1.32	0.711	3.45	2.45	29.0	19.0	27.7
38.1	34.9	4.9	62.7	26.57	1.11	0.575	2.79	1.60	21.1		
32.0	29.3	3.9	57.9	22.32	0.93	0.451	1.74	0.78	14.7	9.4	15.0
26.9	24.7	3.9	54.0	18.76	0.78	0.351	1.35	0.47	10.8		
22.6	20.8	3.9	50.2	15.79	0.66	0.274	1.06	0.29	7.7	1.8	3.6
19.1	17.5	8.5	46.3	13.28	0.55	0.217	1.84	0.40	5.3		
9.53	6.73	5.4	37.8	5.10	0.21	0.084	0.45	0.04	1.0	-	-
4.76	3.37	1.4	32.4	2.22	0.09	0.056	-	-	-	-	-
2.38	1.68	3.1	31.0	0.90	0.04	0.046	-	-	-	-	-
1.19	0.84	7.0	27.9	0.43	0.02	0.042	-	-	-	-	-
0.590	0.42	5.4	20.9	-	-	0.040	-	-	-	-	-
0.297	0.21	4.2	15.5	-	-	0.040	-	-	-	-	-
0.149	0.11	3.0	11.3	-	-	0.040	-	-	-	-	-
0.074			8.3						-	-	-

Note: $\Sigma qp_{Oi} = 43.69$; $\Sigma q^2 p_{Oi} = 35.80$; $\tau = 23.99$ N/m^2; and $\overline{q} = 0.82$.

Armor layer computations for TS 4

d_i [mm] (1)	d_{gi} [mm] (2)	p_{Oi} [%] (3)	Σp_{Oi} [%] (4)	τ_c [N/m^2] (5)	τ_c/τ [-] (6)	q [-] (7)	qp_{Oi} [-] (8)	q^2p_{Oi} [-] (9)	Σp_{Ai} [%] (10)	Σp_{Ami} [%] (11)	Σp_{Aci} [%] (12)
215.3	197.4	-	100.0	150.18	5.53	1.000	-	-	100.0	100.0	100.0
181.0	166.0	-	100.0	126.27	4.65	1.000	-	-	100.0	100.0	100.0
152.2	139.6	1.3	100.0	106.19	3.91	1.000	1.30	1.30	100.0	100.0	100.0
128.0	117.4	1.9	98.7	89.28	3.28	1.000	1.90	1.90	94.4	93.7	95.6
107.6	98.7	2.0	96.8	75.07	2.76	0.999	2.00	2.00	86.3	79.5	84.9
90.5	83.0	1.9	94.8	63.14	2.32	0.990	1.88	1.86	77.7	58.3	67.6
76.1	69.8	2.6	92.9	53.09	1.95	0.953	2.48	2.36	69.6	46.5	57.0
64.0	58.7	2.7	90.3	44.64	1.64	0.870	2.35	2.04	59.0	35.8	46.5
53.8	49.4	2.6	87.6	37.56	1.38	0.749	1.95	1.46	48.9		
45.3	41.5	3.7	85.0	31.60	1.16	0.612	2.27	1.39	40.6	16.3	24.9
38.1	34.9	2.8	81.3	26.57	0.98	0.484	1.36	0.66	30.9		
32.0	29.3	3.7	78.5	22.32	0.82	0.377	1.39	0.53	25.1	7.0	12.0
26.9	24.7	3.8	74.8	18.76	0.69	0.293	1.11	0.33	19.1		
22.6	20.8	3.8	71.0	15.79	0.58	0.231	0.88	0.20	14.3	2.3	4.7
19.1	17.5	10.1	67.2	13.28	0.49	0.185	1.87	0.35	10.5		
9.53	6.73	7.6	57.1	5.10	0.19	0.077	0.59	0.05	2.5	-	-
4.76	3.37	5.5	49.5	2.22	0.08	0.054	-	-	-	-	-
2.38	1.68	6.4	44.0	0.90	0.03	0.045	-	-	-	-	-
1.19	0.84	9.3	37.6	0.43	0.02	0.042	-	-	-	-	-
0.590	0.42	9.0	28.3	-	-	0.040	-	-	-	-	-
0.297	0.21	6.3	19.3	-	-	0.040	-	-	-	-	-
0.149	0.11	2.7	13.0	-	-	0.040	-	-	-	-	-
0.074			10.3						-	-	-

Note: $\Sigma qp_{Oi} = 23.31$; $\Sigma q^2 p_{Oi} = 16.41$; $\tau = 27.18$ N/m^2; and $\overline{q} = 0.70$.

Armor layer computations for TS 5

d_i [mm] (1)	d_{gi} [mm] (2)	p_{Oi} [%] (3)	Σp_{Oi} [%] (4)	τ_c [N/m^2] (5)	τ_c/τ [-] (6)	q [-] (7)	qp_{Oi} [-] (8)	q^2p_{Oi} [-] (9)	Σp_{Ai} [%] (10)	Σp_{Ami} [%] (11)	Σp_{Aci} [%] (12)
215.3	197.4	-	100.0	150.18	7.00	1.000	-	-	100.0	100.0	100.0
181.0	166.0	-	100.0	126.27	5.88	1.000	-	-	100.0	100.0	100.0
152.2	139.6	-	100.0	106.19	4.95	1.000	-	-	100.0	100.0	100.0
128.0	117.4	1.3	100.0	89.28	4.16	1.000	1.30	1.30	100.0	97.0	98.2
107.6	98.7	2.9	98.7	75.07	3.50	1.000	2.90	2.90	95.9	93.6	95.9
90.5	83.0	2.9	95.8	63.14	2.94	1.000	2.90	2.90	86.9	82.7	88.0
76.1	69.8	3.3	92.9	53.09	2.47	0.995	3.28	3.27	77.9	70.1	78.1
64.0	58.7	4.2	89.6	44.64	2.08	0.971	4.08	3.96	67.6	54.7	64.8
53.8	49.4	4.3	85.4	37.56	1.75	0.906	3.89	3.53	54.9		
45.3	41.5	5.3	81.1	31.60	1.47	0.796	4.22	3.36	42.8	29.0	39.5
38.1	34.9	3.3	75.8	26.57	1.24	0.661	2.18	1.44	29.6		
32.0	29.3	3.3	72.5	22.32	1.04	0.528	1.74	0.92	22.8	13.7	20.9
26.9	24.7	3.3	69.2	18.76	0.87	0.412	1.36	0.56	17.4		
22.6	20.8	3.3	65.9	15.79	0.74	0.321	1.06	0.34	13.2	4.5	8.2
19.1	17.5	10.1	62.6	13.28	0.62	0.252	2.54	0.64	9.9		
9.53	6.73	6.9	52.5	5.10	0.24	0.091	0.62	0.06	1.9	-	-
4.76	3.37	1.6	45.6	2.22	0.10	0.058	-	-	-	-	-
2.38	1.68	2.6	44.0	0.90	0.04	0.046	-	-	-	-	-
1.19	0.84	5.6	41.4	0.43	0.02	0.043	-	-	-	-	-
0.590	0.42	13.5	35.8	-	-	0.040	-	-	-	-	-
0.297	0.21	13.0	22.3	-	-	0.040	-	-	-	-	-
0.149	0.11	4.5	9.3	-	-	0.040	-	-	-	-	-
0.074			4.8						-	-	-

Note: $\Sigma qp_{Oi} = 31.95$; $\Sigma q^2p_{Oi} = 24.98$; $\tau = 21.47$ N/m^2; and $\overline{q} = 0.78$.

Armor layer computations for TS 12

d_i [mm] (1)	d_{gi} [mm] (2)	p_{Oi} [%] (3)	Σp_{Oi} [%] (4)	τ_c [N/m^2] (5)	τ_c/τ [-] (6)	q [-] (7)	qp_{Oi} [-] (8)	q^2p_{Oi} [-] (9)	Σp_{Ai} [%] (10)	Σp_{Ami} [%] (11)	Σp_{Aci} [%] (12)
215.3	197.4	-	100.0	150.18	-	1.000	-	-	100.0	100.0	100.0
181.0	166.0	-	100.0	126.27	-	1.000	-	-	100.0	100.0	100.0
152.2	139.6	-	100.0	106.19	9.76	1.000	-	-	100.0	100.0	100.0
128.0	117.4	-	100.0	89.28	8.21	1.000	-	-	100.0	100.0	100.0
107.6	98.7	-	100.0	75.07	6.90	1.000	-	-	100.0	100.0	100.0
90.5	83.0	-	100.0	63.14	5.80	1.000	-	-	100.0	97.8	98.7
76.1	69.8	1.3	100.0	53.09	4.88	1.000	1.30	1.30	100.0	96.1	97.7
64.0	58.7	2.3	98.7	44.64	4.10	1.000	2.30	2.30	96.3	90.0	93.5
53.8	49.4	2.2	96.4	37.56	3.45	1.000	2.20	2.20	89.9		
45.3	41.5	2.4	94.2	31.60	2.90	1.000	2.40	2.40	83.7	63.9	73.3
38.1	34.9	3.3	91.8	26.57	2.44	0.994	3.28	3.26	76.9		
32.0	29.3	3.5	88.5	22.32	2.05	0.967	3.39	3.28	67.7	40.0	50.2
26.9	24.7	3.6	85.0	18.76	1.72	0.898	3.23	2.90	58.1		
22.6	20.8	3.8	81.4	15.79	1.45	0.786	2.99	2.34	49.0	19.1	27.2
19.1	17.5	17.9	77.6	13.28	1.22	0.651	11.65	7.58	40.6		
9.53	6.73	13.3	59.7	5.10	0.47	0.176	2.34	0.41	7.8	-	-
4.76	3.37	5.4	46.4	2.22	0.20	0.081	0.44	0.04	1.2	-	-
2.38	1.68	9.2	41.0	0.90	0.08	0.054	-	-	-	-	-
1.19	0.84	12.0	31.8	0.43	0.04	0.046	-	-	-	-	-
0.590	0.42	10.1	19.8	-	-	0.040	-	-	-	-	-
0.297	0.21	5.7	9.7	-	-	0.040	-	-	-	-	-
0.149	0.11	1.6	4.0	-	-	0.040	-	-	-	-	-
0.074			2.4						-	-	-

Note: $\Sigma qp_{Oi} = 35.51$; $\Sigma q^2 p_{Oi} = 28.01$; $\tau = 10.88$ N/m^2; and $\bar{q} = 0.79$.

Armor layer computations for TS 17

d_i [mm] (1)	d_{gi} [mm] (2)	p_{Oi} [%] (3)	Σp_{Oi} [%] (4)	τ_c [N/m^2] (5)	τ_c/τ [-] (6)	q [-] (7)	qp_{Oi} [-] (8)	q^2p_{Oi} [-] (9)	Σp_{Ai} [%] (10)	Σp_{Ami} [%] (11)	Σp_{Aci} [%] (12)
215.3	197.4	-	100.0	150.18	7.49	1.000	-	-	100.0	100.0	100.0
181.0	166.0	-	100.0	126.27	6.30	1.000	-	-	100.0	100.0	100.0
152.2	139.6	-	100.0	106.19	5.30	1.000	-	-	100.0	100.0	100.0
128.0	117.4	-	100.0	89.28	4.45	1.000	-	-	100.0	100.0	100.0
107.6	98.7	-	100.0	75.07	3.74	1.000	-	-	100.0	100.0	100.0
90.5	83.0	-	100.0	63.14	3.15	1.000	-	-	100.0	98.2	98.9
76.1	69.8	4.5	100.0	53.09	2.65	0.998	4.49	4.48	100.0	95.5	97.0
64.0	58.7	4.5	95.5	44.64	2.23	0.984	4.43	4.36	83.9	90.4	93.2
53.8	49.4	4.5	91.0	37.56	1.87	0.937	4.22	3.95	67.9		
45.3	41.5	4.5	86.5	31.60	1.58	0.844	3.80	3.21	52.8	46.4	55.8
38.1	34.9	3.3	82.0	26.57	1.32	0.716	2.36	1.69	39.1		
32.0	29.3	3.4	78.7	22.32	1.11	0.579	1.97	1.14	30.6	24.6	32.8
26.9	24.7	3.3	75.3	18.76	0.94	0.455	1.50	0.68	23.5		
22.6	20.8	3.4	72.0	15.79	0.79	0.355	1.21	0.43	18.2	9.4	14.6
19.1	17.5	11.4	68.6	13.28	0.66	0.277	3.16	0.87	13.8		
9.53	6.73	7.2	57.2	5.10	0.25	0.095	0.69	0.07	2.5	-	-
4.76	3.37	3.6	50.0	2.22	0.11	0.059	-	-	-	-	-
2.38	1.68	4.9	46.4	0.90	0.04	0.047	-	-	-	-	-
1.19	0.84	10.1	41.5	0.43	0.02	0.043	-	-	-	-	-
0.590	0.42	11.1	31.4	-	-	0.040	-	-	-	-	-
0.297	0.21	7.1	20.3	-	-	0.040	-	-	-	-	-
0.149	0.11	1.3	13.2	-	-	0.040	-	-	-	-	-
0.074			11.9						-	-	-

Note: $\Sigma qp_{Oi} = 27.82$; $\Sigma q^2 p_{Oi} = 20.88$; $\tau = 20.05$ N/m^2; and $\overline{q} = 0.75$.

Least square analysis between GoldSize photographic sizing and area-by-weight sample for TS 2 (upstream)

GoldSize Photographic Sizing

d_i [mm]	Cd_i [mm]	n [-]	q_i^P [%]	d_{gi} [mm]	$q_i^P \cdot d_{gi}^x$ [-]	Σp_i^P [%]
215.3	198.1	-	-	197.4	-	100.0
181.0	166.5	-	-	166.0	-	100.0
152.2	140.0	1	0.2	139.6	61,495.08	100.0
128.0	117.8	5	0.9	117.4	196,334.91	95.7
107.6	99.0	9	1.5	98.7	225,481.59	81.8
90.5	83.3	13	2.2	83.0	207,942.26	65.8
76.1	70.0	21	3.6	69.8	214,482.56	51.2
64.0	58.9	16	2.7	58.7	104,346.96	36.0
53.8	49.5	29	5.0	49.4	120,986.79	28.6
45.3	41.7	38	6.5	41.5	100,952.09	20.1
38.1	35.1	37	6.3	34.9	62,763.44	12.9
32.0	29.4	38	6.5	29.3	40,978.67	8.5
26.9	24.7	36	6.2	24.7	24,944.50	5.6
22.6	20.8	36	6.2	20.7	15,785.30	3.8
19.0	17.5	54	9.2	17.4	15,100.92	2.7
16.0	14.7	60	10.3	14.7	10,841.52	1.7
13.5	12.4	57	9.8	12.4	6,628.64	0.9
11.3	10.4	55	9.4	10.4	4,055.70	0.4
9.5	8.7	42	7.2	8.7	1,950.70	0.1
8.0	7.4	37	6.3	-	-	-
	$\Sigma =$	584	100.0		1,415,071.65	

Standard Sieve Analysis

ϕ [-]	d_i [mm]	w_i [kg]	p_i^A [%]	Σp_i^A [%]
-7.00	128.0	-	-	100.0
-6.75	107.6	9.458	10.6	89.4
-6.50	90.5	15.135	16.9	72.6
-6.25	76.1	13.158	14.7	57.9
-6.00	64.0	12.988	14.5	43.4
-5.75	53.8	9.272	10.3	33.0
-5.50	45.3	10.505	11.7	21.3
-5.25	38.1	3.779	4.2	17.1
-5.00	32.0	4.459	5.0	12.1
-4.75	25.4	4.651	5.2	6.9
-4.50	22.6	2.120	2.4	4.6
-4.00	16.0	3.014	3.4	1.2
-3.50	11.3	1.086	1.2	-
	< 11.3	-	-	-
	$\Sigma =$	89.625	100.0	

Mean Square Analysis

	d^P_i [mm]	d^A_i [mm]
d_{90}	109.7	108.2
d_{80}	97.1	97.7
d_{70}	87.1	87.8
d_{60}	77.7	78.0
d_{50}	69.1	69.3
d_{40}	61.6	60.5
d_{30}	51.1	51.5
d_{20}	41.6	42.9
d_{10}	31.2	29.1
$\Sigma(d^A_i - d^P_i)^2 =$		10.7

$x = 2.59$
$C = 0.92$

Least square analysis between GoldSize photographic sizing and area-by-weight sample for TS 2 (downstream)

GoldSize Photographic Sizing

d_i [mm]	Cd_i [mm]	n [-]	q_i^P [%]	d_{gi} [mm]	$q_i^P \cdot d_{gi}^x$ [-]	Σp_i^P [%]
215.3	204.5	-	-	197.4	-	100.0
181.0	172.0	-	-	166.0	-	100.0
152.2	144.6	-	-	139.6	-	100.0
128.0	121.6	7	1.4	117.4	733,528.32	100.0
107.6	102.2	11	2.2	98.7	714,073.51	79.3
90.5	86.0	14	2.8	83.0	563,402.11	59.2
76.1	72.3	20	4.1	69.8	499,006.11	43.3
64.0	60.8	16	3.3	58.7	247,511.87	29.3
53.8	51.1	22	4.5	49.4	211,418.97	22.3
45.3	43.0	28	5.7	41.5	166,343.44	16.3
38.1	36.2	41	8.3	34.9	151,013.90	11.6
32.0	30.4	42	8.5	29.3	95,463.82	7.4
26.9	25.6	55	11.2	24.7	78,026.33	4.7
22.6	21.5	46	9.3	20.7	40,074.76	2.5
19.0	18.1	38	7.7	17.4	20,499.08	1.4
16.0	15.2	44	8.9	14.7	14,903.33	0.8
13.5	12.8	32	6.5	12.4	6,776.86	0.4
11.3	10.7	35	7.1	10.4	4,561.58	0.2
9.5	9.0	24	4.9	8.7	1,911.26	0.1
8.0	7.6	17	3.5	-	-	-
	$\Sigma =$	492	100.0		3,548,515.25	

Standard Sieve Analysis

ϕ [-]	d_i [mm]	w_i [kg]	p_i^A [%]	Σp_i^A [%]
-7.00	128.0	-	-	100.0
-6.75	107.6	7.507	8.4	91.6
-6.50	90.5	29.434	33.1	58.5
-6.25	76.1	11.484	12.9	45.6
-6.00	64.0	11.314	12.7	32.9
-5.75	53.8	7.010	7.9	25.0
-5.50	45.3	4.472	5.0	20.0
-5.25	38.1	4.290	4.8	15.2
-5.00	32.0	4.473	5.0	10.1
-4.75	25.4	4.517	5.1	5.1
-4.50	22.6	1.539	1.7	3.3
-4.00	16.0	2.178	2.4	0.9
-3.50	11.3	0.789	0.9	-
	< 11.3	-	-	-
	$\Sigma =$	89.007	100.0	

Mean Square Analysis

	$d^P{}_i$ [mm]	$d^A{}_i$ [mm]
d_{90}	111.8	106.8
d_{80}	102.8	101.3
d_{70}	94.3	96.1
d_{60}	86.6	91.2
d_{50}	77.8	80.7
d_{40}	69.4	70.5
d_{30}	61.4	60.1
d_{20}	47.8	45.3
d_{10}	33.8	31.8
$\Sigma(d^A{}_i - d^P{}_i)^2 =$		75.2

$x = 2.76$
$C = 0.95$

Least square analysis between GoldSize photographic sizing and area-by-weight sample for TS 17

GoldSize Photographic Sizing

d_i [mm]	Cd_i [mm]	n [-]	q_i^P [%]	d_{gi} [mm]	$q_i^P \cdot d_{gi}^x$ [-]	Σp_i^P [%]
215.3	206.7	-	-	197.4	-	100.0
181.0	173.8	-	-	166.0	-	100.0
152.2	146.1	-	-	139.6	-	100.0
128.0	122.9	-	-	117.4	-	100.0
107.6	103.3	-	-	98.7	-	100.0
90.5	86.9	4	0.4	83.0	41,462.92	100.0
76.1	73.1	10	0.9	69.8	65,616.34	93.6
64.0	61.4	30	2.7	58.7	124,611.90	83.5
53.8	51.6	53	4.7	49.4	139,620.34	64.2
45.3	43.5	42	3.7	41.5	69,844.14	42.7
38.1	36.6	55	4.9	34.9	57,896.93	31.9
32.0	30.7	72	6.4	29.3	47,763.56	23.0
26.9	25.8	78	6.9	24.7	32,964.63	15.6
22.6	21.7	76	6.8	20.7	20,146.94	10.5
19.0	18.2	104	9.3	17.4	17,430.79	7.4
16.0	15.4	128	11.4	14.7	13,745.53	4.7
13.5	13.0	121	10.8	12.4	8,291.87	2.6
11.3	10.8	116	10.3	10.4	4,996.43	1.3
9.5	9.1	126	11.2	8.7	3,387.93	0.5
8.0	7.7	109	9.7	-	-	-
	$\Sigma =$	1,124	100.0		647,780.24	

Standard Sieve Analysis

ϕ [-]	d_i [mm]	w_i [kg]	p_i^A [%]	Σp_i^A [%]
-7.00	128.0	-	-	100.0
-6.75	107.6	-	-	100.0
-6.50	90.5	-	-	100.0
-6.25	76.1	0.874	2.0	98.0
-6.00	64.0	4.687	10.9	87.1
-5.75	53.8	9.330	21.7	65.3
-5.50	45.3	8.710	20.3	45.1
-5.25	38.1	4.063	9.5	35.6
-5.00	32.0	4.671	10.9	24.7
-4.75	25.4	3.652	8.5	16.2
-4.50	22.6	2.007	4.7	11.6
-4.00	16.0	3.312	7.7	3.8
-3.50	11.3	1.653	3.8	-
	< 11.3	-	-	-
	$\Sigma =$	42.959	100.0	

Mean Square Analysis

	d^P_i [mm]	d^A_i [mm]
d_{90}	68.7	67.1
d_{80}	59.5	60.5
d_{70}	54.4	55.9
d_{60}	49.9	51.4
d_{50}	46.1	47.2
d_{40}	41.7	41.2
d_{30}	35.2	34.8
d_{20}	28.7	28.1
d_{10}	21.1	21.1
$\Sigma(d^A_i - d^P_i)^2 =$		9.7

$x = 2.64$
$C = 0.96$